MSc-research Thesis

Joint Inversion of Surface Waves and Ps-converted Waves

Niels Grobbe
Utrecht University, the Netherlands
August 18, 2010

Supervised by: Dr. J. A. M. Paulssen
Utrecht University, the Netherlands

Table of Contents

Table of contents **-2-**

Abstract **-3-**

Introduction **-4-**

Methods **-11-**

Monte Carlo-search -11-

Iterative linearized least-squares inversion -14-

Results & Discussion **-16-**

Monte Carlo-search with phase velocity dispersion data and receiver function data -16-

Three-layered crust over a half-space -16-

Three-layered crust over a varying mantle -26-

Modelling with a different number of layers than the number of layers of the true model -28-

Monte Carlo-search with phase velocity dispersion data, receiver functions and group velocity dispersion data -33-

Results iterative linearized least-squares inversion with phase velocity dispersion data and receiver functions -48-

Vp/Vs ratio -51-

Damping -55-

General approach developed -55-

Iterative linearized least-squares inversion with many layers -58-

Iterative linearized least-squares inversion with phase velocity dispersion data, receiver functions and group velocity dispersion data -60-

Conclusions **-66-**

Recommendations for future research **-68-**

Acknowledgements **-68-**

References **-69-**

Abstract

To put constraints on the crustal and upper-mantle structure, seismologists have often made use of the sensitivity of surface wave dispersion observations and teleseismic P-wave receiver functions to the shear velocity structure of the medium.

Receiver functions are primarily sensitive to the shear wave velocity contrasts of interfaces in the medium and the vertical traveltimes (relative traveltime of the converted waves reverberated between those interfaces). In contrast, surface wave dispersion measurements are sensitive to vertical shear wave velocity averages (absolute).

Both types of datasets have their own limitations in resolution. In this study, it was investigated if the resolution gaps can be bridged (and hence leading to tighter constraints on the shear wave velocity structure), by doing a joint interpretation of surface wave dispersion data and teleseismic P-wave receiver functions. This joint inversion of surface wave dispersion data and Ps-receiver functions was based upon fundamental mode Rayleigh wave phase and group velocity measurements and teleseismic P-wave receiver functions.

To solve the joint inverse problem, two different solution techniques were closely investigated: a Monte Carlo-search and an iterative linearized least-squares inversion.

The results of this study clearly show that performing a joint inversion with surface wave phase velocity dispersion data and receiver function data significantly improves the retrieved shear wave velocity structure. Using group velocity dispersion data in the joint inversion (in addition to phase velocity dispersion data and receiver functions), improves the retrieved shear wave velocity structure even more.

The non-uniqueness problem of the receiver functions is tackled remarkably well by the joint inversion. Nevertheless, the joint inverse problem remains highly non-linear. Therefore, with the iterative linearized least-squares inversion, a final solution which resembles the true shear wave velocity structure perfectly is almost impossible to obtain even with the application of a general approach for the iterative linearized least-squares inversion developed in this study. During this development it has become clear that the choice of the starting model does influence the end-result obtained, but the most important influencing part is formed by the Vp/Vs ratio of the starting model which was kept fixed in the inversion.

A Monte Carlo-search is in general the best solution technique, while this results in a range of possible models that give a clear indication of the real shear wave velocity structure. However, also the iterative linearized least-squares inversion results in quite good shear wave velocity-depth plots.

Introduction

Using seismic recordings, elastic properties of the subsurface can be inferred. The process of reconstructing an earth model from geophysical observables recorded at the surface is called an inverse problem. The forward problem deals with computing the data **d**, given a model **m**. It can be described by the following equation: $\mathbf{d} = A(\mathbf{m})$, where **m** is the model vector, **d** is the data vector and *A* is an operator acting on the model parameters. The inverse problem in contrast, deals with the question what gave rise to a specific set of observed data. In other words, trying to reconstruct a model from a set of measurements. The inverse problem often is not unique, i.e. the data can be explained equally well by many different models. This is a consequence of the fact that in general it is tried to reconstruct a model with many degrees of freedom, using a finite amount of data. Therefore, there is not sufficient information in the data to determine the model uniquely. This has as a consequence, that the obtained model from the inversion is not necessarily the true model.

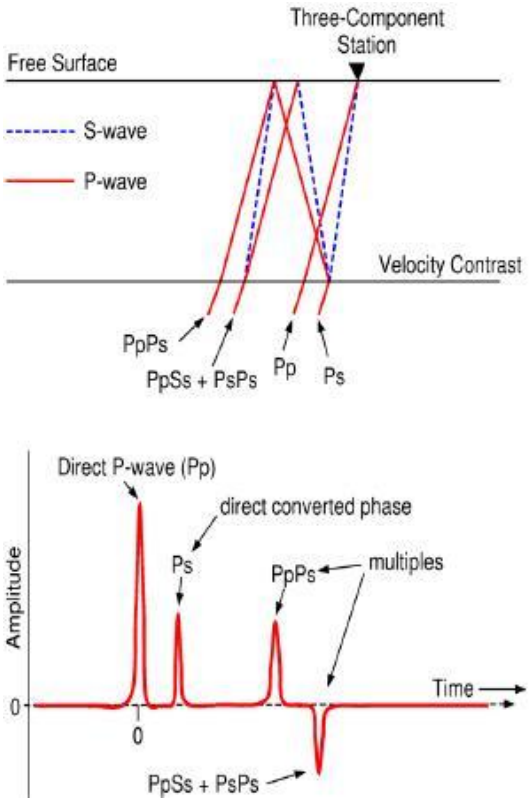

Figure 1
Top: Ray diagram (simplified) showing the P-to-S converted phases reverberating in a single layer over a half-space.
Bottom: The corresponding receiver function (From: http://web.wits.ac.za/NR/rdonlyres)

When a linear inverse problem is considered, and it is assumed that the model can be characterized by a finite number of parameters, the following relation holds: $\mathbf{d} = \mathbf{A}\mathbf{m} + \mathbf{e}$. Here, **m** is the model vector (containing the finite number of model parameters), **d** is the data vector containing the observed data and **A** represents a matrix that relates the data to the model through the product **Am**. To account for the errors **e** that contaminate the data in reality, the term **e** is added. The observed data is used to make an estimation of the model. In practice, this estimated model differs from the true model. Therefore, $\tilde{\mathbf{m}}$ is often used to denote the estimated model, and **m** to denote the true model. To estimate a model, it is often tried to find the model $\tilde{\mathbf{m}}$ that minimizes the difference, measured by the L_2-norm, between the data vector **d** and the recalculated data $\mathbf{A}\tilde{\mathbf{m}}$. In other words, search for the model that minimizes the following misfit function:

$S = \|\mathbf{d} - \mathbf{A}\mathbf{m}\|^2$. This model is the least-squares solution. Other measurements than the L_2-norm for minimizing the difference are also possible. However, for the iterative linearized least-squares inversion performed in this study the L_2-norm will be used.
However, all of the above is described for linear inverse problems. When dealing with non-linear inverse problems, as is the case in this study, the estimation problem is considerably complicated by the non-linearity. However, non-linearity not only affects the estimation problem, it also affects the so-called appraisal problem. The latter deals with the relation between the estimated model $\tilde{\mathbf{m}}$ and the true model **m**. So, non-linear inverse problems are much more difficult to solve. This and more detailed information on inverse problems can be found in e.g. *Snieder and Trampert (1999)* or *Stein and Wysession (2003)*.

To put constraints on the crustal and upper-mantle structure, seismologists have often made use of the sensitivity of surface wave dispersion observations and teleseismic P-wave receiver functions to the shear velocity structure of the medium.

Receiver functions can be computed from three-component seismograms. As described clearly in *Ammon et al. (1990)*, the receiver functions are dominated by P-to-S converted phases. These waves reverberate in the structure beneath the seismometer. This situation is shown in the simplified ray diagram of figure 1 (top). Figure 1 (bottom) shows the actual receiver function, corresponding to the model of figure 1 (top).
By modelling the timing and amplitude of those reverberating waves, important constraints are provided on the underlying Earth structure.

The characteristics of a teleseismic P wave limit the information contained in a receiver function and hence, are worth recapitulating. A teleseismic P-wave has a steep angle of incidence, indicated by the relatively large horizontal phase velocity. A plane wave approximation can be used due to the fact that this relative large horizontal phase velocity (of about 15-25 km/s), is also constant. As a consequence of the steep angle of incidence, the particle motion is polarized, resulting in P-waves dominating the vertical component (and shear waves that are preferentially recorded on the horizontal components). A second effect of the steep angle of incidence is that at horizontal interfaces, the reflection and conversion coefficients are small for the direct and reverberating phases. Consequently, these phases are easily contaminated by scattering from a more complicated Earth structure.

In single-station studies, it is often assumed that the velocity structure is laterally homogeneous and horizontal (or slightly dipping). Whether this assumption is valid or not, depends on the frequency content of the signal and the lateral extent of the sampled structure.
Roughly speaking, the lateral extent of the area that is sampled by the P-waveform is equal to the depth of the deepest reflecting interface. In this study, the deepest reflecting interface is the Moho, set at a depth of 35 km. So, the lateral area sampled has a radius of roughly 35 km.
The lateral homogeneous assumption often does not hold for high-frequency data, because high-frequency waveforms (which have short periods) are more sensitive to the effects of small-scale structure (which often results in sensitivity to the effects of a more complicated structure).
As shown by *Kennett (1986)*, a useful view of complicated velocity heterogeneity in the Earth, is lateral heterogeneity superimposed on a vertically varying velocity structure. So, for modelling complicated velocity heterogeneity in the Earth, determination of the vertical component of velocity variation is essential. In this study, the retrieved shear wave velocity structure shows how the shear wave velocity changes with depth (i.e. the vertical component of the velocity variation is determined).

Both the amplitudes of the arrivals in a receiver function and their timing depend on the incidence angle of the impinging P-wave (ray parameter). In addition, the amplitude depends on the size of the velocity contrasts that generate the conversions (Ps) and multiples. Furthermore, the arrival times are determined by the depth of the velocity contrast and the P- and S-velocity between the contrast and the surface.

Lots of different information can be retrieved from teleseismic P waveforms, for example: information related to the source time history, the source orientation, the near-source structure, the propagation effects and the near-receiver structure. For receiver function studies, the near-receiver structure effects must be isolated from the source and distant structure effects. Then, detailed modelling of the first 20-30 s of the waveform provides constraints on the local velocity structure beneath the receiver.
When three-component data is used, the arrivals generated by the vertical component of the velocity structure can be separated from the total wavefield (as described by *Zandt et al., 1988* and *Owens et al., 1989*). Furthermore, when this response of the vertically varying velocity structure is isolated from the lateral heterogeneity effects, the source information on the three components can be applied to equalize the source and near-source structure effects and to isolate the receiver structure effects on the waveforms. This procedure of source equalization was developed by

Langston (1979). In fact, it is a deconvolution of the vertical component from the horizontal components of ground motion. The result is a time series which is dominated by local structure effects: the receiver function. The deconvolution itself is performed in the frequency domain. For a comprehensive discussion on deconvolution methods, the reader is referred to *Oldenburg (1981)*. *Langston (1979)* used a deconvolution with a water-level stabilization method and a low-pass Gaussian filter. The Gaussian filter was added in order to remove the high-frequency noise that was not filtered by the water-level. This will be discussed in more detail in the section *'Methods'*. Further details about the source equalization procedure can be found in *Langston (1979)*.

Receiver functions are primarily sensitive to the shear wave velocity contrasts of interfaces in the medium, and the vertical traveltimes (relative traveltime of the converted waves reverberated between those interfaces). So, the receiver functions contain very little absolute-velocity information. This may cause an apparent depth-velocity trade-off, which is a problem when interpreting the data (as described by *Ammon et al., 1990*). For example, the same average differential time can be produced by both a slow, thin layer and a fast, thick layer (*Özalaybey et al., 1997*). In other words, the solutions of the inverse problem are non-unique. Non-uniqueness is, as the word already suggests, the problem that properties of an Earth model can be varied without the consequence of worsening the fit to the observed data. As mentioned before, the results of the source equalization procedure are horizontal receiver functions (radial and tangential components). Bear in mind that because P-to-S converted phases dominate the horizontal components, the receiver functions are most sensitive to the shear velocity structure beneath the station *(Owens, 1984, Özalaybey et al., 1997)*.

Obtaining shear wave velocities, instead of compressional wave velocities, has some benefits. Shear waves travel at shorter wavelengths than compressional waves for a given frequency, because of the lower velocity values for shear waves compared with the values for compressional waves ($\lambda=v/f$, with wavelength λ, velocity v and frequency f). Due to this travelling of shear waves at shorter wavelengths, higher resolution is obtained *(Owens, 1987, Özalaybey et al., 1997)*. Another beneficial property of shear waves is that they display stronger anomalies for e.g. the presence of seismic anisotropy, fluids and fractures in crustal rocks and so on, than compressional waveforms do (*Özalaybey et al., 1997)*.

Besides the non-uniqueness problem, the receiver function inverse problem is known to be highly non-linear. *Ammon et al. (1990)*, performed several synthetic tests. Their results clearly showed that the final models were dependent on the initial models. Nevertheless, the inverse problem is often tackled using a linearized inversion. This, due to the simplicity of implementation of the associated

forward problem (*Harland et al., 2009*). Other methods to deal with the non-uniqueness and non-linearity of this inverse problem were also developed. For example, *Zhu and Kanamori (2000)*, describe a simple 2D grid search, using a minimal model which consists of a single layer over a half-space. With this method, they focus on the Moho depth variations. Due to its simplicity, the method is widely applied. However, when more intra-crustal detail is demanded, this approach is not suitable.

Another alternative for the linearized inversion is the Monte Carlo-search. The main advantage of this global optimization technique is that by using a Monte Carlo-search, solutions trapped in local minima of the objective function are avoided. *Shibutani et al. (1996)* used genetic algorithm inversion in order to tackle the non-uniqueness and non-linearity of the receiver function inverse problem.

In this study, both a Monte Carlo-search and an iterative linearized least-squares inversion are applied to the inverse problem.

Besides teleseismic P-wave receiver functions, surface wave dispersion observations are also sensitive to the shear velocity structure of the medium. In contrast to the receiver functions, which are (as discussed before) primarily sensitive to the shear wave velocity contrasts of interfaces in the medium and to the vertical traveltimes, surface wave dispersion measurements are sensitive to vertical shear wave velocity averages (absolute).

Surface waves are large, longer period waves that arrive after the P- and S-waves in the seismogram. Their energy is concentrated near the Earth's surface. Two main types of surface waves are Rayleigh waves and Love waves. Love waves consist of SH-motions, whereas Rayleigh waves are a combination of P- and SV-motions. Surface waves have an important property: dispersion. Dispersive waves of different frequencies propagate at different speeds. Looking at this property in another way, it can be stated that the surface wave velocities vary, depending on the depth range sampled by each period. Longer period waves sample more of the velocity in the underlying half-space. This is a valuable property for studying the Earth's structure. Important to note is that the sensitivity of local isotropic phase (or group) velocity to a perturbation in shear wave velocity at a certain depth is described by sensitivity kernels.

Figure 2a and b show some sensitivity kernels for the phase- and group velocity at various periods, respectively. To construct the kernels, the model PREM was used in which the ocean was replaced by a sedimentary layer. As is visible, each period has a maximum sensitivity at a certain depth, but is also sensitive at other depths. Thus, the sensitivity varies over a depth range.

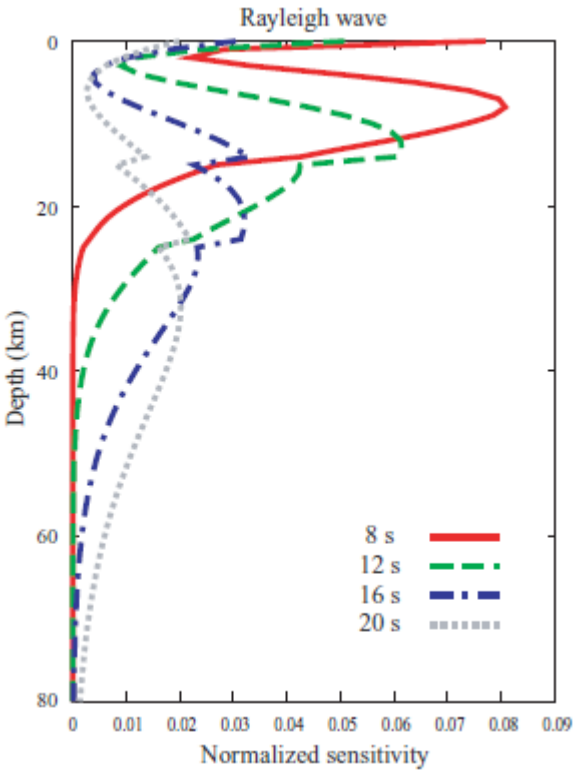

Figure 2a: Sensitivity kernels for the Rayleigh wave phase velocity at periods of 8-,12-,16- and 20-s, calculated with the 1-D PREM model in which the ocean is replaced by a sedimentary layer. From: Lin et al., 2008

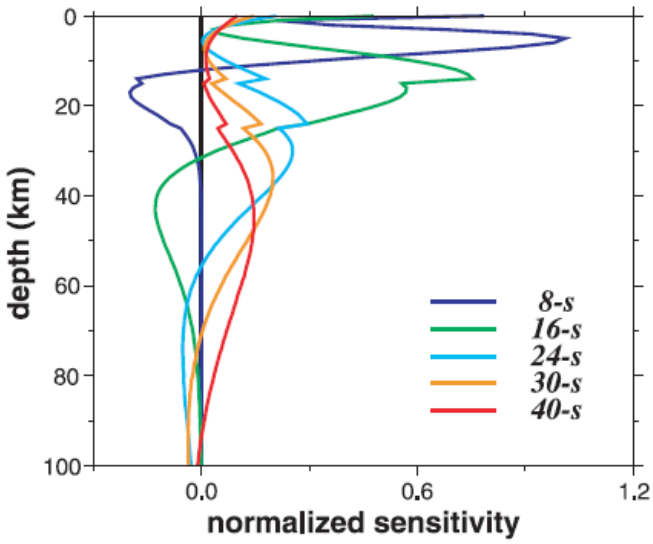

Figure 2b: Sensitivity kernels for the Rayleigh wave group velocity at periods of 8-,16-,24-,30- and 40-s, calculated with the 1-D PREM model in which the ocean is replaced by a sedimentary layer. From: Moschetti et al., 2007

When comparing the sensitivity kernels for the Rayleigh wave phase velocity with the sensitivity kernels for the Rayleigh wave group velocity, it is clearly visible that the group velocity is more sensitive to the shallower shear wave velocity structure. For example, the 12 s phase velocity kernel of figure 2a corresponds closely with the 16 s group velocity kernel of figure 2b (the green lines). In general, longer period data is sensitive to deeper parts of the shear wave velocity structure. As can be clearly seen, the 16 s group velocity kernel shows sensitivities similar to the 12 s phase velocity kernel. In this way, a group velocity at a period of 12 s is sensitive to a shallower structure than a phase velocity at a period of 12 s, i.e. group velocity data are more sensitive to the shallower shear wave velocity structure.

The dispersion of Love waves depends on the shear velocity, whereas the dispersion of Rayleigh waves depends on both the compressional and the shear velocities. Two types of dispersion measurements can be distinguished: phase velocity dispersion measurements and group velocity

dispersion measurements. Further details about dispersion can be found in e.g. *Stein and Wysession (2003)* and *Aki and Richards (2002).*

In this study, fundamental mode Rayleigh wave phase velocity measurements are used. These fundamental mode Rayleigh waves (considering moving from left to right) have particle motions, that can be described by an elliptical, retrograde (counterclockwise) motion. As an extension of this study, the possibility of using fundamental mode Rayleigh wave group velocity measurements as well in the joint inversion will be investigated.

So, both surface wave dispersion observations and teleseismic P-wave receiver functions can provide information about the shear velocity structure of the medium. The main problem is that both types of datasets have their own limitations in resolution. The next step is therefore to combine the two.

By doing a joint interpretation of surface wave dispersion data and teleseismic P-wave receiver functions, the resolution gaps may be bridged (which leads to tighter constraints on the shear velocity structure). Furthermore, by matching two independent data sets simultaneously, the likelihood of overinterpretation is reduced. In order to combine the two, receiver functions and surface wave dispersion curves are jointly inverted.

The main purpose of this study is to investigate how well the joint inversion method works. The focus lies on obtaining the methods that yield the best resolution. In contrast to studies done by e.g. Julià et al (2000), it is attempted to put less constraints on parameters dealing with smoothness. In relation to this, the number of layers which will be used in the modelling, will be reduced significantly.

The study is a theoretical one, using synthetic seismograms. First of all, forward modelling is used to calculate the surface waves and Ps converted waves for a given structure.

Then, the inverse problem is considered: can the structure be retrieved from the surface waves and Ps-converted waves, using a joint inversion of surface wave dispersion data and Ps-receiver functions, and how well?

Methods

As already mentioned in the introduction, the joint inversion of surface wave dispersion data and Ps-receiver functions was based upon fundamental mode Rayleigh wave phase velocity measurements and teleseismic P-wave receiver functions. To solve the joint inverse problem, two different solution techniques were investigated. Specific points that were addressed are:

- What a priori information is needed?
- What role does the parameterization play?
- What adaptations can be made to the inversion procedure, and what are the consequences for the structural model?
- Investigate both noise-free synthetic data and synthetic data with simulated noise.
- Investigate both the use of phase and group velocity dispersion curves, in combination with receiver function data.

Monte Carlo-search

First of all, a Monte Carlo-search was performed. This, in order to get a first idea of how well the joint inversion approach works, and what influence the different parameters and uncertainty constraints have on the results of the Monte Carlo-search. As pointed out before, the study performed is purely theoretical and made use of synthetic data solely. This data was created in a forward modelling step. An uncertainty was assigned to this synthetic data, in order to simulate the presence of noise.

The general idea of the Monte Carlo-search was as follows. A certain reference model was randomly perturbed by the program to create a new model: V_s was changed, and by keeping the V_p/V_s ratio constant (i.e. the V_p/V_s ratio of the reference model), V_p was changed as well. Subsequently, it was checked whether the model (i.e. the corresponding calculated phase velocity curve) matched the phase velocity data (the 'true' data) within the uncertainties for all frequencies of the phase velocity curve, or not. If so, then the receiver functions of the accepted phase velocity models were checked. If these receiver functions also lay within the uncertainties of the 'true' receiver function, then the corresponding model was kept, as well as the phase velocity curve and the receiver function. In this way, a whole range of accepted models was derived, which indicated the possible shear wave velocity structures.

When in addition to the phase velocity dispersion data and the receiver function data also group velocity dispersion data was used, the concept of the Monte Carlo-search remained the same (it only introduced an additional constraint in the Monte Carlo-search).

The Monte Carlo-searches performed in this study had in general a total number of 16000 random models. However, in some cases the total number of random models was changed in such a way that sufficient accepted models (which gave a clear result) were obtained.

As mentioned before, creating the phase velocity data, group velocity data and receiver function data was done in a forward modelling step. For this step, several programs were used.

For the surface waves, the program 'rayleigh' (*Nolet, 2008*) was used (in a slightly adapted form). The program computes eigenfunctions and phase and group velocities of Rayleigh waves in spherical (1D) Earth models. From the output, tables with periods and phase velocities and periods and group velocities could be extracted, representing the dispersion data.

For computing the receiver function data, two programs were used: 'respknt' and 'pwaveqn'.

These are programs of a program package developed mainly and described by *Ammon (1997)*. In the Monte Carlo-search, first the program 'respknt' is called and after that the program 'pwaveqn'. 'Respknt' computes body-wave responses of the structure; i.e. in the case of this study, the response of the structure to an incident teleseismic P-wave. George Randall has written this program, which is based on the approach of Kennett (1983), to compute the seismic response of a cylindrically symmetric medium by using the reflectivity approach. By running 'respknt', SAC files are generated, which represent the response to the incoming plane wave (not the receiver functions). As already mentioned in the introduction, in order to calculate the receiver functions, the source equalization procedure needs to be applied on these files (*Langston, 1979*). This is performed by the program 'pwaveqn'. *Langston's (1979)* source equalization procedure tries to remove the effects of near-source structure and source time functions as good as possible. The procedure involves a frequency-domain deconvolution. If ω represents the angular frequency ($\omega = 2\pi f$), Z(ω) the Fourier transform of the vertical component of motion, R(ω) the Fourier transform of the radial component of motion, then E_R(ω), the Fourier transform of the radial receiver function, is defined by:

$E\_R(\omega) = \frac{R(\omega)Z*(\omega)}{Z(\omega)Z*(\omega)}$ where $Z*(\omega)$ is the complex conjugate of Z(ω). Similarly, an equation can be written for the tangential component of motion, which then defines the tangential receiver function. To remove high-frequency noise, *Langston (1979)* introduced a low-pass Gaussian filter G(ω), which resulted into the following expression for the Fourier transform of the radial receiver function: $E\_R(\omega) = \frac{G(\omega)R(\omega)Z*(\omega)}{Z(\omega)Z*(\omega)}$. Using a Gaussian as a filter, has several advantages, e.g.: the simple shape of the Gaussian, zero phase distortion and lack of side-lobes. This low-pass filter will be treated in more detail later on in this section. The last equation, which is the definition of a receiver function, cannot be used to compute observed seismograms. This has to do with numerical problems that occur when the term $Z(\omega)Z*(\omega)$ in the denominator, is very small or zero. To avoid this problem,

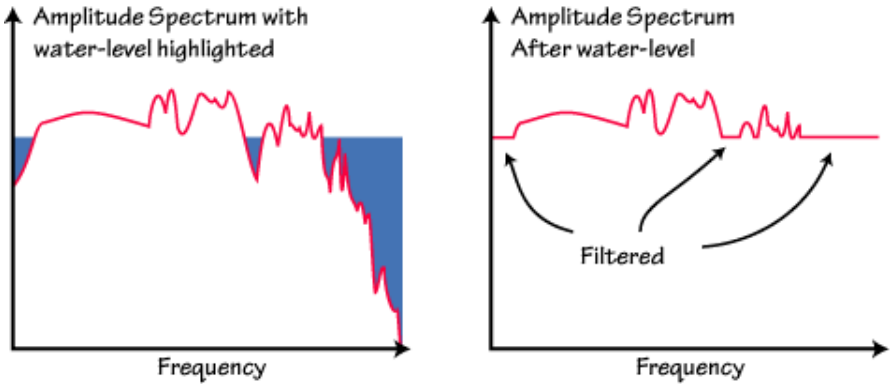

Figure 3: Amplitude spectra for and after water-level deconvolution

several approaches can be used. In the program 'pwaveqn', a so called water-level deconvolution (*Langston, 1979*) is used. In water-level deconvolution, division by small numbers is avoided by replacing these small values in the denominator by values which are a fraction of the maximum value of the denominator. This fraction, which is called the water-level parameter, is the same for all frequencies. The water-level itself is then the fraction (water-level parameter) multiplied with the maximum amplitude of the denominator (see figure 3).

The water-level parameter is determined by trial and error. Using a water-level deconvolution, and hence replacing small values in the denominator by larger values, consequently attenuates the frequencies for which the vertical component has a small amplitude.

The trial and error procedure is used to determine the lowest water-level that produces acceptable noise levels in the receiver function. It is controlled by the signal-to-noise ratio and nature of the vertical component seismogram. Due to the fact that the water-level filter can cause distortions of the receiver function, the smaller the value that you choose for the water-level parameter, the better it is. In this study, a value of 0.0001 for the water-level parameter c is chosen. Important to note is that this value has to be identical for both the 'true' synthetic data modelling step and the synthetic forward modelling step.

As mentioned before, *Langston (1979)* introduced a low-pass Gaussian filter $G(\omega)$ in order to remove high-frequency noise in the receiver functions. The Gaussian filter that is often used can be described by the following expression: $G(\omega) = \exp\left(-\frac{\omega^2}{4a^2}\right)$, where a is the Gaussian filter-width parameter. This parameter controls the frequency content. At ω=0, the filter gain is unity. A nice property of a Gaussian is, that the Fourier transform of it also is a Gaussian.

In this study, a was chosen to be 1.0 in the Monte Carlo-search. This value for the Gaussian filter-width parameter implies that $G(\omega)$has decayed to a value of 0.1 for a frequency of 0.5 Hz. The width of the Gaussian pulse in the time domain is about $\frac{5}{3*\mathrm{sqrt}\,(a)}$ = 1.67 s.

For further details on the programs 'respknt' and 'pwaveqn', the reader is referred to *Ammon (1997)*.

Iterative linearized least-squares inversion

In the second part of this study an iterative linearized least-squares inversion (non-linear inversion) was used to solve the inverse problem.

As already mentioned in the introduction, in this study the L_2-norm is used as a measure for minimizing the difference between the data vector **d** and the recalculated data $\mathbf{A}\tilde{\mathbf{m}}$. The misfit function for a linearized problem is then given by $S = \left\|\mathbf{d} - \mathbf{A}\mathbf{m}\right\|^2$. The model that minimizes this misfit function is the least-squares solution. While in the iterative linearized least-squares inversion of this study normalized residuals are used, the corresponding normalized misfit function (for either the phase velocity data, group velocity data or receiver function data) can be described by:

$S_{normalized} = \sum_{i=1}^{N} \left(\frac{d_i^{observed} - d_i^{theoretical}}{\sigma_i} \right)^2$, where σ_i is the standard deviation of the i[th] data point and *N* is the total number of data points. When working with real data, the standard deviations of the datasets will be used for the normalization of the misfit function. However, in this study only synthetic data is used. Therefore, an uncertainty value of 1% is used for the phase velocity data. Furthermore, a reasonable absolute receiver function uncertainty value of 0.02 was used, to normalize the residual vector of the receiver function. When in addition to the Rayleigh wave phase velocity data and the receiver function data also Rayleigh wave group velocity data was used in the joint inversion, an uncertainty of 2% was utilized for the normalization of the group velocity data. The value of the 'standard deviation' of the phase and group velocity data, used for normalizing the misfit function, was calculated by multiplying the 'true' data with the uncertainties (the percentage values divided by 100) of respectively the phase and group velocity data. For the receiver function data, the standard deviation was equal to the absolute uncertainty value that was chosen.

The total normalized misfit function is then given by:

$S_{total} = w_{recfn} S_{recfn} + w_{phasevel} S_{phasevel} + w_{groupvel} S_{groupvel}$, where *w* accounts for the relative weights of respectively the receiver function misfit, the phase velocity misfit and the group velocity misfit. *S* represents the normalized misfit function ($S_{normalized}$) for respectively the receiver function data, the phase velocity data and the group velocity data.

Both the programs for the phase (and group) velocity curves and for the receiver functions, are called in a 'Matlab'-based main program. This in order to perform the joint-inversion. For the iterative linearized least-squares inversion, the 'Matlab' built-in function 'lsqnonlin' is used with the Levenberg-Marquardt algorithm.

One of the advantages of the iterative linearized least-squares inversion is that it is much faster than the Monte Carlo-search. Several parameters were changed, e.g. the weights of the different residual vectors (phase velocity vs. receiver function), applying damping or not and so on. These different inversion configurations will be thoroughly discussed in the following section ‘Results’.

Results & Discussion

Monte Carlo-search with phase velocity dispersion data and receiver function data

In this section, it will be investigated how well the phase velocity curves and the receiver functions determine the Earth's structure. Focus will lie on the influence of the different parameters and uncertainty constraints on the results of the Monte Carlo-search. As already discussed in the section 'Methods', for calculating the receiver function a trough filter of 0.0001 and a Gaussian scale a of 1.0 will be used. The part of the receiver function considered in this study is from 0 till 25 s.

Three-layered crust over a half-space

In order to do so, first of all a three-layered crustal model (sedimentary layer, upper-crust and lower-crust) over a half-space (mantle) will be considered. The half-space is taken to have a constant (shear wave) velocity until a depth of 210 km.

First of all, the effect of the phase velocity curve on the retrieved structure is investigated. So, no receiver function constraints are taken into account. A reasonable uncertainty (which can be regarded as a simulation of the presence of noise) of 1% in the phase velocity curve for the 'true, measured' data, is considered. Hence, 1% phase velocity curve variations are allowed in the Monte Carlo inversion. Two situations are compared: the case where the phase velocity curve is considered to be determined for the periods from 8 s to 43 s (referred to as the short period phase velocity curve), and the situation where the phase velocity curve is determined for the periods from 13 s to 43 s (referred to as the long period phase velocity curve). This is done because of the fact that shorter periods are in practice more difficult to determine.

Figure 4 shows the phase velocity curves obtained by a Monte Carlo search for an input model with a short period phase velocity curve, which allows uncertainties in the phase velocities of $\pm$ 1% and has no constraints from the receiver functions. Velocity variations of $\pm$ 10% from the 'true' model are allowed for the three crustal layers, whereas the discontinuities are almost fixed at their correct position (discontinuity depth variations of $\pm$ 2% from the 'true' model). Figure 5 represents phase velocity curves for a similar model, except for the period range of the phase velocities. This input model uses phase velocity data in the period range of 13-43 s, which is referred to as long period phase velocity data. So, the only difference between the two input models is the period range of the Rayleigh waves.

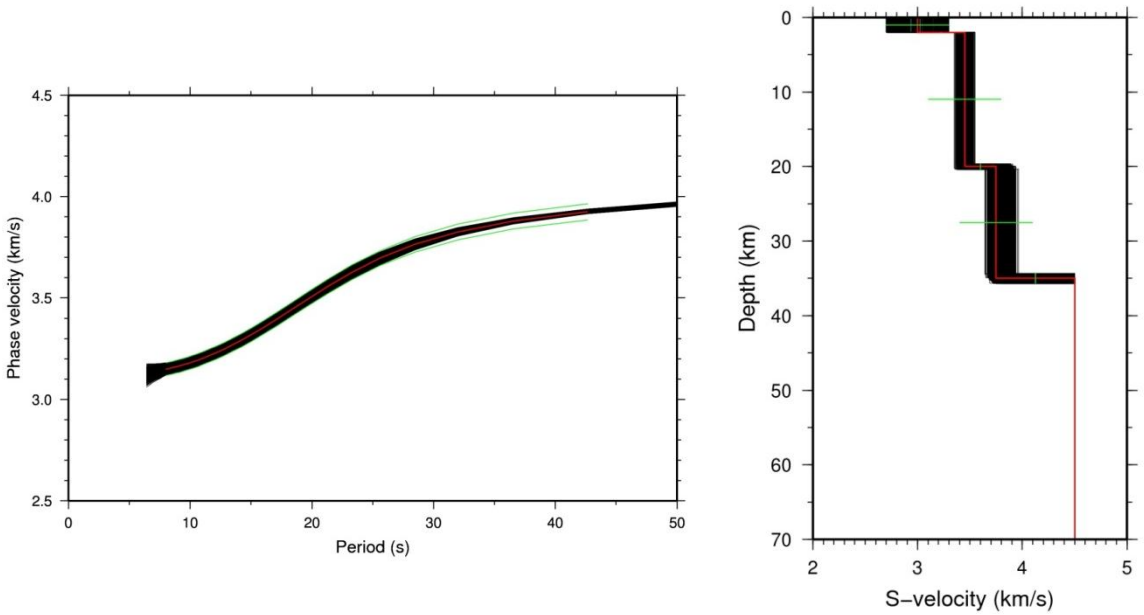

Figure 4: Results of a Monte Carlo-search for an input model with a short period phase velocity curve (8-43 s), uncertainties in the phase velocities of ±1%, no receiver function constraints, velocity variations per layer of ±10% from the 'true' model and discontinuity depth variations of ±2% from the 'true' model.
a) Left: Phase velocity curves obtained. The red line represents the 'real', measured data. The black lines are the phase velocity curves obtained by the Monte Carlo-search (corresponding to accepted models). The green lines indicate the phase velocity bounds (±1%)
b) Right: Obtained shear wave velocity – depth plots of the accepted three-layered crustal models. The red line represents the 'true' model, the horizontal green lines indicate the velocity range per layer (minimum and maximum velocity, specified in the input model) and the vertical green lines show the discontinuity range (minimum and maximum depth of the discontinuity, specified in the input model). The black lines represent the accepted models.

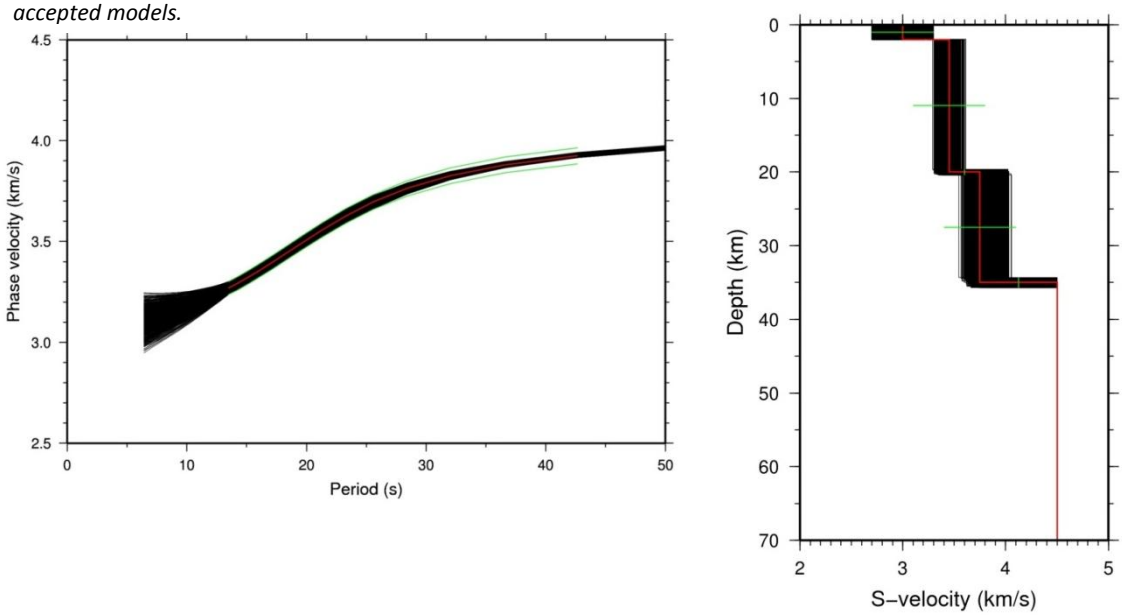

Figure 5: Results of a Monte Carlo-search for an input model with a long period phase velocity curve (13-43 s), uncertainties in the phase velocities of ±1%, no receiver function constraints, velocity variations per layer of ±10% from the 'true' model and discontinuity depth variations of ±2% from the 'true' model.
a) Left: Phase velocity curves obtained. The red line represents the 'real', measured data. The black lines are the phase velocity curves obtained by the Monte Carlo-search (corresponding to accepted models). The green lines indicate the phase velocity bounds (±1%).
b) Right: Obtained shear wave velocity – depth plots of the accepted three-layered crustal models. The red line represents the 'true' model, the horizontal green lines indicate the velocity range per layer (minimum and maximum velocity, specified in the input model) and the vertical green lines show the discontinuity range (minimum and maximum depth of the discontinuity, specified in the input model). The black lines represent the accepted models.

Figures 4b and 5b above, show the shear wave velocity (V_s) - depth plots of the accepted models, as obtained from the Monte Carlo-search. Figure 4b corresponds to the Monte Carlo-search with the input model containing Rayleigh wave periods in the range 8-43 s. Figure 5b is the result of using an input model that contains Rayleigh wave periods in the range 13-43 s.

It can be observed that for both cases models are accepted which have shear wave velocities over the whole 10% velocity range for the first layer. For the deeper layers (second and third), models with a greater velocity range (around the 'true' velocity) are accepted for the input model with Rayleigh wave periods 13-43 s (see figure 5b). This can be explained as follows. A Rayleigh wave with a period of 8 s corresponds to a maximum sensitivity of that wave at a depth of about 8 km (see figure 2a). However, this wave is also sensitive at greater/shallower depths (it is a sensitivity curve). The Rayleigh waves with the period range 8-13 s, are not taken into account in the case of figure 5b. Consequently, less constraint is put on greater depths, resulting in a wider shear wave velocity range for the accepted models.

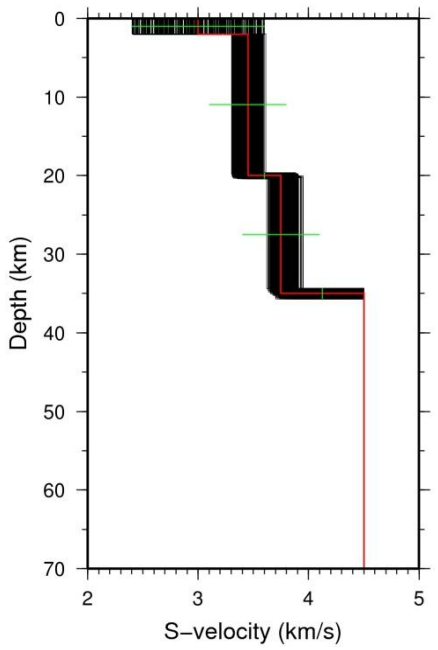

Figure 6: Shear wave velocity – depth plots of the accepted three-layered crustal models, obtained for an input model with a short period phase velocity curve (8-43 s), allowed velocity variations for the first layer of ± 20% and of ± 10% for the other two layers and discontinuity depth variations of ± 2%. Furthermore, this input model allows ± 1% uncertainty in the phase velocities and has no receiver function constraints.
The red line represents the 'true' model, the horizontal green lines indicate the velocity range per layer (minimum and maximum velocity, specified in the input model) and the vertical green lines show the discontinuity range (minimum and maximum depth of the discontinuity, specified in the input model). The black lines represent the accepted models.

As can be observed in the figures above, the obtained range of shear wave velocities for the first layer equals the complete range of allowed velocity variations.

Hence, to investigate the effects of the different parameters and constraints for the first layer more clearly, velocity variations of ± 20% are now allowed in the first layer (sediment layer).

Figure 6 represents the V_s-depth plots obtained for an input model with only phase velocity constraints (±1%), short period phase velocity data, allowed velocity variations for the first layer of ± 20% and of ± 10% for the other two layers and discontinuity depth variations of ± 2%.

When comparing figure 6 with figure 4b, it can be clearly observed that allowing a greater velocity variation in the first layer, results in accepted models with a greater range of shear wave velocities in the first and second layer. The shear wave velocity range for the third layer is shifted more symmetrically around the 'true' model. What can be concluded from this observation, is that the phase velocity

data do not determine the shear wave velocity in the sediment layer. Furthermore, it can be observed that the obtained discontinuity depth range of the accepted models equals the complete range of allowed discontinuity depth variations. To investigate how well the discontinuities are retrieved, an input model will now be considered, which also allows a depth variation of the discontinuity of $\pm$ 10%, instead of $\pm$ 2%. The Rayleigh wave period range of this model is 8-43 s. Logically, by allowing a depth variation of $\pm$ 10%, the depth parameters play a more important role in the Monte Carlo-search. Hence, by varying the depth of the discontinuity over a greater distance from the 'true' model, less models will be accepted, which was indeed observed.

Comparing figure 7 with figure 4b (the input model with $\pm$ 2% discontinuity depth variation), some important similarities and differences can be recognized. It can be observed again, that for both cases models are accepted, which have shear wave velocities over the whole velocity range for the first layer. However, the first discontinuity depth range of the accepted models is slightly greater for the input model of figure 7.

Comparing the second layer for both cases, no significant differences can be observed. However, figure 7 clearly shows a greater shear wave velocity range (models accepted over almost the whole allowed velocity range) for the third layer than in figure 4b. In addition, great differences can be observed looking at the second and third discontinuities. The depth range of these discontinuities is far greater for the accepted models of figure 7. The range of the accepted models equals the total range of the allowed discontinuity variations. So, when the Monte Carlo-search was performed allowing even a greater range of discontinuity variations, probably also a wider range would be observed in the discontinuity depths of the accepted models. This would probably also be the case for the shear wave velocity range of the third layer, when a greater shear wave velocity range was allowed in the Monte Carlo-search. So, the shear wave velocity of the third layer and the discontinuity depths are not very well retrieved when only phase velocity data is taken into account.

Furthermore, in figure 7 an important step-wise pattern can be recognized (at the high velocity side of the second discontinuity and at the low velocity side of the third discontinuity).

This indicates a trade-off between the shear wave velocity and depth: a discontinuity with a shear wave velocity which is lower than the 'true' velocity, is also at a shallower depth. In contrast, a discontinuity with a higher shear wave velocity is at greater depth.

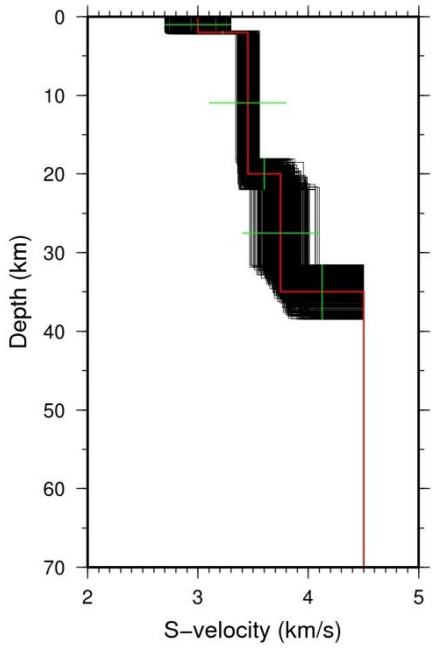

Figure 7: Shear wave velocity – depth plots of the accepted models, obtained from a Monte Carlo-search for an input model which allows discontinuity depth variations of ±10%, as well as crustal velocity variation. The input model has a short period phase velocity curve (8-43 s), allows uncertainties in the phase velocities of 1% and takes no receiver function constraints into account. The red line represents the 'true' model, the horizontal green lines indicate the velocity range per layer (minimum and maximum velocity, specified in the input model) and the vertical green lines show the discontinuity range (minimum and maximum depth of the discontinuity, specified in the input model). The black lines represent the accepted models.

As was concluded above, the phase velocity data solely does not provide enough constraints to retrieve the shear wave velocity structure well enough. Therefore, the receiver function constraints will now also be taken into account in the Monte Carlo-search. The effects of this joint inversion on the retrieved shear wave velocity structure will be thoroughly investigated.

When the receiver function constraints are taken into account as well, with an allowed uncertainty of ± 0.02, the shear wave velocity-depth plots, phase velocity curves and receiver functions of figure 8 are obtained.

Comparing figure 8b with figure 4, it can be observed that for figure 8b the model phase velocity curves are closer to the 'real' phase velocity curve. In other words, tighter constraints result in phase velocity curves that are closer to the 'real' phase velocity curve. This phenomenon can be observed most clearly at the longer periods (T > 20 s).

Next, examining figure 8a more closely, a decrease in the range of the shear wave velocities, with respect to figure 4b, can be observed for all three layers. Thus, the shear wave velocities obtained for the different models are much closer to the 'true' model when the receiver function constraint is taken into account. All the receiver functions corresponding to the models kept are shown in black in figure 8c. These models have met all the constraints of the two datasets (phase velocity dispersion data and receiver function data). As is visible in figure 8c, all the black lines lie perfectly in-between the green lines, which indicate the set uncertainty value.

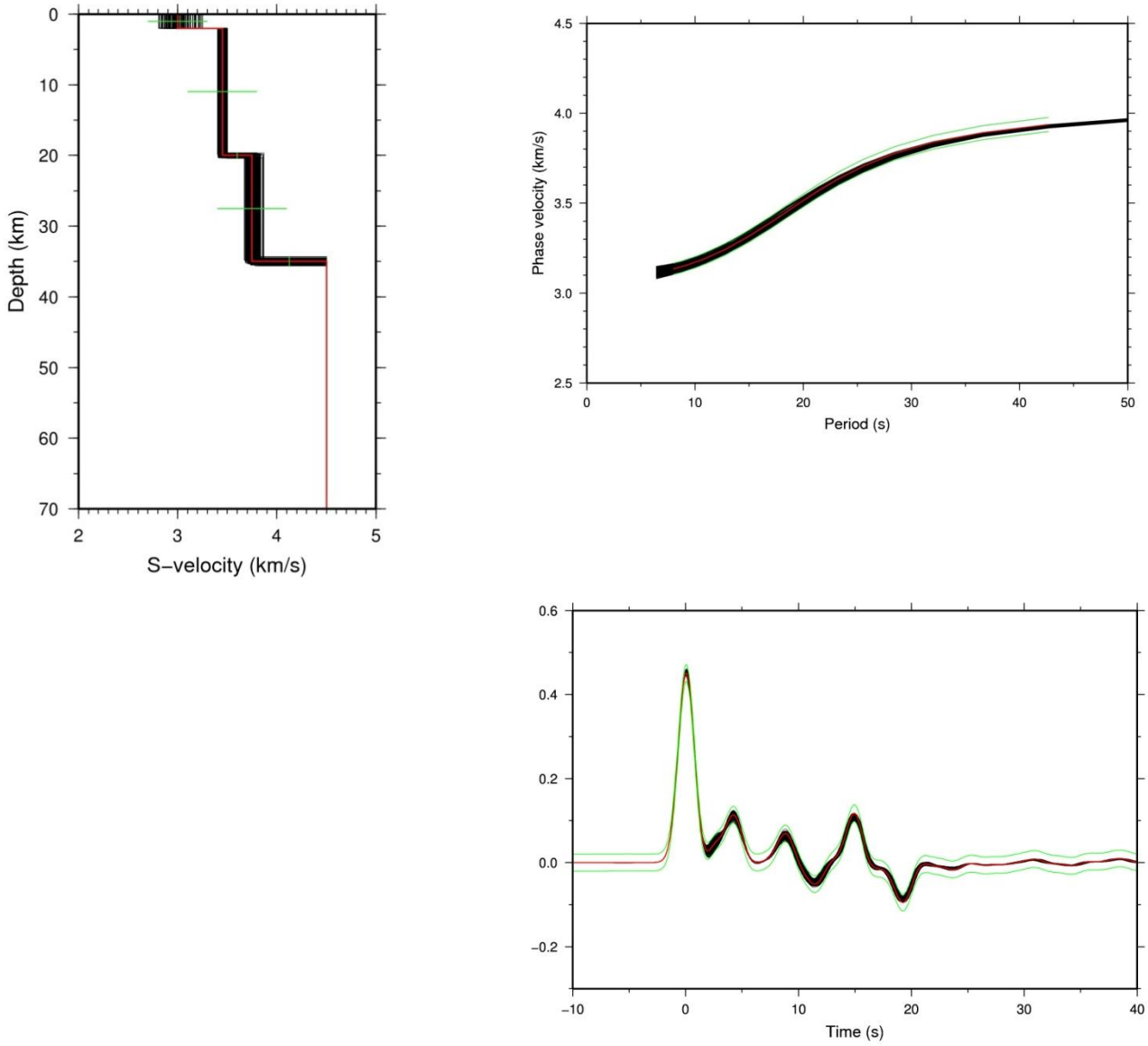

Figure 8: Results of a Monte Carlo-search for an input model with a short period phase velocity curve (8-43 s), uncertainties in the phase velocities of ±1%, an absolute receiver function uncertainty range of ±0.02 , velocity variations per layer of ± 10% from the 'true' model and discontinuity depth variations of ±2% from the 'true' model.

- *a) Left: Shear wave velocity – depth plots of the accepted three-layered crustal models. The red line represents the 'true' model, the horizontal green lines indicate the velocity range per layer (minimum and maximum velocity, specified in the input model) and the vertical green lines show the discontinuity range (minimum and maximum depth of the discontinuity, specified in the input model). The black lines represent the accepted models.*
- *b) Right: Phase velocity curves obtained. The red line represents the 'real', measured data. The black lines are the phase velocity curves obtained by the Monte Carlo-search (corresponding to accepted models). The green lines indicate the phase velocity bounds (±1%)*
- *c) Below: Receiver functions obtained. Again, the red line represents the true model, the green lines represent the absolute value uncertainty set, and the black lines are all the receiver functions corresponding to the models kept (which meet all the constraints of the Monte Carlo-search)*

.

The previous results of the Monte Carlo-search have shown the beneficial effects of adding the receiver function constraints to the inversion on the obtained shear wave velocity structure. However, due to the fact that the allowed discontinuity depth variations in the Monte Carlo-search were set to ± 2% (and again models were accepted covering this whole range), no clear conclusions could be drawn with respect to possible improvement of the retrieved discontinuity depths. To investigate this possible improvement of the retrieved discontinuity depths further (among other possible effects of adding receiver function constraints), now a joint inversion of long period phase velocity data (13-43 s) with receiver function data will be considered, whereby discontinuity depth variations of ± 10% are allowed. The results of this joint inversion will be compared with an inversion that uses only long period phase velocity data. Figure 9a below shows the phase velocity curves obtained for an input model with a long period phase velocity curve (13-43 s), velocity variations per layer of ± 10%, a discontinuity depth range of ± 10%, 1% uncertainty in the phase velocities and receiver function bounds of ± 0.02. Figure 10a represents the phase velocity curves obtained for the same input model, except that receiver function constraint is not taken into account. When comparing these two figures, it can be seen that the phase

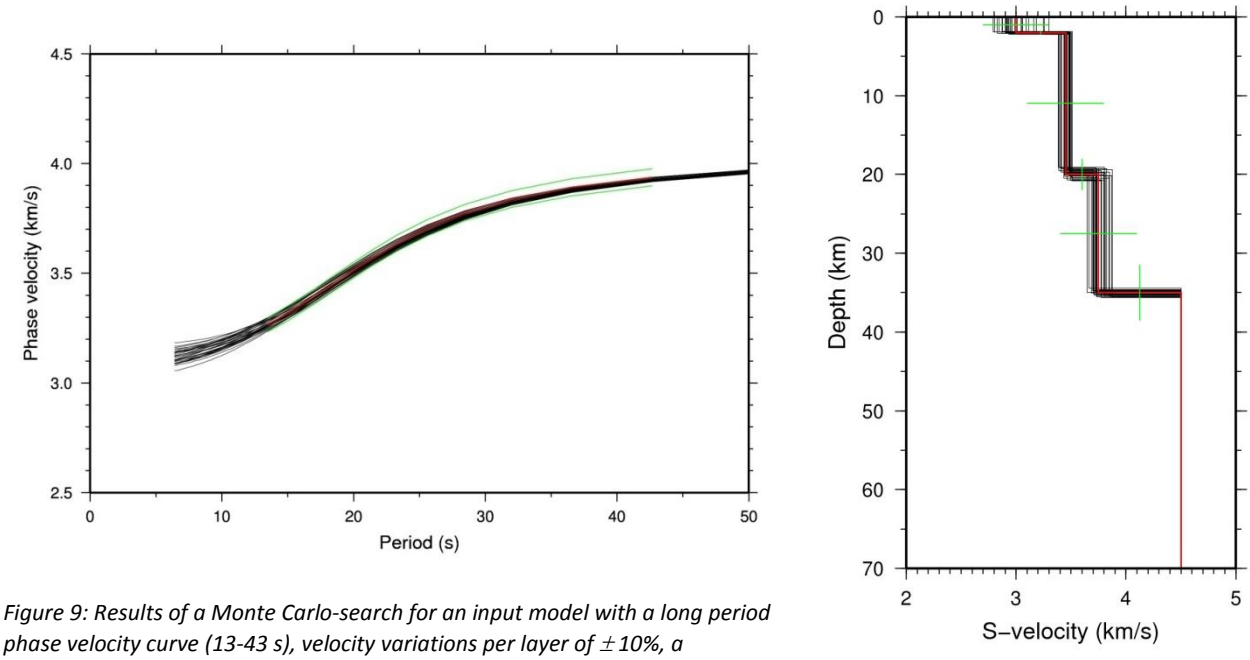

Figure 9: Results of a Monte Carlo-search for an input model with a long period phase velocity curve (13-43 s), velocity variations per layer of ± 10%, a discontinuity depth range of ± 10%, 1% uncertainty in the phase velocities and receiver function bounds of ± 0.02.
a) Left: Phase velocity curves obtained. The red line represents the 'real', measured data. The black lines are the phase velocity curves obtained by the Monte Carlo-search (corresponding to accepted models). The green lines indicate the phase velocity bounds (± 1%).
b) Right: Obtained shear wave velocity – depth plots of the accepted three-layered crustal models. The red line represents the 'true' model, the horizontal green lines indicate the velocity range per layer (minimum and maximum velocity, specified in the input model) and the vertical green lines show the discontinuity range (minimum and maximum depth of the discontinuity, specified in the input model). The black lines represent the accepted models.

velocity curves of the accepted models are more close to the 'real' data for the case with the receiver function constraint taken into account. This effect is very nicely visible in the period range of 8-13 s. Where figure 10a shows curves in that range that are not based upon either phase velocity or receiver function uncertainty constraints, figure 9a shows curves that are more close to the 'real' data in that range. So, despite a missing phase velocity uncertainty constraint in that range, the considered receiver function constraints have a significant effect on the range of the phase velocity curves.

Figures 9b and 10b represent the shear wave velocity-depth plots obtained for the same input model

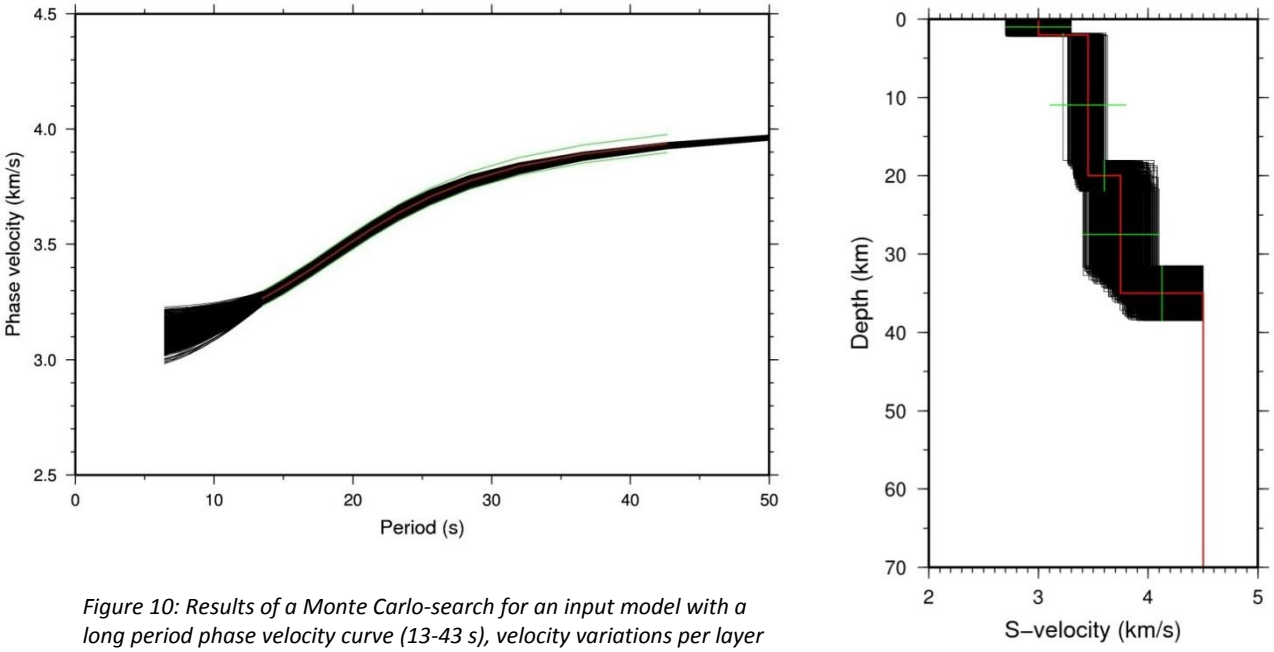

Figure 10: Results of a Monte Carlo-search for an input model with a long period phase velocity curve (13-43 s), velocity variations per layer of ±10%, a discontinuity depth range of ±10%, 1% uncertainty in the phase velocities and no receiver function constraints.
a) Left: Phase velocity curves obtained. The red line represents the 'real', measured data. The black lines are the phase velocity curves obtained by the Monte Carlo-search (corresponding to accepted models). The green lines indicate the phase velocity bounds (±1%).
b) Right: Obtained shear wave velocity – depth plots of the accepted three-layered crustal models. The red line represents the 'true' model, the horizontal green lines indicate the velocity range per layer (minimum and maximum velocity, specified in the input model) and the vertical green lines show the discontinuity range (minimum and maximum depth of the discontinuity, specified in the input model). The black lines represent the accepted models.

configuration that resulted in figures 9a and 10a.

As can be clearly observed, by taking the receiver function constraint into account, the range in accepted shear wave velocities is decreased significantly, especially for the second and third layer). In addition, the range in discontinuity depths is much smaller: in figure 10b, models over the whole allowed depth range for the discontinuities are accepted, whereas figure 9b only shows accepted models with discontinuities at depths close to the 'true' model. Nevertheless, the shear wave velocity in the sedimentary layer is still not determined very well by using a combination of phase velocity data and receiver functions (a very small improvement is however visible). So, performing a joint-inversion of

long period phase velocity dispersion data and receiver function data has significant beneficial effects on the retrieved shear wave velocity structure.

The results presented above were obtained using a joint inversion of long period (13-43 s) phase velocity data and receiver function data. Now, it will be investigated what further positive effects a joint inversion of short period phase velocity data (8-43 s) and receiver function data has on the retrieved shear wave velocity structure. In order to do so, a Monte Carlo-search is performed using the same input model as for figure 9b, but now with a short period phase velocity curve (8-43 s). This results in the V_s-depth plots shown in figure 11 below. Comparing this figure with figure 10b, it can be recognized that (as already observed before in figures 4b and 5b), by taking the short period phase velocities into account (and hence uncertainty constraints in that range), the range of shear wave velocities of the accepted models is reduced further. This is now not only visible in the second and third layers but also slightly in the first layer. Also, a small decrease in discontinuity depth variation (second and third discontinuity) can be observed.

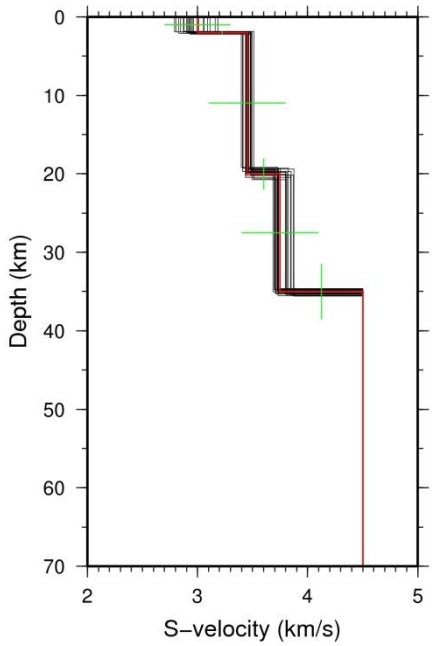

Figure 11: Shear wave velocity – depth plots of the accepted models, obtained from a Monte Carlo-search for an input with a short period phase velocity curve (8-43 s), velocity variations per layer of ±10%, a discontinuity depth range of ±10%, 1% uncertainty in the phase velocities and receiver function bounds of ±0.02. The red line represents the 'true' model, the horizontal green lines indicate the velocity range per layer (minimum and maximum velocity, specified in the input model) and the vertical green lines show the discontinuity range (minimum and maximum depth of the discontinuity, specified in the input model). The black lines represent the accepted models.

Until now, the receiver function constraint has only been applied in combination with the phase velocity constraint. To get a better insight in the effects of the receiver function data on the retrieved shear wave velocity structure, a Monte Carlo-search with only receiver function constraints will be performed (so, no phase velocity constraints will be taken into account). An input model with receiver function bounds of ± 0.02 and allowed velocity and discontinuity depth variations of ± 10% is considered. Figures 12a and 12b show respectively the receiver functions and V_s-depth plots obtained.

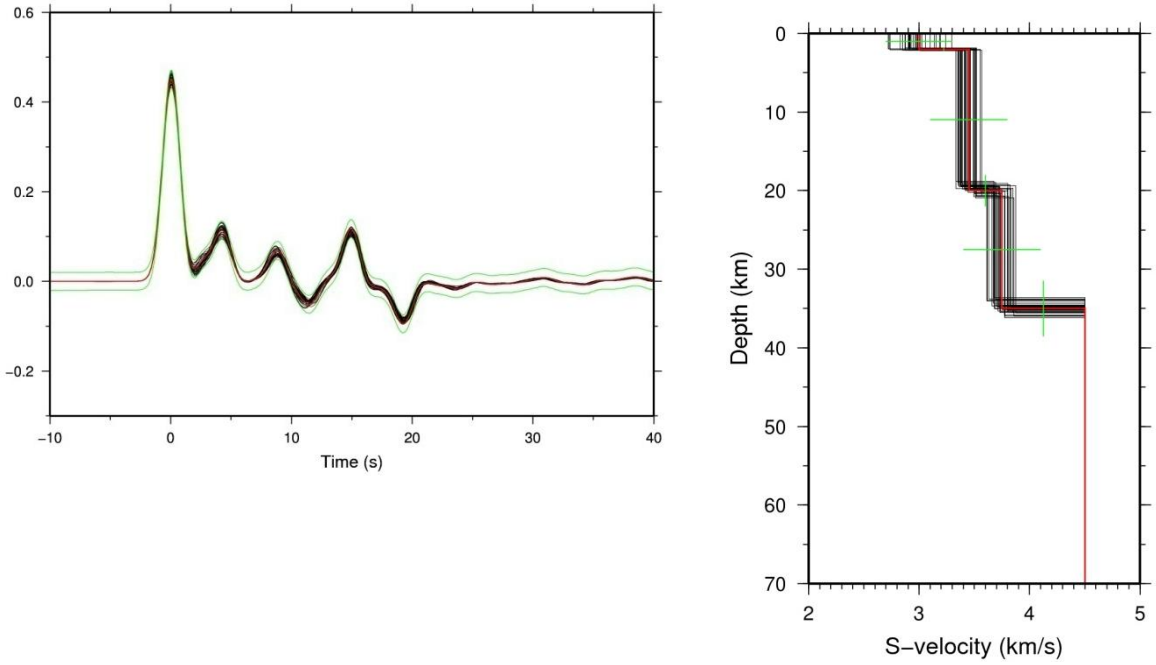

Figure 12: Results of a Monte Carlo-search for an input model that has only receiver function constraints with an uncertainty set at ±0.02. The allowed velocity and discontinuity depth variations are ±10%.
a) Left: Receiver functions obtained. The red line represents the true model, the green lines represent the absolute value uncertainty set, and the black lines are all the receiver functions corresponding to the models kept.
b) Right: Obtained shear wave velocity – depth plots of the accepted three-layered crustal models. The red line represents the 'true' model, the horizontal green lines indicate the velocity range per layer (minimum and maximum velocity, specified in the input model) and the vertical green lines show the discontinuity range (minimum and maximum depth of the discontinuity, specified in the input model). The black lines represent the accepted models.

Figure 12b shows that, despite the fact that only receiver function constraints are taken into account, the range in obtained shear wave velocities is quite restricted. The depth of the first discontinuity is also obtained accurately. Additionally, the depth ranges of the second and third are limited as well. However, the step-wise pattern visible around the second and third discontinuity indicates a velocity-depth trade-off (as discussed before in this section): a discontinuity with a shear wave velocity which is lower than the 'true' velocity, is also at a shallower depth. This is an example of the non-uniqueness problem of the receiver function inversion: the same average differential arrival time can be produced by either a slow, thin layer or a fast, thick layer. As visible, models which have roughly the same receiver function data fit (i.e. all lie in between the uncertainty bounds set, as visible in figure 8), produce final shear wave velocity models with differing velocities.

When comparing this figure 12b with figure 11, the beneficial effects on the shear wave velocity ranges and on the discontinuity depth ranges, of using both phase velocity constraints and receiver function constraints, can be observed clearly. Furthermore, the step-wise pattern indicating the velocity-depth trade-off is almost completely removed in figure 11. This is a clear indication that the

receiver function non-uniqueness problem can be addressed by combining receiver function data with surface wave dispersion data in a joint inversion, as already mentioned in the 'Introduction'.

Three-layered crust over a varying mantle

Until now, the mantle was assumed to have a constant shear wave velocity of 4.5 km/s until a depth of 210 km. Next, it will be investigated what the consequences are for the retrieved structure, when besides the crustal velocity also the mantle velocity is varied. In other words, what effects (positive or negative) the introduction of another velocity parameter has on the retrieved shear wave velocity structure.

To investigate these effects, a Monte Carlo-search was performed for an input model with short

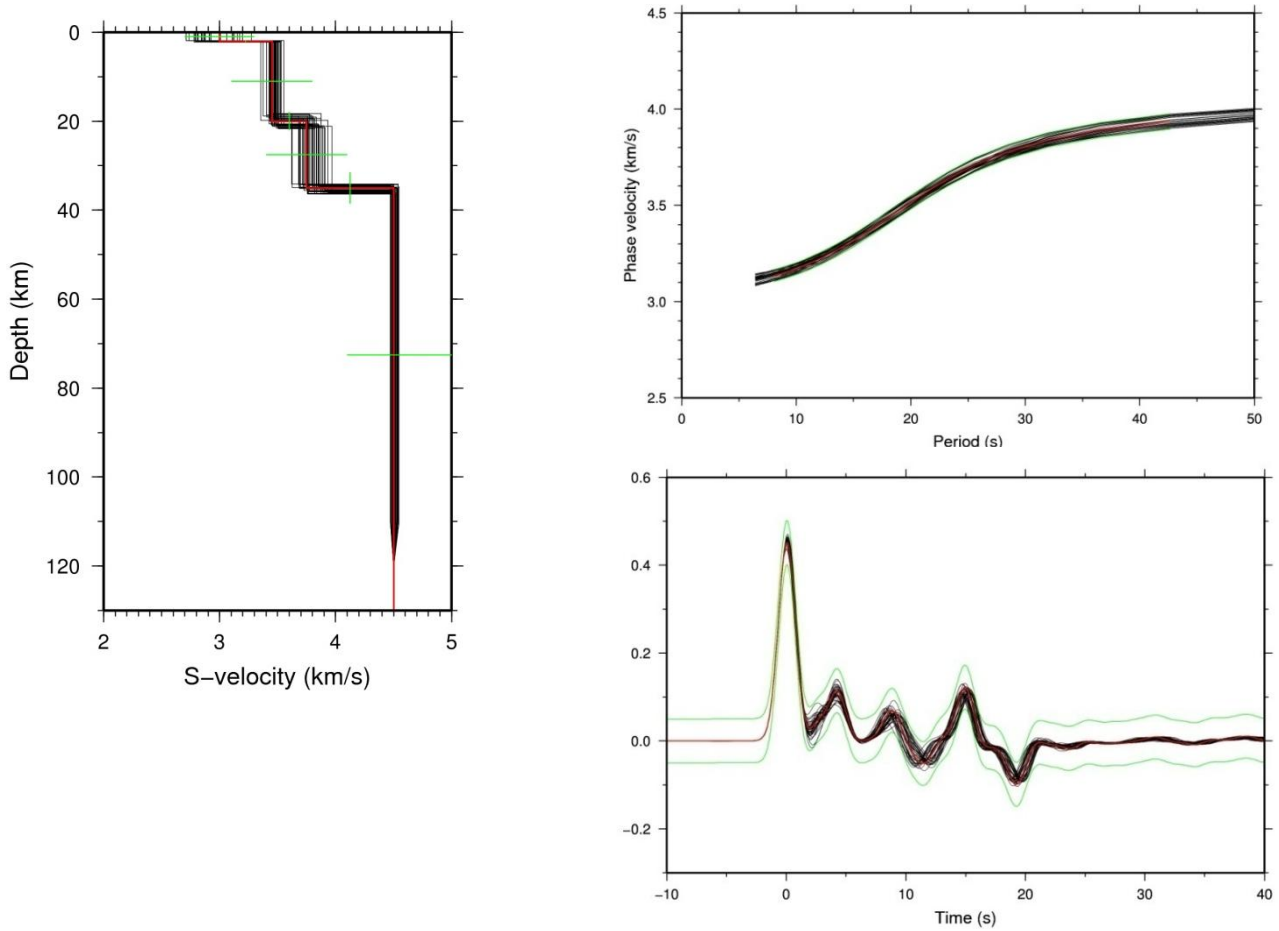

Figure 13: Results of a Monte Carlo-search for an input model with short period phase velocity data (8-43 s), allowed velocity variations of ± 10% (also the mantle velocity is changed), allowed discontinuity depth variations of ± 10%, 1% uncertainty in the phase velocities and receiver function bounds of ±0.05.
a) Top-left: Obtained shear wave velocity-depth profiles of the accepted three-layered crustal models over a varying mantle. The red line represents the 'true' model, the horizontal green lines indicate the velocity range per layer (minimum and maximum velocity, specified in the input model) and the vertical green lines show the discontinuity range (minimum and maximum depth of the discontinuity, specified in the input model). The black lines represent the accepted models.
b) Top-right: Obtained phase velocity dispersion curves. The red line represents the 'real', measured data. The black lines are the phase velocity curves obtained by the Monte Carlo-search (corresponding to accepted models). The green lines indicate the phase velocity bounds (±1%).
c) Bottom: Receiver functions obtained. The red line represents the true model, the green lines represent the absolute value uncertainty set, and the black lines are all the receiver functions corresponding to the models kept.

period phase velocity data, allowed velocity variations of ± 10% (also for the mantle velocity), allowed discontinuity depth variations of ± 10%, 1% uncertainty in the phase velocities and receiver function bounds of $\pm$ 0.05. So, both phase velocity constraints and receiver function constraints were taken into account. It is assumed that the mantle velocity varies as a whole until a depth of 110 km. After that, the mantle shear wave velocity is again kept constant at a value of 4.5 km/s, until a depth of 210 km.

The results of this Monte Carlo-search, which are visible in figure 13, will be compared with the results of a Monte Carlo-search that had the same input model, except for the fact that it did not

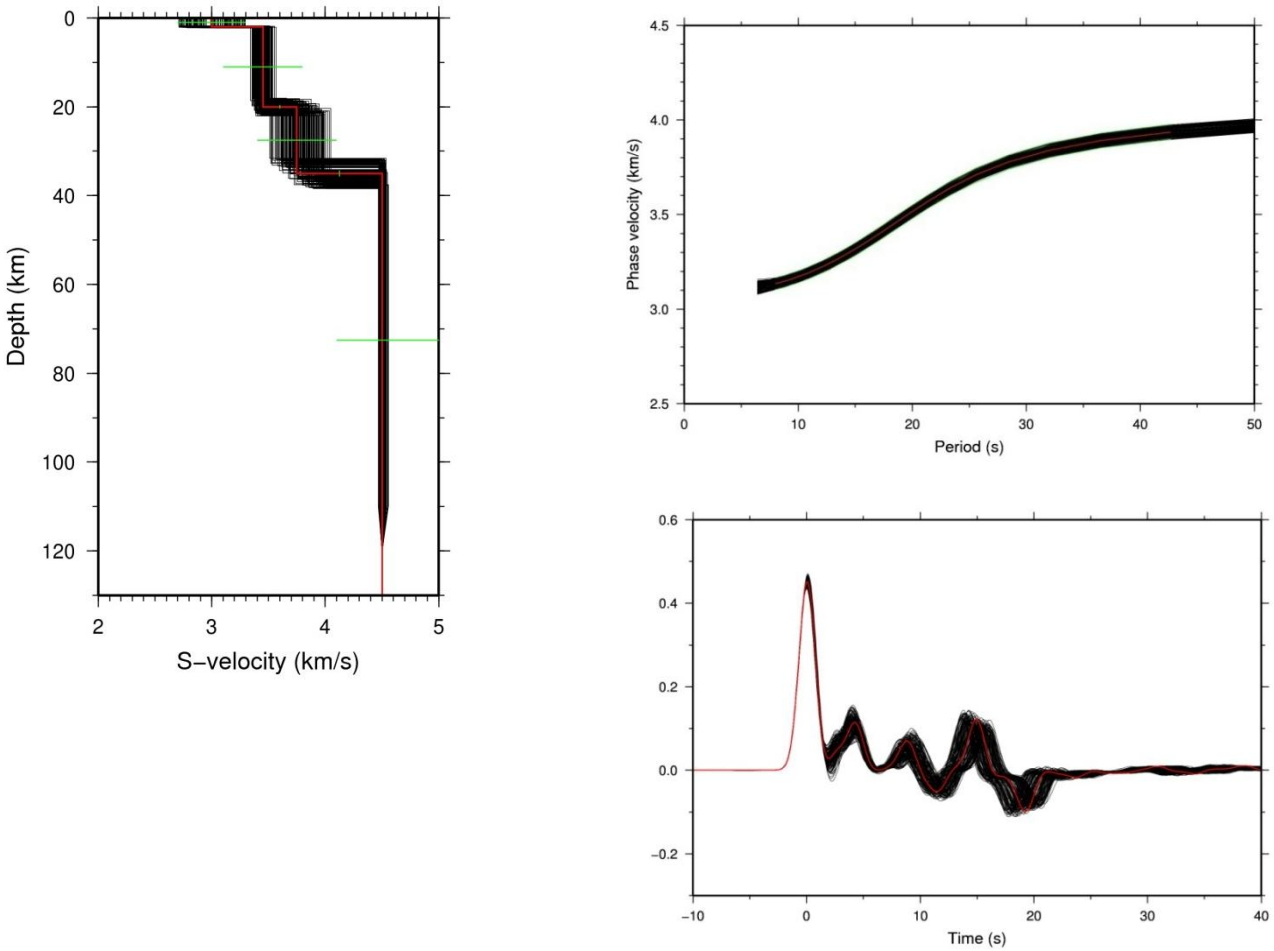

Figure 14: Results of a Monte Carlo-search for an input model with short period phase velocity data (8-43 s), allowed velocity variations of ± 10% (also the mantle velocity is changed), allowed discontinuity depth variations of ± 10%, 1% uncertainty in the phase velocities and no receiver function constraints.
a) Top-left: Obtained shear wave velocity-depth profiles of the accepted three-layered crustal models over a varying mantle. The red line represents the 'true' model, the horizontal green lines indicate the velocity range per layer (minimum and maximum velocity, specified in the input model) and the vertical green lines show the discontinuity range (minimum and maximum depth of the discontinuity, specified in the input model). The black lines represent the accepted models.
b) Top-right: Obtained phase velocity dispersion curves. The red line represents the 'real', measured data. The black lines are the phase velocity curves obtained by the Monte Carlo-search (corresponding to accepted models). The green lines indicate the phase velocity bounds ($\pm$1%).
c) Bottom: Receiver functions obtained. The red line represents the true model and the black lines are all the receiver functions corresponding to the models kept. No green lines representing the uncertainty are visible, due to the fact that the receiver function constraint was not taken into account.

take any receiver function constraints into account (see figure 14). In this way the effects of performing a joint inversion on the retrieved shear wave velocity structure (when an additional velocity parameter is involved) will be clearly observable.

When looking at figure 13a, it can be clearly seen that when the mantle velocity is varied (over a range of ± 10%), the velocity structure is still obtained quite well. So, adding an additional velocity parameter does not negatively influence the retrieved shear wave velocity structure after performing a joint inversion. Comparing figures 13a and 14a, it is again evident that a joint inversion of receiver functions and surface wave dispersion curves has beneficial effects on the retrieved shear wave velocity-depth profile. By adding the receiver function constraints (which resulted in figure 13), first of all a clear improvement of the discontinuity depths (second and third discontinuity) is obtained. In addition to the improved discontinuity depths, also a clear enhanced lower crustal shear wave velocity is retrieved. No significant improvement of the upper crustal shear wave velocity and the mantle shear wave velocity is visible after adding the receiver function constraints.

As found before, a slightly better fit is visible in the plot of the phase velocity curves, when the receiver function constraint is taken into account (compare figures 13b and 14b).

Modelling with a different number of layers than the number of layers of the true model

Until now the 'real' structure was tried to be retrieved by modelling with the same number of layers. However, in reality the 'real' structure is of course not known. Therefore, it will now be investigated how well the structure is retrieved when the modelling is done with one layer less than the true model or with one layer more than the true model.

First of all, three layers will be modelled with two layers (so, the mantle shear wave velocity is again fixed at a constant value). The phase velocity uncertainty again set to ±1%, and the absolute receiver function uncertainty value was set to 0.05. An input model with a short period Rayleigh wave phase velocity curve (8-43 s) is considered. An allowed velocity range of ± 10% for the second layer and from 2 till 3.8 km/s for the first layer is considered, together with allowed discontinuity depth variations of ± 10%. What can be observed, when looking at the data fit of both the phase velocity curves and receiver functions, is that the obtained phase velocity curves and receiver functions lie close to the 'real' data (see figure 15). For the receiver functions, this is especially the case at greater times. As a result, what can be seen in figure 15 below, the velocity structure for the second and third layer is retrieved quite well. Looking at the discontinuities, the third discontinuity (Moho) is obtained nicely. Only the sedimentary layer is not retrieved, when modelling with one layer less than the 'true' structure.

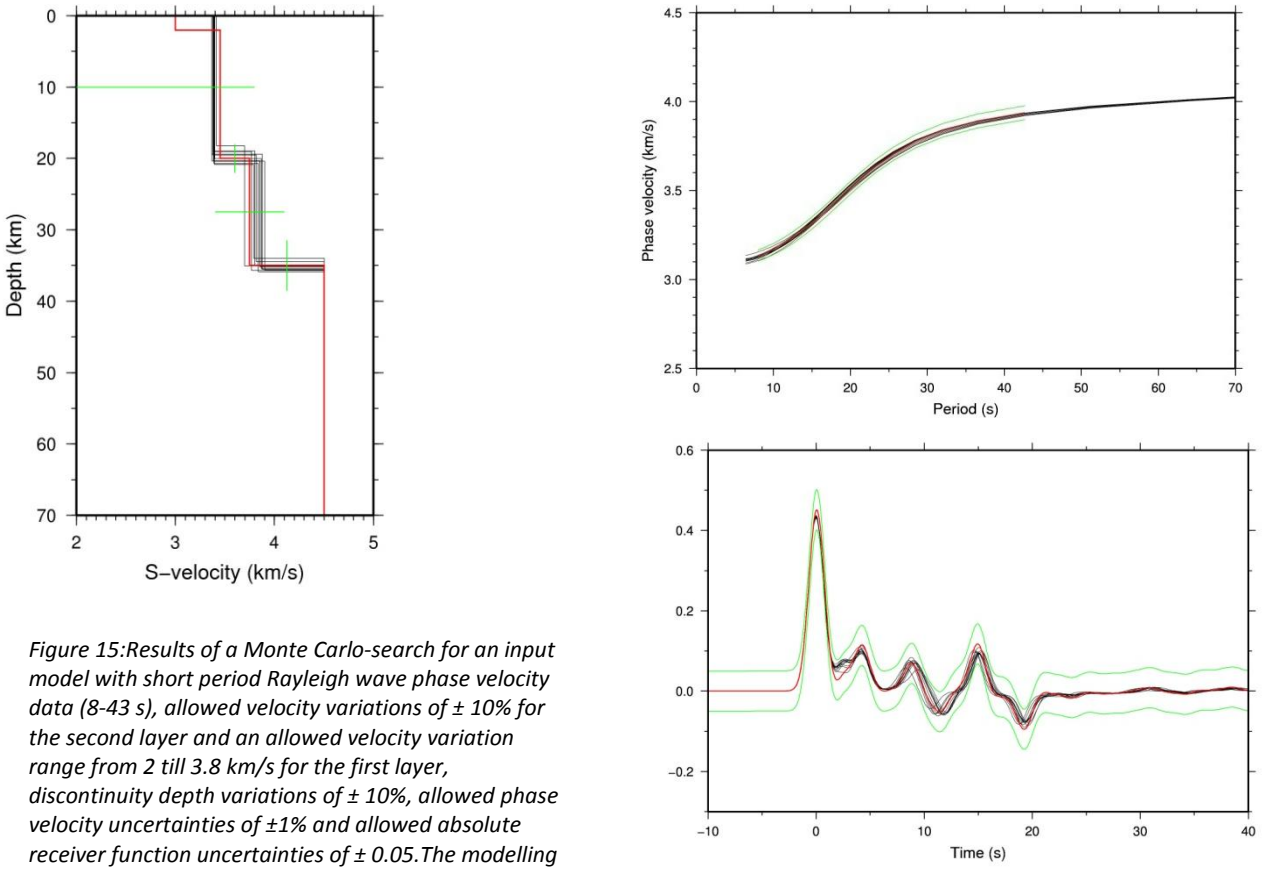

Figure 15:Results of a Monte Carlo-search for an input model with short period Rayleigh wave phase velocity data (8-43 s), allowed velocity variations of ± 10% for the second layer and an allowed velocity variation range from 2 till 3.8 km/s for the first layer, discontinuity depth variations of ± 10%, allowed phase velocity uncertainties of ±1% and allowed absolute receiver function uncertainties of ± 0.05.The modelling of a true structure with 3 layers, is done with 2 layers (1 layer less than the true structure).
a) Top-left: Obtained shear wave velocity-depth profiles of the accepted models. The red line represents the 'true' model, the horizontal green lines indicate the velocity range per layer (minimum and maximum velocity, specified in the input model) and the vertical green lines show the discontinuity range (minimum and maximum depth of the discontinuity, specified in the input model). The black lines represent the accepted models.
b) Top-right: Obtained phase velocity dispersion curves. The red line represents the 'real', measured data. The black lines are the phase velocity curves obtained by the Monte Carlo-search (corresponding to accepted models). The green lines indicate the phase velocity bounds (±1%).
c) Bottom: Receiver functions obtained. The red line represents the true model and the black lines are all the receiver functions corresponding to the models kept. The green lines represent the receiver function uncertainties.

Important to note is that the modelling with two layers in this case probably gives such good results, because of the fact that the sedimentary layer is chosen to be modelled together with the upper crustal layer as one layer. As already shown before, the surface wave dispersion data and receiver function data are not very sensitive to the sedimentary layer, so taking this layer together with the upper crustal layer does not influence the results of the Monte Carlo-search very much. When taking for example the upper and lower crustal layers together as one layer, this could end-up in results that are not so good as the results of figure 15. However, choosing to model with one very thin layer (sedimentary layer) and one very thick layer (upper and lower crust together) does not seem to be an intuitively logical choice. Furthermore, the small sensitivity of the data to the shear wave velocity structure of the sedimentary layer was already shown before in this study, so this a priori information can be taken into account when deciding which modelling set-up will be used.

Next, it will be investigated how well the structure is retrieved when the modelling is done with one layer more than the true model. Therefore, a 'true' structure consisting of two layers over a half-space, will be modelled with three layers over a half-space. The results of two Monte Carlo-searches will be compared: one that takes only phase velocity constraints into account and one that uses both phase velocity and receiver function data. An input model using short period Rayleigh wave phase velocity data (8-43 s) will be used in both cases. Furthermore, the allowed discontinuity depth variations are $\pm$ 10%, the allowed velocity variations are $\pm$ 10% for the second and third layer, and the allowed velocity range for the first layer is from 2 till 3.8 km/s. The phase velocity uncertainties are again set to ±1%. When the receiver function constraint is taken into account, the allowed absolute receiver function uncertainty is ± 0.05.

Figure 16 shows the results of the Monte Carlo-search that uses only phase velocity data.

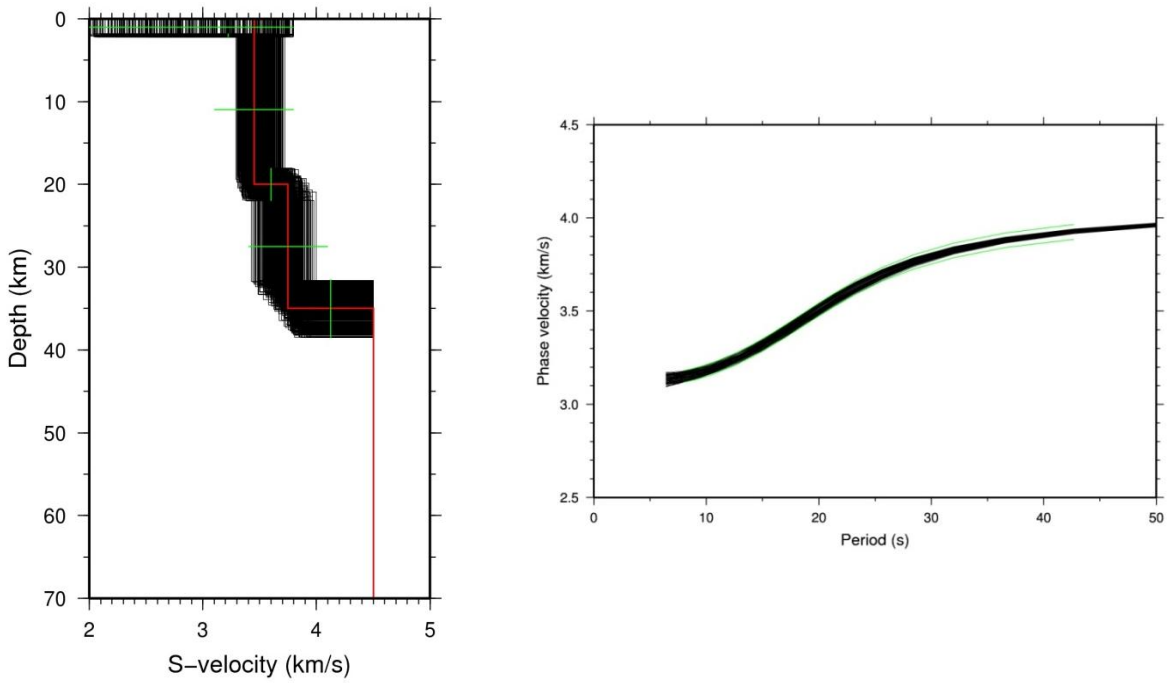

Figure 16:Results of a Monte Carlo-search for an input model with short period Rayleigh wave phase velocity data (8-43 s), allowed velocity variations of ± 10% for the second layer and third layer and an allowed velocity variation range from 2 till 3.8 km/s for the first layer, discontinuity depth variations of ± 10%, allowed phase velocity uncertainties of ±1% and no receiver function constraints. The modelling of a true structure with 2 layers, is done with 3 layers (1 layer more than the true structure).
a) Left: Obtained shear wave velocity-depth profiles of the accepted models. The red line represents the 'true' model, the horizontal green lines indicate the velocity range per layer (minimum and maximum velocity, specified in the input model) and the vertical green lines show the discontinuity range (minimum and maximum depth of the discontinuity, specified in the input model). The black lines represent the accepted models.
b) Right: Obtained phase velocity dispersion curves. The red line represents the 'real', measured data. The black lines are the phase velocity curves obtained by the Monte Carlo-search (corresponding to accepted models). The green lines indicate the phase velocity bounds ($\pm$ 1%).

Figure 17 presents the results of the Monte Carlo-search that used both phase velocity constraints and receiver function constraints.

When two layers are modelled with three layers, the data fit is different. The phase velocity curves are obtained reasonably close to the 'real' data (see figure 16b or 17b). However, the receiver functions fit the data less well, as can be seen in figure 17c (when comparing with figure 15). Now,

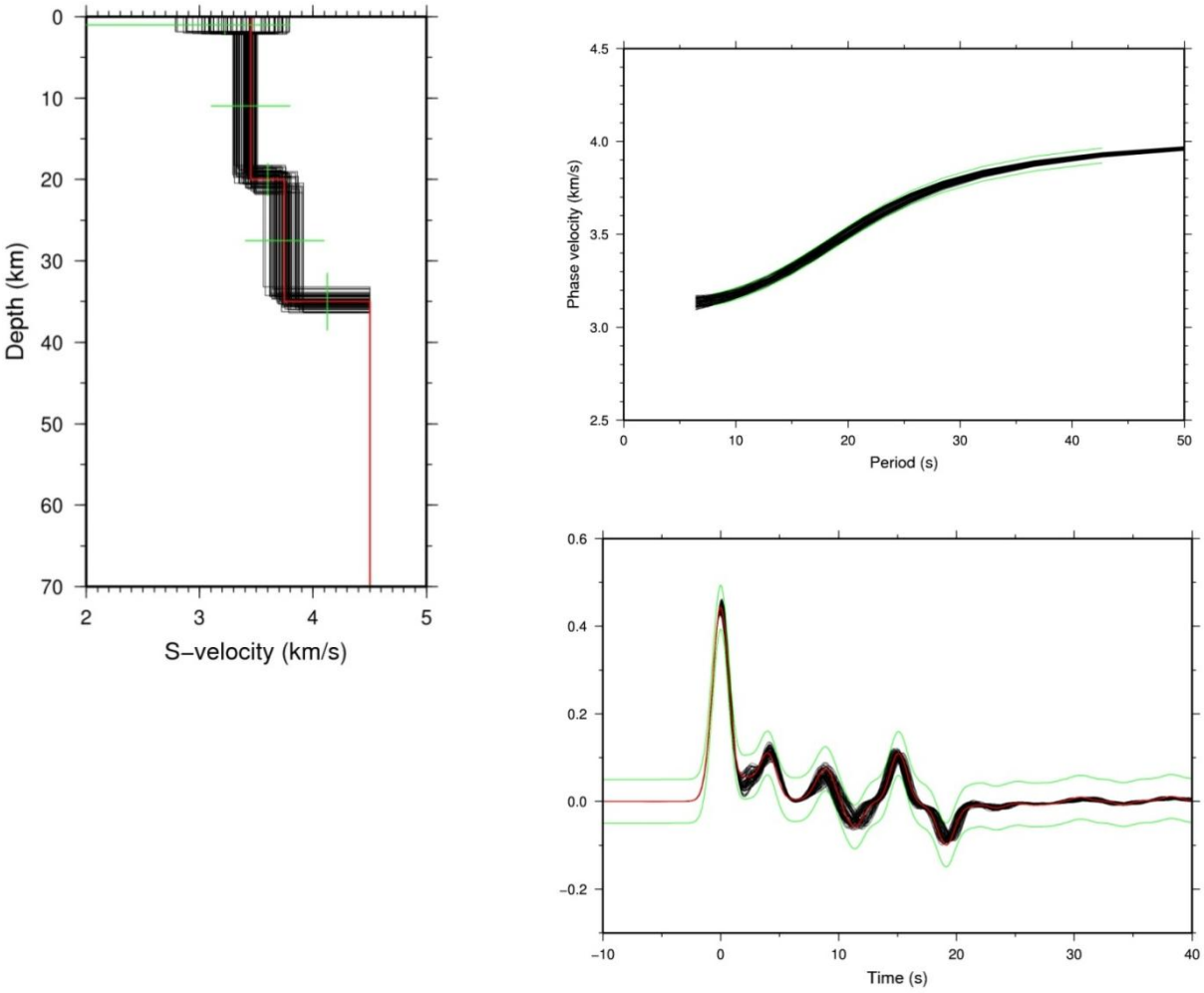

Figure 17: Results of a Monte Carlo-search for an input model with short period Rayleigh wave phase velocity data (8-43 s), allowed velocity variations of ± 10% for the second layer and third layer and an allowed velocity variation range from 2 till 3.8 km/s for the first layer, discontinuity depth variations of ± 10%, allowed phase velocity uncertainties of ±1% and an allowed absolute receiver function uncertainty of ± 0.05 . The modelling of a true structure with 2 layers, is done with 3 layers (1 layer more than the true structure).
a) Upper-left: Obtained shear wave velocity-depth profiles of the accepted models. The red line represents the 'true' model, the horizontal green lines indicate the velocity range per layer (minimum and maximum velocity, specified in the input model) and the vertical green lines show the discontinuity range (minimum and maximum depth of the discontinuity, specified in the input model). The black lines represent the accepted models.
b) Upper-right: Obtained phase velocity dispersion curves. The red line represents the 'real', measured data. The black lines are the phase velocity curves obtained by the Monte Carlo-search (corresponding to accepted models). The green lines indicate the phase velocity bounds (± 1%).
c) Bottom: Receiver functions obtained. The red line represents the true model and the black lines are all the receiver functions corresponding to the models kept. The green lines represent the receiver function uncertainties.

comparing the retrieved shear wave velocity structures when both the phase velocity data and the receiver function data are used (figure 17a) with the retrieved shear wave velocity structures of figure 15a (a joint inversion where 3 layers are modelled with 2 layers), several observations can be made. First of all, the velocity structure of the second part of the first layer is retrieved quite well. In contrast, the second layer velocity structure is obtained less well. The second discontinuity (which is in this case the Moho) is better retrieved than the first one.

Comparing the velocity structures obtained when using only phase velocity curves (figure 16a), with the retrieved structures from the joint-inversion (figure 17a), it is clearly observable that the latter yields better results.

What can be concluded from the results discussed above, is that when the structure is modelled with one layer less than the 'true' structure the results are better than when modelling with one layer more than the 'true' structure. However, the main characteristics of the obtained shear wave velocity structures are quite similar for both cases. The fact that modelling with one layer more than the 'true' structure yields worse results than when modelling with one layer less or the same number of layers, can probably be explained by the fact that modelling with one layer more, introduces two more degrees of freedom (shear wave velocity parameter and discontinuity depth parameter) than the number of degrees of freedom for the 'true' structure. This increase in the number of degrees of freedom results in more different possibilities that match the data within the uncertainty bounds set. Hence, the retrieved shear wave velocity structure shows a wider range of accepted models, giving a less clear indication of what the 'true' model looks like (i.e. a worse result of the Monte Carlo-search).

As already mentioned in the introduction, Rayleigh wave group velocity data are more sensitive to the shallower shear wave velocity structure than Rayleigh wave phase velocity data. This was clearly visible when comparing the sensitivity kernels of the Rayleigh wave phase and group velocities. So, when also Rayleigh wave group velocity dispersion data is taken into account in the joint inversion, tighter constraints on the shear velocity structure could possibly be obtained, especially for the shallower parts.

Monte Carlo-search with phase velocity dispersion data, receiver functions and group velocity dispersion data

To investigate the effects of the group velocity data on the retrieved shear wave velocity structure, a Monte Carlo-search is performed that takes only group velocity constraints into account. The allowed velocity variations and discontinuity depth variations are ± 10% and an allowed group velocity uncertainty of ± 2% is used. Group velocity data in the period range from 10-28 s are used.
In figure 18a below the obtained shear wave velocity structure is presented, when performing a Monte Carlo search with only group velocity constraints. It is clearly visible that the group velocity data is mainly sensitive to the shallower parts of the shear wave velocity structure. The Rayleigh wave group velocity sensitivity kernel, as discussed in the introduction, is clearly recognizable in the obtained shear wave velocity structure below.
Despite the fact that the no phase velocity constraints were used, the obtained phase velocity curves fit the data quite nicely (see figure 18b). When in contrast looking at figure 18d, it is observable that the obtained receiver functions do not fit the data well. For completeness, the obtained phase velocity curves and receiver functions are shown in figure 18 (despite the fact that they did not put any constraints on the retrieved shear wave velocity models).

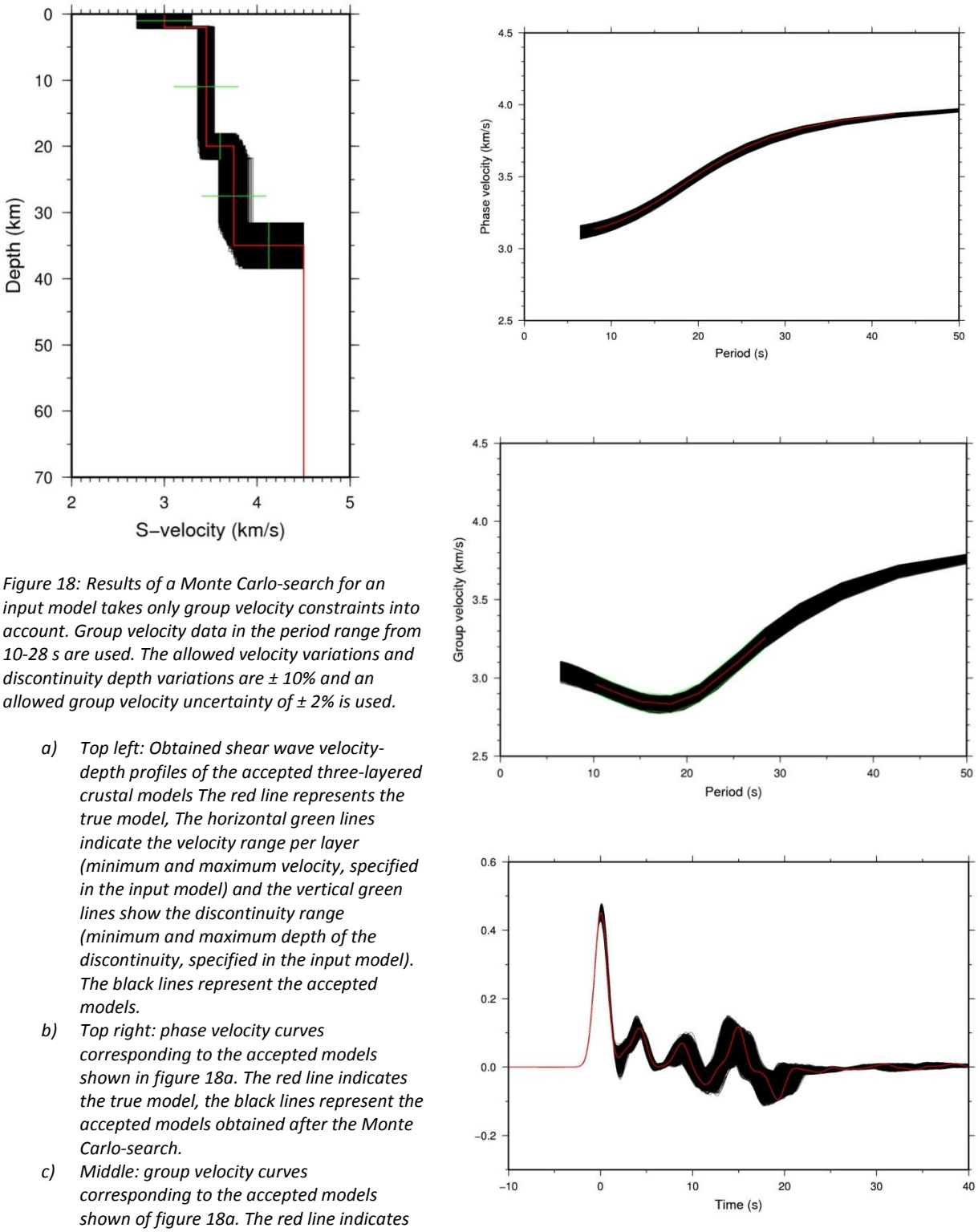

Figure 18: Results of a Monte Carlo-search for an input model takes only group velocity constraints into account. Group velocity data in the period range from 10-28 s are used. The allowed velocity variations and discontinuity depth variations are ± 10% and an allowed group velocity uncertainty of ± 2% is used.

- *a) Top left: Obtained shear wave velocity-depth profiles of the accepted three-layered crustal models The red line represents the true model, The horizontal green lines indicate the velocity range per layer (minimum and maximum velocity, specified in the input model) and the vertical green lines show the discontinuity range (minimum and maximum depth of the discontinuity, specified in the input model). The black lines represent the accepted models.*
- *b) Top right: phase velocity curves corresponding to the accepted models shown in figure 18a. The red line indicates the true model, the black lines represent the accepted models obtained after the Monte Carlo-search.*
- *c) Middle: group velocity curves corresponding to the accepted models shown of figure 18a. The red line indicates the true model, the black lines represent the accepted models obtained after the Monte Carlo-search. The green lines illustrate the allowed uncertainty range.*
- *d) Lower right: Receiver functions corresponding to the accepted models shown of figure 18a. The red line indicates the true model, the black lines represent the accepted models obtained after the Monte Carlo-search.*

Now that the effect of using only group velocity constraints on the retrieved structure has been studied, the next step is to investigate whether adding the Rayleigh wave group velocity dispersion data to the joint inversion has beneficial effects on the retrieved shear wave velocity structure or not. First of all, the effects of performing a joint inversion of only surface wave dispersion data will be studied (i.e. using both phase and group velocity constraints in the Monte Carlo-search). Thereby, the effect of assigning two different uncertainties to the group velocity data will be investigated.

The results of three different Monte Carlo-searches will be compared. In all cases, an input model with allowed velocity and discontinuity depth variations of ± 10% will be considered. Furthermore, short period phase velocity data will be used (8-43 s), with allowed phase velocity uncertainties of ± 1%. In all three cases, the receiver functions do not constrain the data. Group velocity data in the period range from 10-28 s are used. When the group velocity constraint was used, two different group velocity uncertainties were assigned: ± 2% and ± 4%. The input models for the Monte Carlo-search resulting in figures 19 and 20 imply a joint inversion of phase velocity data (with an accepted uncertainty of ± 1%) and group velocity data (with an accepted uncertainty of ± 2% and ± 4%, respectively).

Comparing figures 19 and 20, the effect of assigning different group velocity uncertainties on the retrieved shear wave velocity structure is mainly visible looking at the lower crustal shear wave velocity: when allowing ± 4% group velocity uncertainty, the shear wave velocity structure is less constrained than when a ± 2% group velocity uncertainty is accepted. However, as visible when comparing figure 20 with figure 21 (which has only phase velocity constraints), there is still some significant improvement in the upper and lower crustal shear wave velocity when a group velocity uncertainty of ± 4% is accepted.

So, when comparing figures 19 and 20 with figure 21, it is clearly observable that introducing the additional group velocity constraint again improves the upper and lower crustal shear wave velocity significantly. However, by introducing the additional group velocity constraints no clear improving effects on the discontinuities are visible. This can probably be explained by the fact that in this case a joint inversion with only phase and group velocity data (which are mainly sensitive to the absolute shear wave velocity values) was performed. So, no receiver function constraints were taken into account. As mentioned before, the receiver functions are mainly sensitive to the shear wave velocity contrasts (i.e. discontinuities), so when not using receiver function data in the joint inversion, it is intuitively logical that the discontinuities are not resolved very well.

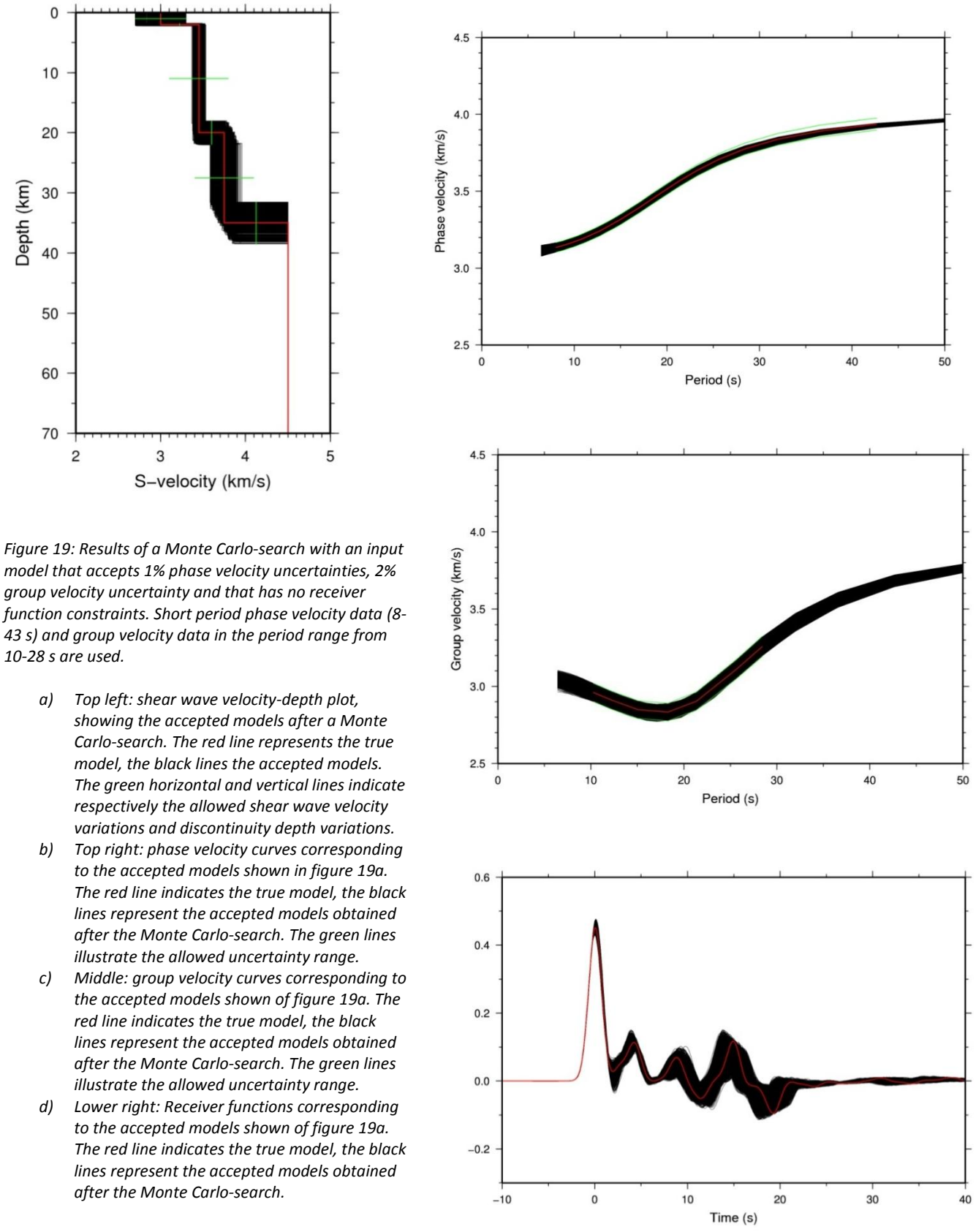

Figure 19: Results of a Monte Carlo-search with an input model that accepts 1% phase velocity uncertainties, 2% group velocity uncertainty and that has no receiver function constraints. Short period phase velocity data (8-43 s) and group velocity data in the period range from 10-28 s are used.

a) Top left: shear wave velocity-depth plot, showing the accepted models after a Monte Carlo-search. The red line represents the true model, the black lines the accepted models. The green horizontal and vertical lines indicate respectively the allowed shear wave velocity variations and discontinuity depth variations.

b) Top right: phase velocity curves corresponding to the accepted models shown in figure 19a. The red line indicates the true model, the black lines represent the accepted models obtained after the Monte Carlo-search. The green lines illustrate the allowed uncertainty range.

c) Middle: group velocity curves corresponding to the accepted models shown of figure 19a. The red line indicates the true model, the black lines represent the accepted models obtained after the Monte Carlo-search. The green lines illustrate the allowed uncertainty range.

d) Lower right: Receiver functions corresponding to the accepted models shown of figure 19a. The red line indicates the true model, the black lines represent the accepted models obtained after the Monte Carlo-search.

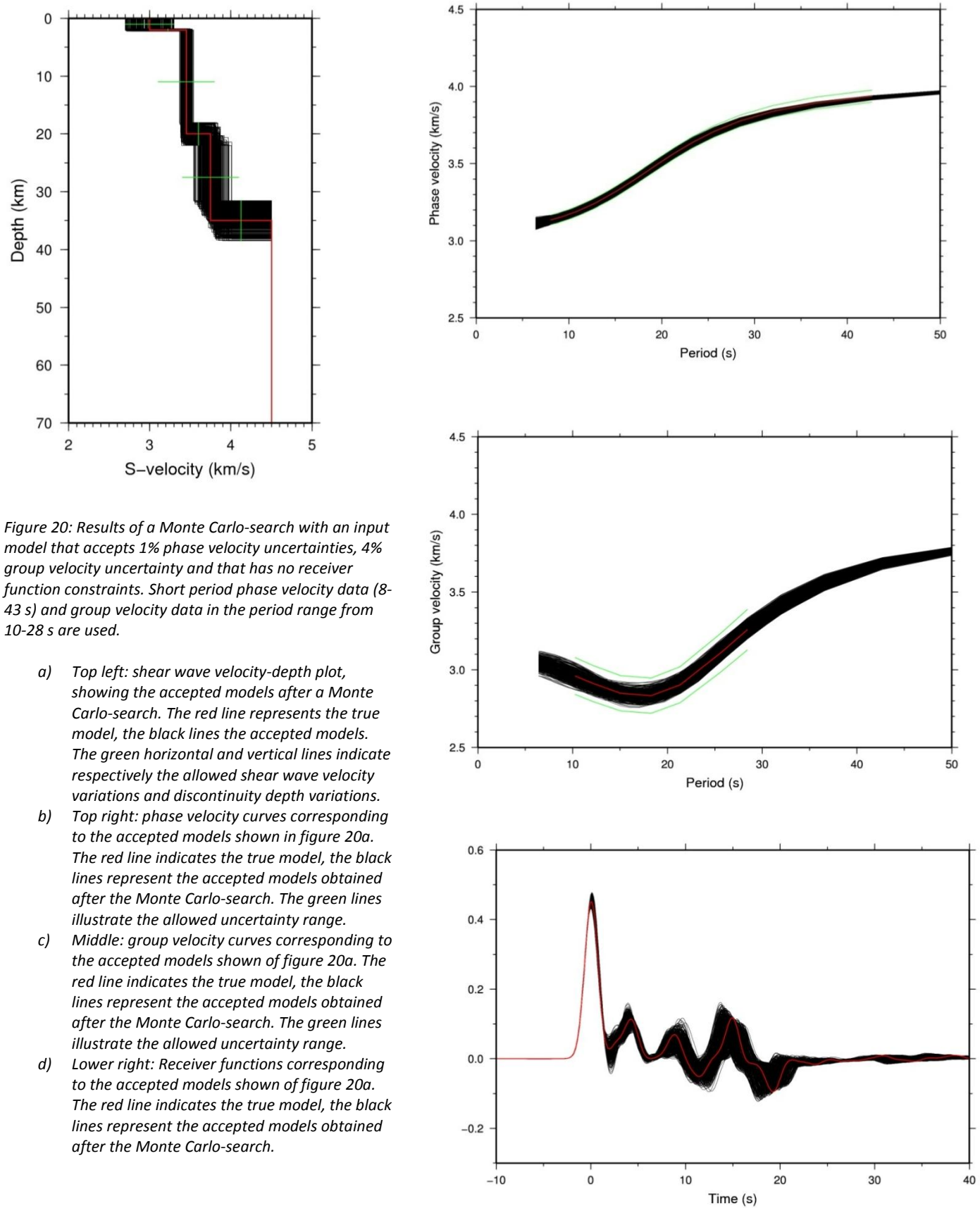

Figure 20: Results of a Monte Carlo-search with an input model that accepts 1% phase velocity uncertainties, 4% group velocity uncertainty and that has no receiver function constraints. Short period phase velocity data (8-43 s) and group velocity data in the period range from 10-28 s are used.

a) *Top left: shear wave velocity-depth plot, showing the accepted models after a Monte Carlo-search. The red line represents the true model, the black lines the accepted models. The green horizontal and vertical lines indicate respectively the allowed shear wave velocity variations and discontinuity depth variations.*
b) *Top right: phase velocity curves corresponding to the accepted models shown in figure 20a. The red line indicates the true model, the black lines represent the accepted models obtained after the Monte Carlo-search. The green lines illustrate the allowed uncertainty range.*
c) *Middle: group velocity curves corresponding to the accepted models shown of figure 20a. The red line indicates the true model, the black lines represent the accepted models obtained after the Monte Carlo-search. The green lines illustrate the allowed uncertainty range.*
d) *Lower right: Receiver functions corresponding to the accepted models shown of figure 20a. The red line indicates the true model, the black lines represent the accepted models obtained after the Monte Carlo-search.*

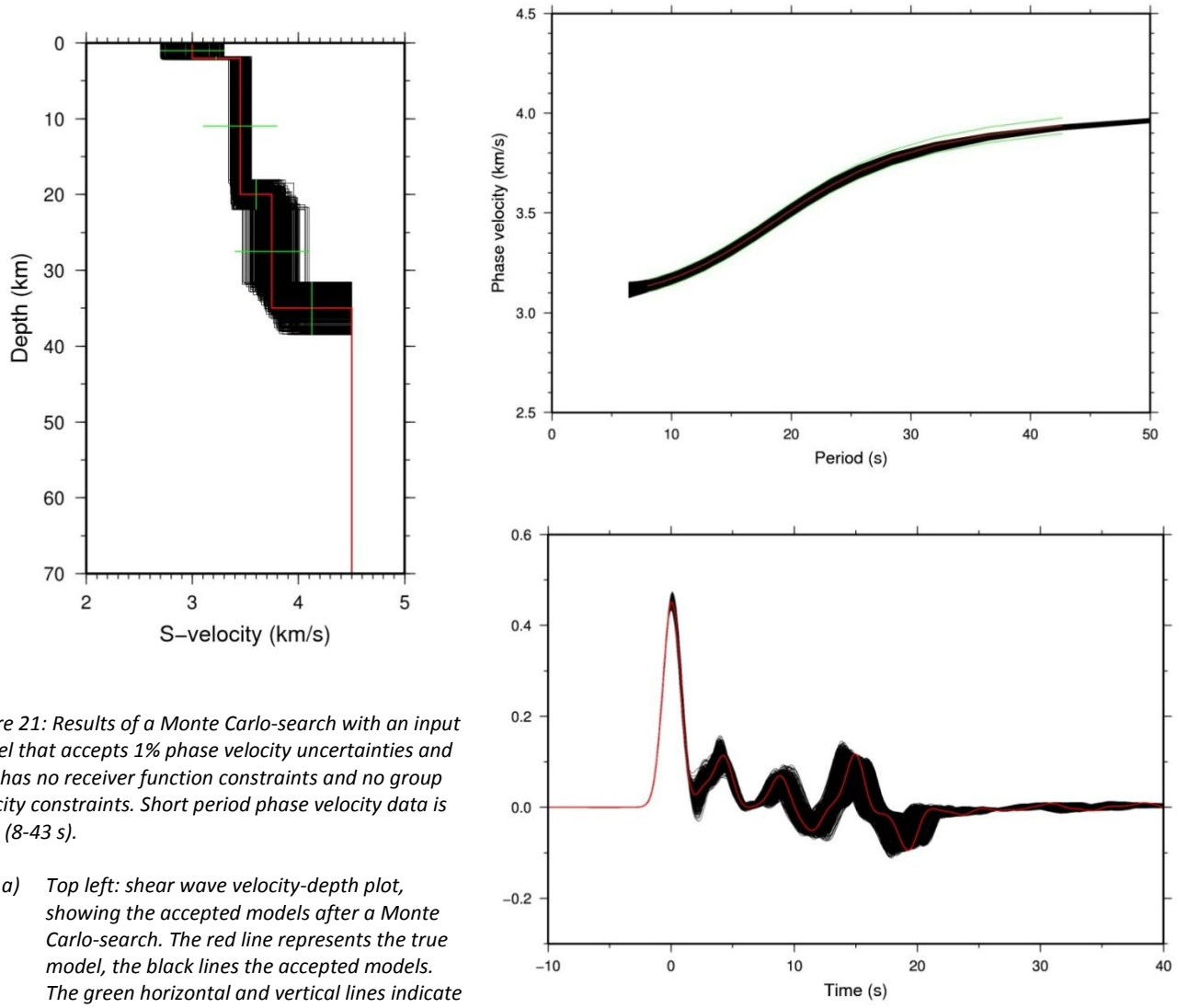

Figure 21: Results of a Monte Carlo-search with an input model that accepts 1% phase velocity uncertainties and that has no receiver function constraints and no group velocity constraints. Short period phase velocity data is used (8-43 s).

- *a) Top left: shear wave velocity-depth plot, showing the accepted models after a Monte Carlo-search. The red line represents the true model, the black lines the accepted models. The green horizontal and vertical lines indicate respectively the allowed shear wave velocity variations and discontinuity depth variations.*
- *b) Top right: phase velocity curves corresponding to the accepted models shown in figure 21a. The red line indicates the true model, the black lines represent the accepted models obtained after the Monte Carlo-search. The green lines illustrate the allowed uncertainty range.*
- *c) Lower right: Receiver functions corresponding to the accepted models shown of figure 21a. The red line indicates the true model, the black lines represent the accepted models obtained after the Monte Carlo-search.*

Now that the effects of using solely group velocity data, and using both phase and group velocity data on the retrieved shear wave velocity structure are investigated, the next step is to investigate a joint inversion of phase velocity data, group velocity data and receiver function data. To illustrate the effects of adding group velocity constraints to the joint inversion, the results of two Monte Carlo-searches will be compared: one that uses only phase velocity constraints and receiver function constraints (figure 22), and one that uses all three types of data (figure 23). The input models for both searches use short period phase velocity data and allow uncertainties in the phase velocities of 1%. In both cases, absolute value uncertainties for the receiver functions of 0.05 are allowed.

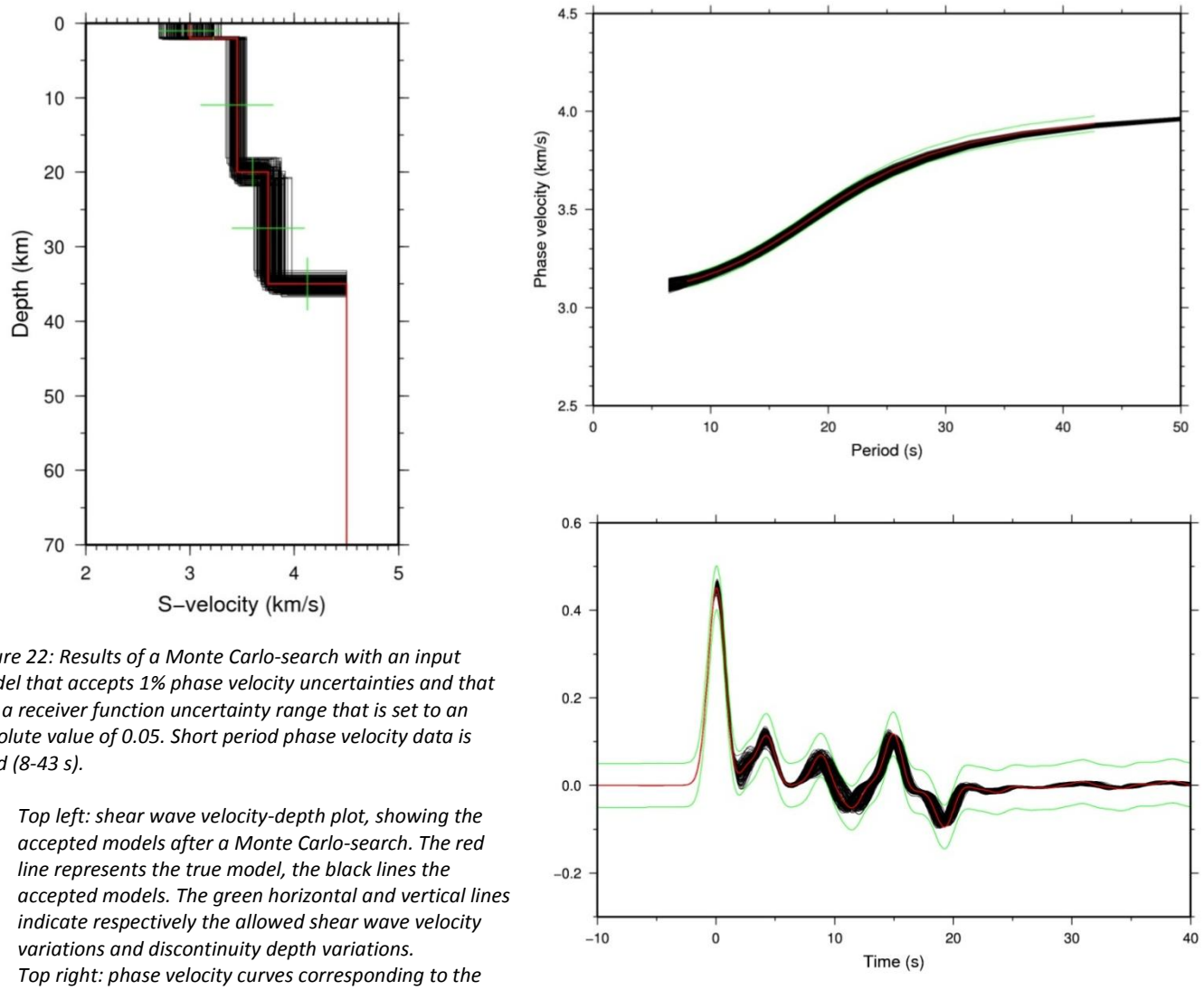

Figure 22: Results of a Monte Carlo-search with an input model that accepts 1% phase velocity uncertainties and that has a receiver function uncertainty range that is set to an absolute value of 0.05. Short period phase velocity data is used (8-43 s).

a) *Top left: shear wave velocity-depth plot, showing the accepted models after a Monte Carlo-search. The red line represents the true model, the black lines the accepted models. The green horizontal and vertical lines indicate respectively the allowed shear wave velocity variations and discontinuity depth variations.*
b) *Top right: phase velocity curves corresponding to the accepted models shown in figure 22a. The red line indicates the true model, the black lines represent the accepted models obtained after the Monte Carlo-search. The green lines illustrate the allowed uncertainty range.*
c) *Lower right: Receiver functions corresponding to the accepted models shown of figure 22a. The red line indicates the true model, the black lines represent the accepted models obtained after the Monte Carlo-search. The green lines illustrate the allowed uncertainty range.*

Velocity variations of ± 10% from the 'true' model are allowed for the three crustal layers and also depth variations of the discontinuities of ± 10% are permitted. For producing the results of figure 23, also group velocity data was taken into account, with allowed uncertainties of 2%.

When comparing figures 22a and 23a, it is again clearly visible that when taking the group velocity data additionally into account, the shear wave velocity for especially the upper crust is much better constrained. Furthermore, the lower crustal shear wave velocity is improved by introducing the group velocity data and also the Moho is better determined. As already discussed above, there is a trade-off between the shear wave velocity and depth. So, when improving the lower crustal velocity, this also influences the retrieved Moho depth. This effect is less visible for the 2nd discontinuity, which is overall not clearly improved. So, by adding the group velocity data to the joint inversion the shear wave velocities are much better determined and also the Moho discontinuity is slightly better resolved. The shear wave velocity of the sedimentary layer is still not better constrained by adding the group velocity data to the joint inversion.

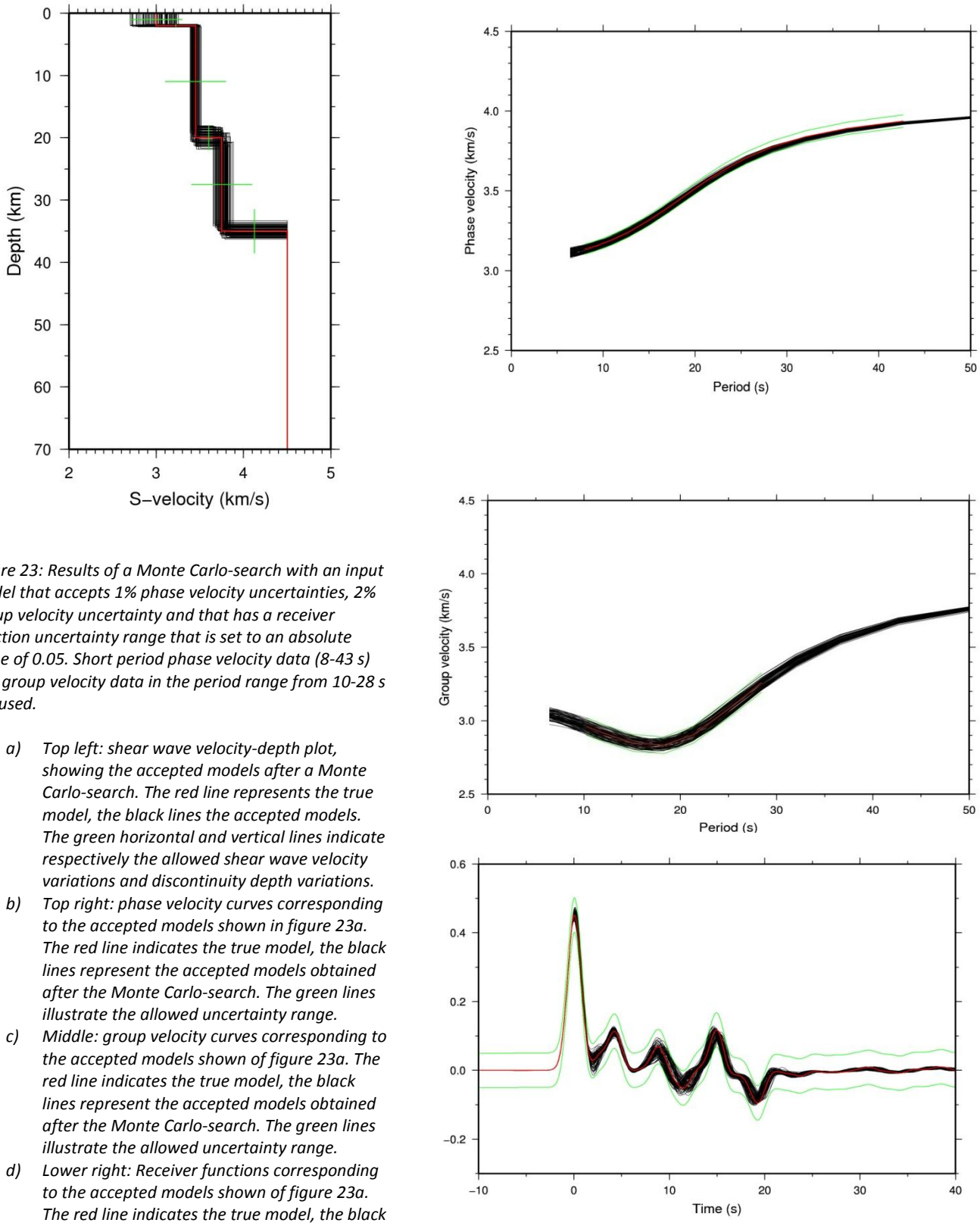

Figure 23: Results of a Monte Carlo-search with an input model that accepts 1% phase velocity uncertainties, 2% group velocity uncertainty and that has a receiver function uncertainty range that is set to an absolute value of 0.05. Short period phase velocity data (8-43 s) and group velocity data in the period range from 10-28 s are used.

a) *Top left: shear wave velocity-depth plot, showing the accepted models after a Monte Carlo-search. The red line represents the true model, the black lines the accepted models. The green horizontal and vertical lines indicate respectively the allowed shear wave velocity variations and discontinuity depth variations.*
b) *Top right: phase velocity curves corresponding to the accepted models shown in figure 23a. The red line indicates the true model, the black lines represent the accepted models obtained after the Monte Carlo-search. The green lines illustrate the allowed uncertainty range.*
c) *Middle: group velocity curves corresponding to the accepted models shown of figure 23a. The red line indicates the true model, the black lines represent the accepted models obtained after the Monte Carlo-search. The green lines illustrate the allowed uncertainty range.*
d) *Lower right: Receiver functions corresponding to the accepted models shown of figure 23a. The red line indicates the true model, the black lines represent the accepted models obtained after the Monte Carlo-search. The green lines represent the allowed uncertainty range.*

Again, the situation of modelling with a different number of layers than the number of layers of the true model will be investigated. First of all, the situation of modelling a real, three layered structure with two layers (one layer less) will be considered. The results of two different input models are presented below in figures 24 and 25. The only difference between the two input models is that figure 24 uses additional group velocity constraints, with an accepted group velocity uncertainty of $\pm$ 2%, and group velocity data in the period range from 10-28 s. The phase velocity uncertainty that is allowed is for both cases $\pm$ 1%, and the absolute value receiver function uncertainty is set to $\pm$ 0.05 for both cases. For both Monte Carlo-searches, short period phase velocity data is used (8-43 s). The allowed velocity variation is ± 10% for the second layer and the allowed velocity range for the first layer is from 2 till 3.8 km/s. The accepted discontinuity depth variations are ± 10%.
When comparing the shear wave velocity-depth plots of both situations, it is clearly recognizable that by adding the group velocity data to the joint inversion, especially the lower crustal shear wave velocity is better constrained. When comparing the receiver function graphs, no clear improvement is visible when adding the group velocity constraint. This is also visible in the comparison of the retrieved shear wave velocity structure, where no improvement of the discontinuity depths can be observed. A small improved upper crustal shear wave velocity can be seen in figure 24. So, adding the group velocity constraint to the joint inversion also has beneficial effects on the retrieved shear wave velocity structure when the modelling is done with one layer less than the number of layers of the 'true' structure.

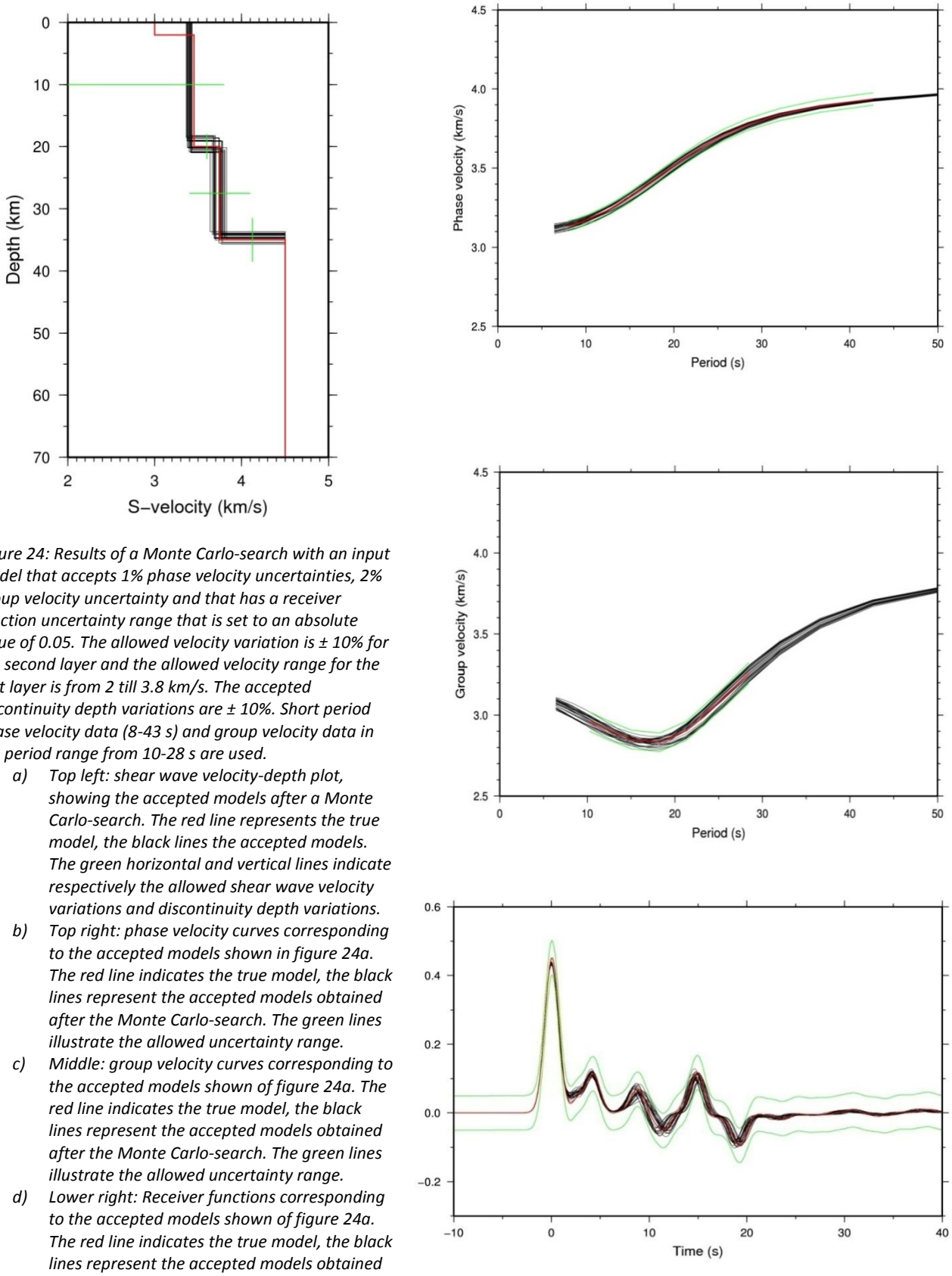

Figure 24: Results of a Monte Carlo-search with an input model that accepts 1% phase velocity uncertainties, 2% group velocity uncertainty and that has a receiver function uncertainty range that is set to an absolute value of 0.05. The allowed velocity variation is ± 10% for the second layer and the allowed velocity range for the first layer is from 2 till 3.8 km/s. The accepted discontinuity depth variations are ± 10%. Short period phase velocity data (8-43 s) and group velocity data in the period range from 10-28 s are used.

a) *Top left: shear wave velocity-depth plot, showing the accepted models after a Monte Carlo-search. The red line represents the true model, the black lines the accepted models. The green horizontal and vertical lines indicate respectively the allowed shear wave velocity variations and discontinuity depth variations.*
b) *Top right: phase velocity curves corresponding to the accepted models shown in figure 24a. The red line indicates the true model, the black lines represent the accepted models obtained after the Monte Carlo-search. The green lines illustrate the allowed uncertainty range.*
c) *Middle: group velocity curves corresponding to the accepted models shown of figure 24a. The red line indicates the true model, the black lines represent the accepted models obtained after the Monte Carlo-search. The green lines illustrate the allowed uncertainty range.*
d) *Lower right: Receiver functions corresponding to the accepted models shown of figure 24a. The red line indicates the true model, the black lines represent the accepted models obtained after the Monte Carlo-search. The green lines represent the allowed uncertainty range.*

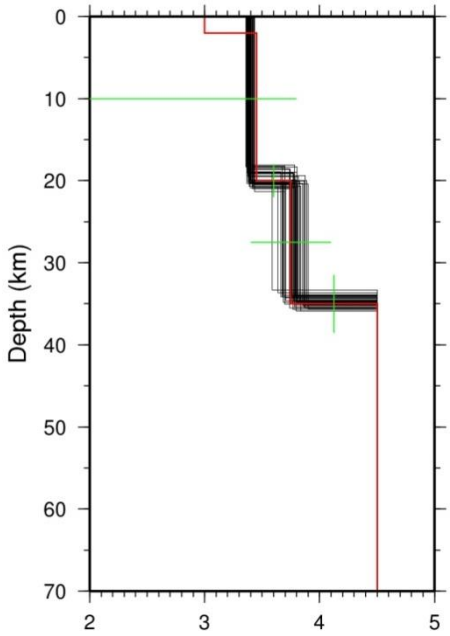

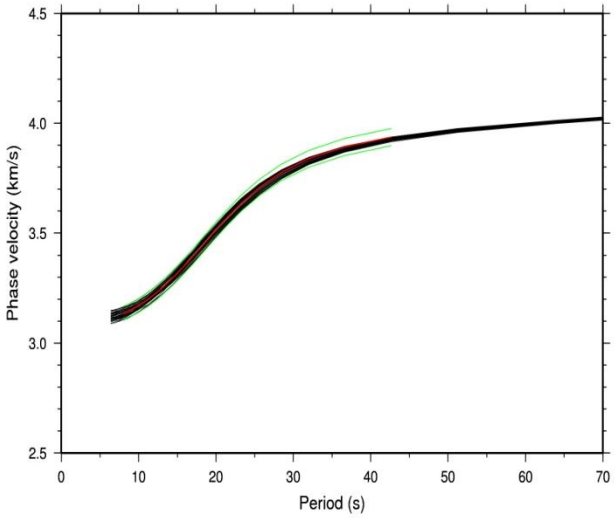

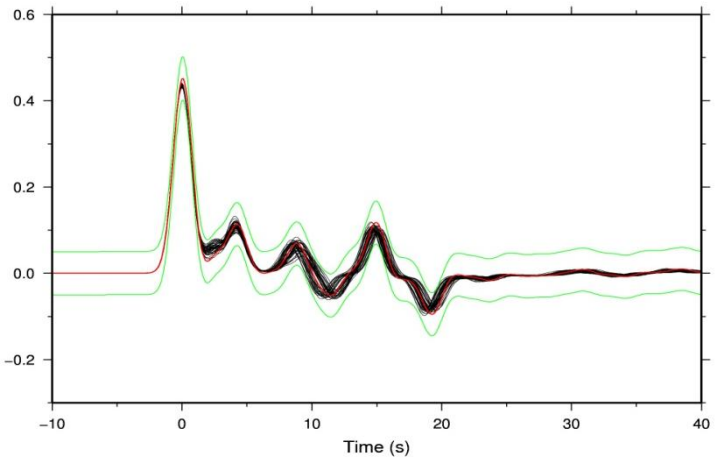

Figure 25: Results of a Monte Carlo-search with an input model that accepts ± 1% phase velocity uncertainties, uses short period phase velocity data (8-43 s) and has a receiver function uncertainty range that is set to an absolute value of ± 0.05. The allowed velocity variation is ± 10% for the second layer and the allowed velocity range for the first layer is from 2 till 3.8 km/s. The accepted discontinuity depth variations are ± 10%. No group velocity constraints are taken into account.

- *a) Top left: shear wave velocity-depth plot, showing the accepted models after a Monte Carlo-search. The red line represents the true model, the black lines the accepted models. The green horizontal and vertical lines indicate respectively the allowed shear wave velocity variations and discontinuity depth variations.*
- *b) Top right: phase velocity curves corresponding to the accepted models shown in figure 25a. The red line indicates the true model, the black lines represent the accepted models obtained after the Monte Carlo-search. The green lines illustrate the allowed uncertainty range.*
- *c) Lower right: Receiver functions corresponding to the accepted models shown of figure 25a. The red line indicates the true model, the black lines represent the accepted models obtained after the Monte Carlo-search.*

Finally, the situation of modelling with one layer more than the true model will be considered.
In other words, a true structure consisting of two layers will be modelled with three layers.
Again, a Monte Carlo-search with two different input models will be investigated. The only difference between the two input models is again the presence or absence of the extra group velocity constraint. The phase velocity uncertainties allowed are for both cases 1%. The receiver function absolute value uncertainty is again 0.05. When the group velocity constraint is added to the joint inversion (which results in figure 27 below), the allowed uncertainties for the group velocities are 2%. Short period phase velocity data is used (8-43 s). The allowed velocity variations are ± 10% for the second layer and third layer and the allowed velocity range for the first layer is from 2 till 3.8 km/s. The accepted discontinuity depth variations are ± 10%.
Figure 26 shows the results of a Monte Carlo-search when only phase velocity and receiver function constraints are used. Figure 27 presents the results when in addition to the phase velocity data and the receiver function data, also group velocity data was used. When comparing the results of the two input models (visible in figures 26 and 27), a very clear improvement in the upper and lower crustal shear wave velocities is recognizable when adding the group velocity constraint (see figure 27). Where in the case of modelling with one layer less, especially the lower crustal velocity was improved by the additional group velocity constraint, in this case also the upper crustal shear wave velocity is enormously enhanced. Again, no clear improved discontinuity depths are observable and, in correspondence to that, the receiver functions do not fit the data better when the group velocity constraint is added to the joint inversion.
What can be concluded from this, is that when modelling with one layer more than the number of layers of the true structure, the obtained shear wave velocity structure is much more reliable when in addition to the joint inversion of phase velocity dispersion data and receiver function data also group velocity dispersion data is taken into account. This conclusion also holds for the case of modelling with one layer less than the number of layers of the true structure. However, for this case reasonable results were already obtained with the use of only phase velocity dispersion data and receiver function data. In contrast, when modelling with one layer more than the true structure, the obtained shear wave velocity structure was not so reliable when only phase velocity dispersion data and receiver function data were used in the joint inversion.

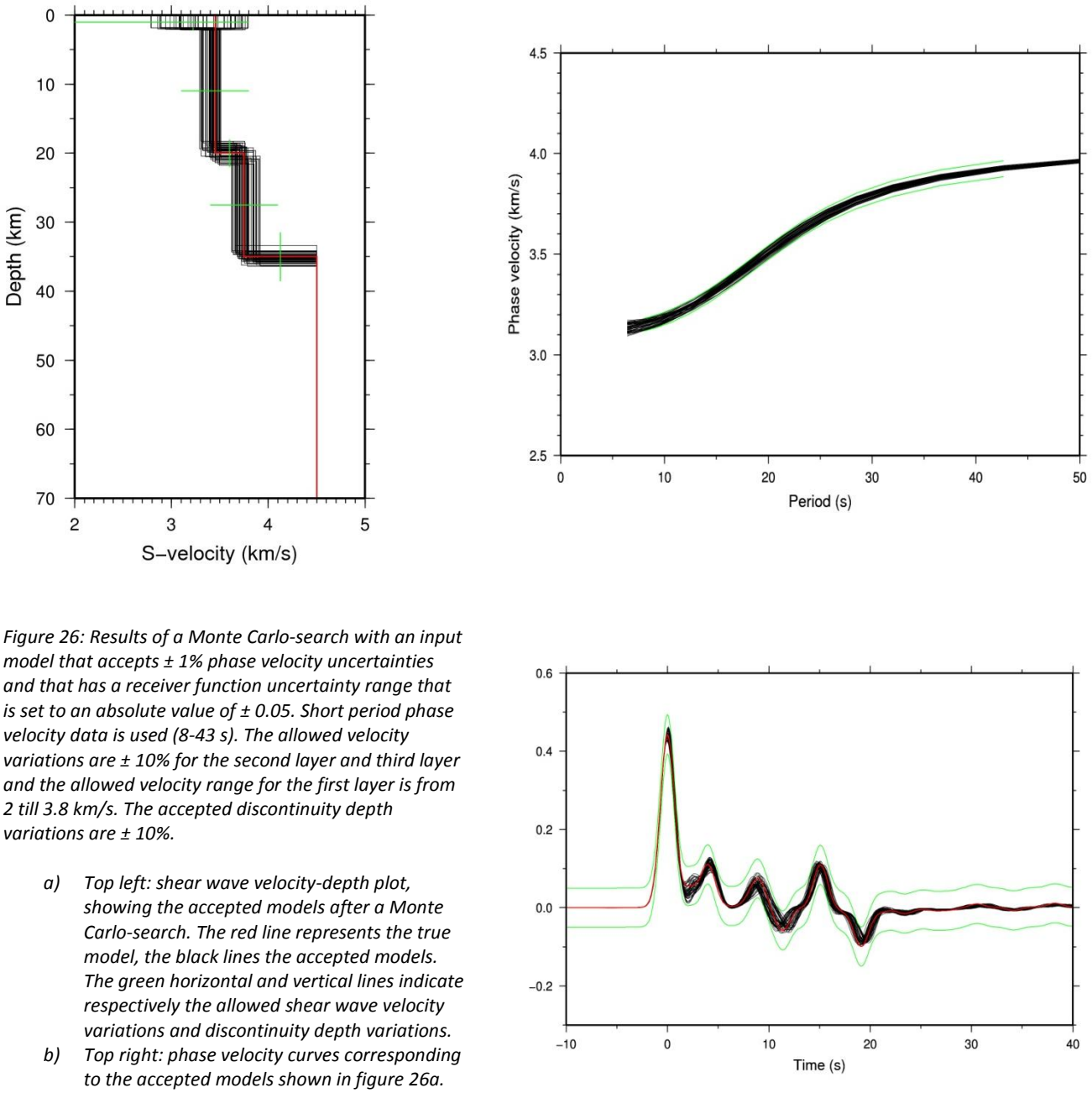

Figure 26: Results of a Monte Carlo-search with an input model that accepts ± 1% phase velocity uncertainties and that has a receiver function uncertainty range that is set to an absolute value of ± 0.05. Short period phase velocity data is used (8-43 s). The allowed velocity variations are ± 10% for the second layer and third layer and the allowed velocity range for the first layer is from 2 till 3.8 km/s. The accepted discontinuity depth variations are ± 10%.

a) Top left: shear wave velocity-depth plot, showing the accepted models after a Monte Carlo-search. The red line represents the true model, the black lines the accepted models. The green horizontal and vertical lines indicate respectively the allowed shear wave velocity variations and discontinuity depth variations.

b) Top right: phase velocity curves corresponding to the accepted models shown in figure 26a. The red line indicates the true model, the black lines represent the accepted models obtained after the Monte Carlo-search. The green lines illustrate the allowed uncertainty range.

c) Lower right: Receiver functions corresponding to the accepted models shown of figure 26a. The red line indicates the true model, the black lines represent the accepted models obtained after the Monte Carlo-search.

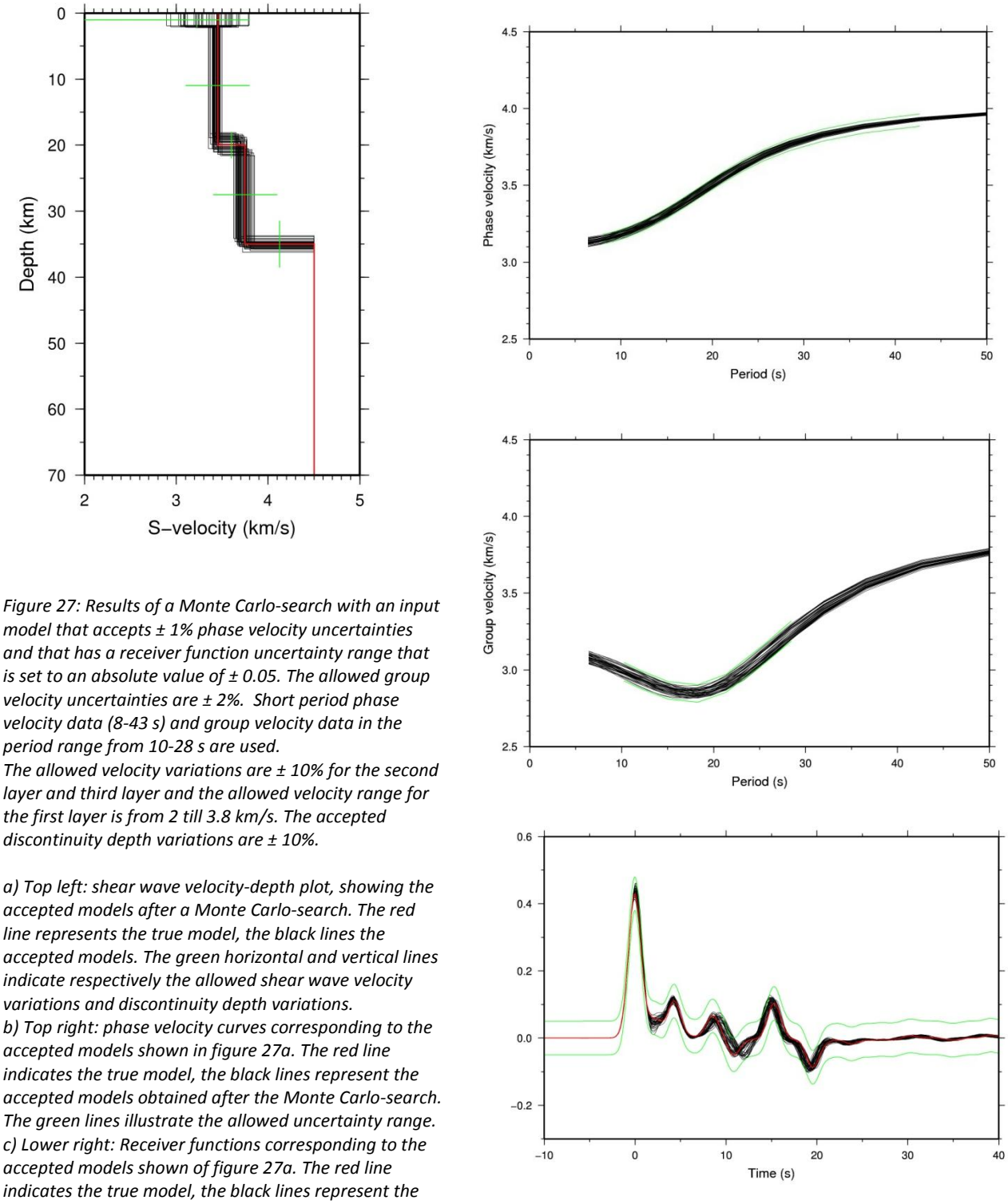

Figure 27: Results of a Monte Carlo-search with an input model that accepts ± 1% phase velocity uncertainties and that has a receiver function uncertainty range that is set to an absolute value of ± 0.05. The allowed group velocity uncertainties are ± 2%. Short period phase velocity data (8-43 s) and group velocity data in the period range from 10-28 s are used.
The allowed velocity variations are ± 10% for the second layer and third layer and the allowed velocity range for the first layer is from 2 till 3.8 km/s. The accepted discontinuity depth variations are ± 10%.

a) Top left: shear wave velocity-depth plot, showing the accepted models after a Monte Carlo-search. The red line represents the true model, the black lines the accepted models. The green horizontal and vertical lines indicate respectively the allowed shear wave velocity variations and discontinuity depth variations.
b) Top right: phase velocity curves corresponding to the accepted models shown in figure 27a. The red line indicates the true model, the black lines represent the accepted models obtained after the Monte Carlo-search. The green lines illustrate the allowed uncertainty range.
c) Lower right: Receiver functions corresponding to the accepted models shown of figure 27a. The red line indicates the true model, the black lines represent the accepted models obtained after the Monte Carlo-search.

Results iterative linearized least-squares inversion with phase velocity dispersion data and receiver functions

As already mentioned in the introduction, especially the receiver function inverse problem is known to be highly non-linear. *Ammon et al. (1990)* performed several synthetic tests. Their results clearly showed that the final models were dependent on the initial models, which indicates the high non-linearity of the receiver function inverse problem. In the case of such a problem, the Monte Carlo approach is in general better, due to the fact that a Monte Carlo-search results in several models that indicate the trend. In the case of the iterative linearized least-squares inversion, only one 'final' model is obtained (which is dependent on the initial model). Nevertheless, the inverse problem is often tackled using such a linearized inversion. This, due to the simplicity of implementation of the associated forward problem (*Harland et al., 2009*). Furthermore, it is much faster than the Monte Carlo-search.
As mentioned before, several parameters can be changed, e.g. weights of the different residual vectors (phase velocity vs. receiver function), applying damping or not and so on.

The dependence of the end-result on the initial model, as shown by *Ammon (1990)* is clearly visible in figures 28 and 29. Again, a 'true' three-layered crustal model (sedimentary layer, upper-crust and lower-crust) over a half-space (mantle) is considered. Short period phase velocity data is used (8-43 s) and the part of the receiver function considered in this study is again from 0 till 25 s. The two different starting models both have a Vp/Vs ratio of 1.78. When the initial model is changed, the end-result is also significantly different. This is a consequence of the non-linearity of the joint-inverse problem, and especially of the receiver function inversion part. The phase velocity inverse problem is also non-linear, but to a less great extent. This amount of non-linearity is already reflected by comparing the shape of the phase velocity curve with the shape of the receiver function: a receiver function has much more peaks and troughs (a much more irregular shape), which results in a greater non-linearity (the higher-frequency a receiver function is, the greater the non-linearity). The phase velocity curve, in contrast, has a quite smooth shape.
Important to note is that for both the examples shown in figures 28 and 29, the obtained end-models do not meet the data well enough (i.e. the synthetic data corresponding to the obtained end-model, does not fit the different datasets within the uncertainty bounds set). So, the final models do not represent the true structure well enough in both cases (in other words are not so reliable). However, the obtained shear wave velocity structure resembles the true structure quite well in both cases.
Furthermore, most parts of the data sets do fit the true data reasonably well (especially the data sets

of figure 29 are almost perfectly matched within the uncertainty bounds set). So, based upon that, the retrieved models can still provide some useful information on the shear wave velocity structure. However, care must still be taken when interpreting such obtained final models.

The receiver function problem also suffers greatly from non-uniqueness issues *(Ammon, 1990)*. Non-uniqueness can be best explained as the problem that properties of an Earth model can be varied without the consequence of worsening the fit to the observed data. In other words, a different shear-wave velocity model yields roughly the same data fit. So, when jointly inverting the phase velocity data and the receiver function data, the final result can be a shear wave velocity model that does not per definition represent the 'true' velocity structure. As already mentioned above, the problem of non-uniqueness can be better solved using a Monte Carlo-search, due to the fact that this results in several accepted models from which the general trend of the shear wave velocity structure can be

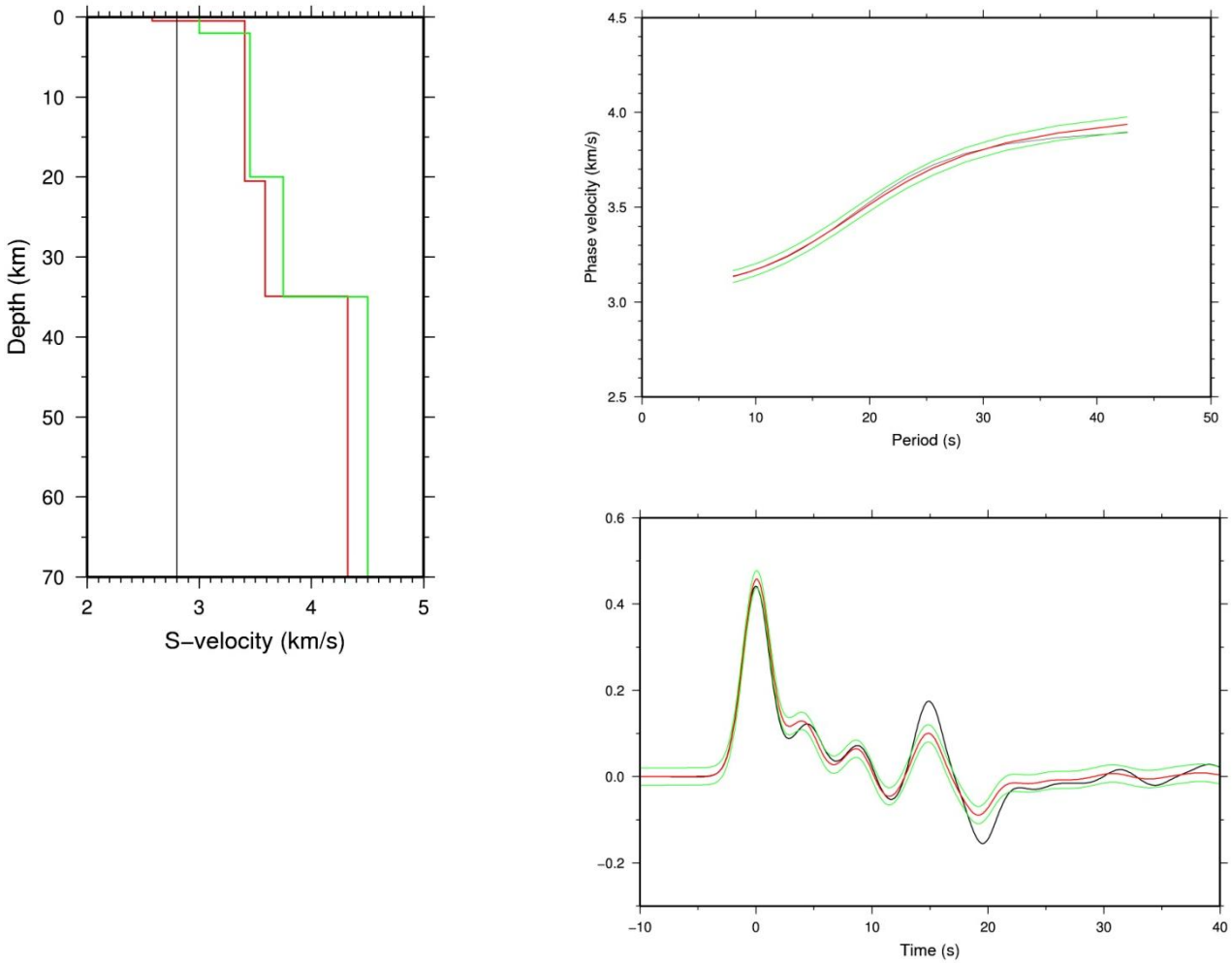

Figure 28:

- *a) Top left: shear wave velocity-depth plot, obtained with an iterative linearized least-squares inversion. The green line represents the true model, the red line the final end-model. The black line illustrates the starting model, which has a Vp/Vs ratio of 1.78.*
- *b) Top right: phase velocity curve corresponding to the obtained model shown in figure 28a. The red line indicates the true model, the black line represents the final end-model. The green lines illustrate the allowed uncertainty range (±1%).*
- *c) Lower right: Receiver functions corresponding to the accepted models shown of figure 28a. The red line indicates the true model, the black line represents the final end-model. The green lines illustrate the allowed uncertainty range (±0.02).*

derived. Due to the non-linearity of the joint-inverse problem, in particular the receiver function inverse problem, the iterative linearized least-squares inversion can suffer from solutions that become 'trapped' in local minima of the objective function.

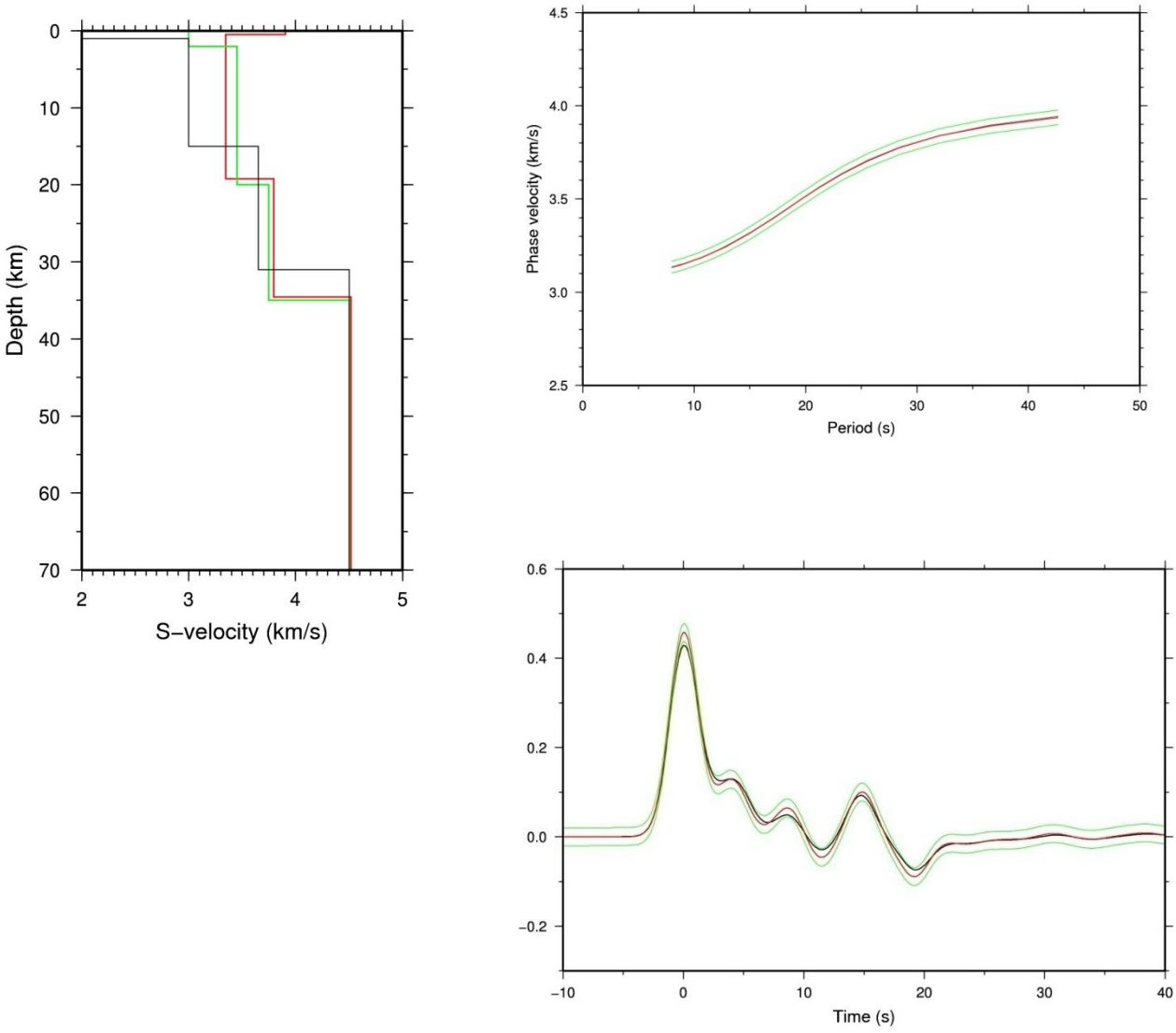

Figure 29:

- *a) Top left: shear wave velocity-depth plot, obtained with an iterative linearized least-squares inversion. The green line represents the true model, the red line the final end-model. The black line illustrates the starting model, which has Vp/Vs ratios for the different layers of 1.78 (for the upper mantle the Vp/Vs ratio is 1.8).*
- *b) Top right: phase velocity curve corresponding to the obtained model shown in figure 29a. The red line indicates the true model, the black line represents the final end-model. The green lines illustrate the allowed uncertainty range (±1%).*
- *c) Lower right: Receiver functions corresponding to the accepted models shown of figure 29a. The red line indicates the true model, the black line represents the final end-model. The green lines illustrate the allowed uncertainty range (±0.02).*

During this study, it was tried to develop a general approach to tackle the problem of solutions that become 'trapped' in local minima of the objective function as best as possible. In other words, to develop an approach that yields quite reliable results, despite the unfortunate fact that the final result is often still a solution trapped in a local minimum.

During this development of a general approach, different situations with different starting models and changed parameters were closely investigated. Examples of changing the parameters are: putting different weights on the different residual vectors, applying damping or not, varying the time of the receiver functions over which the misfit is calculated and varying the Gaussian scale a in the input for the program 'pwaveqn' (which performs the source equalization procedure for the receiver function data). The model parameterization during the iterative linearized least-squares inversion could also be varied. However, in this study only layers, or combinations of layers were used for the parameterization. Other basis functions were also investigated, but did not seem to improve the final result.

Vp/Vs ratio

As mentioned above, the basis of investigating the non-linear inversion was formed by changing the shear wave velocities and discontinuity depths of the reference models (starting models). As is visible in figures 28 and 29 above, it does not really matter whether a reference model which lies closer to the real model and has already a three-layered structure over a half-space (figure 29), or a reference model which has a constant crustal and upper mantle velocity (in this case 2800 m/s, see figure 28) was used. However, when a very good reference model is used (for example one or more shear wave velocities (almost) identical to the true shear wave velocity for that part of the structure), an almost perfect final result can be obtained, as visible in figure 30. The reference model used in this iterative linearized least-squares inversion had Vp/Vs ratios for the different layers varying around √3, except for the upper mantle where the Vp/Vs ratio is 1.8. But not the shear wave velocity values or discontinuity depths themselves play the most important role. The main parameter controlling whether the final solution approaches the 'true' structure close or not, seems to be the Vp/Vs ratio. The importance of this parameter was yet discovered, when performing the iterative linearized least-squares inversion. Due to lack of time, this parameter could not be (further) investigated in the Monte Carlo-search.

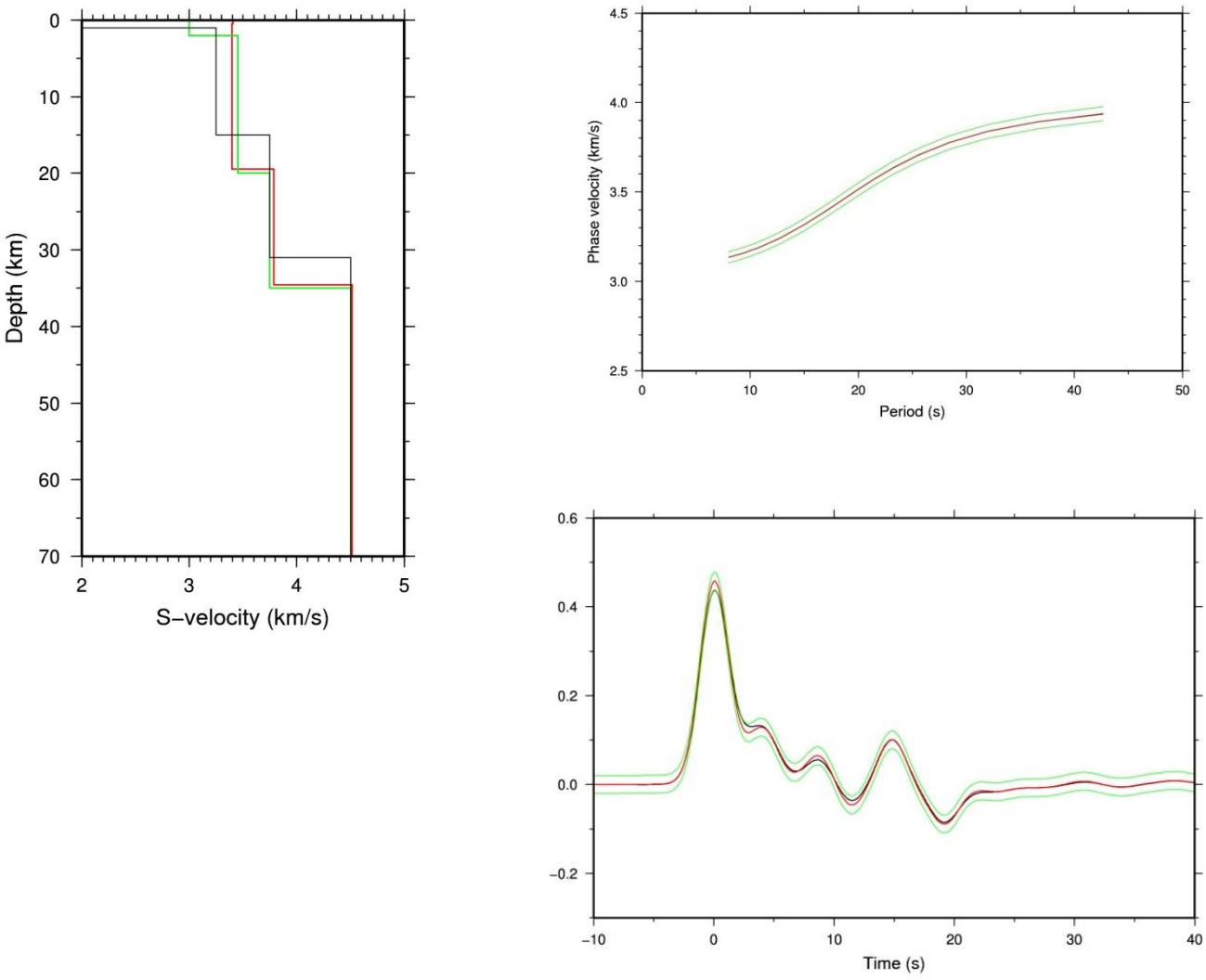

Figure 30:

- *a) Top left: shear wave velocity-depth plot, obtained with an iterative linearized least-squares inversion. The green line represents the true model, the red line the final end-model. The black line illustrates the starting model, which has Vp/Vs ratios for the different layers varying around √3 except for the upper mantle where the Vp/Vs ratio is 1.8.*
- *b) Top right: phase velocity curve corresponding to the obtained model shown in figure 29a. The red line indicates the true model, the black line represents the final end-model. The green lines illustrate the allowed uncertainty range (±1%).*
- *c) Lower right: Receiver functions corresponding to the accepted models shown of figure 29a. The red line indicates the true model, the black line represents the final end-model. The green lines illustrate the allowed uncertainty range (±0.02).*

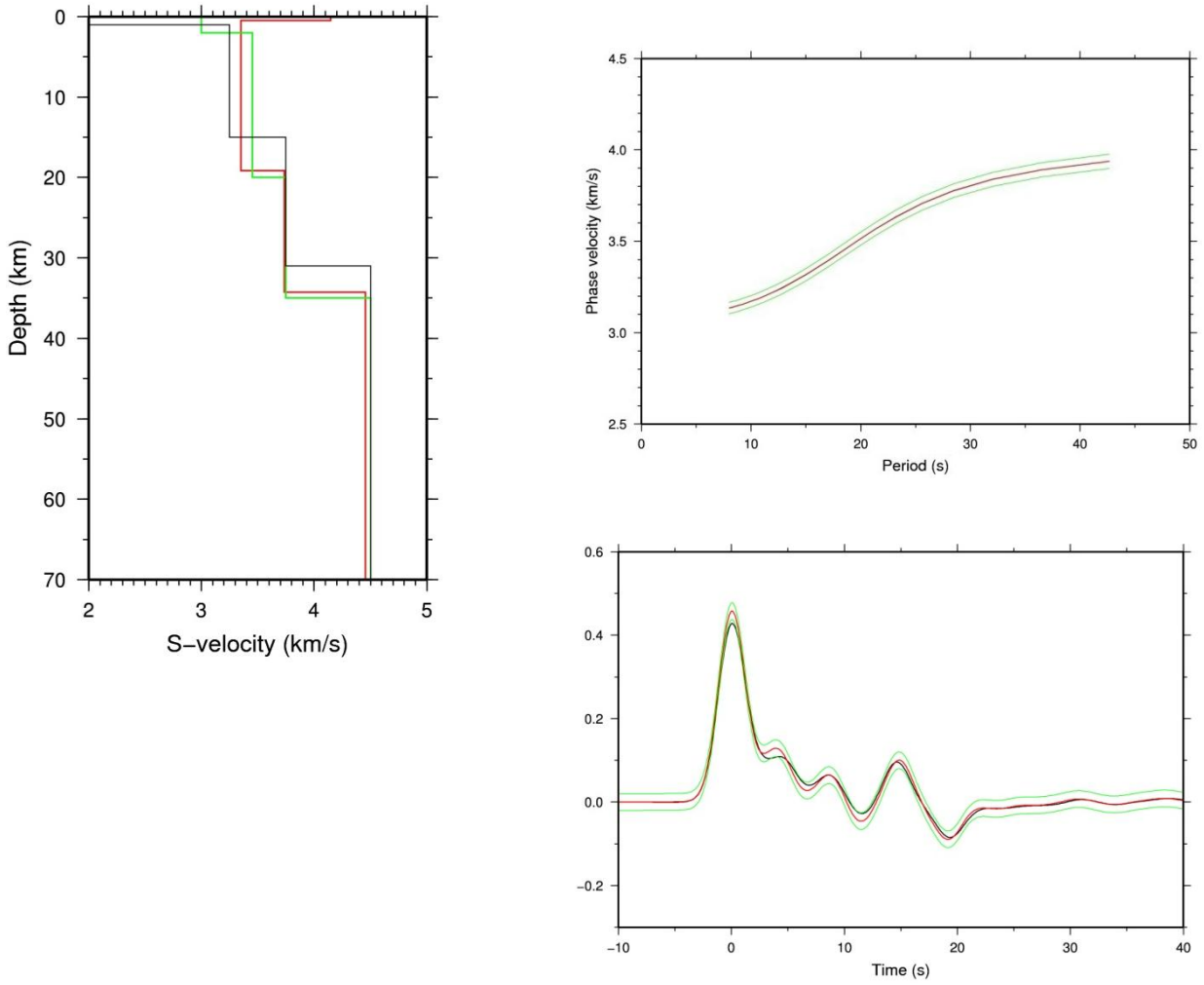

Figure 31:

- *a) Top left: shear wave velocity-depth plot, obtained with an iterative linearized least-squares inversion. The green line represents the true model, the red line the final end-model. The black line illustrates the starting model, which has Vp/Vs ratios of about √3 except for the lower crust where the Vp/Vs ratio is 2 and the upper mantle where the Vp/Vs ratio is 1.8.*
- *b) Top right: phase velocity curve corresponding to the obtained model shown in figure 30a. The red line indicates the true model, the black line represents the final end-model. The green lines illustrate the allowed uncertainty range (±1%).*
- *c) Lower right: Receiver functions corresponding to the accepted models shown of figure 30a. The red line indicates the true model, the black line represents the final end-model. The green lines illustrate the allowed uncertainty range (±0.02).*

The importance of the Vp/Vs ratio can be clearly observed when comparing figures 30 and 31. As has been shown above, the starting model of figure 30 results in an almost perfect final result. However, when the same starting model is used as in figure 30, but a non-realistic Vp/Vs ratio is chosen for only the lower crust (a Vp/Vs ratio of 2), it can be clearly seen in figure 31 that this results in a completely different, not so reliable end-result.
This is also a clear example of non-uniqueness. The figures with the phase velocity curves and receiver functions show again an almost perfect data fit. Nevertheless, comparing the obtained shear wave velocity structure with the structure of figure 30, significant differences can be observed.

When the same starting model is chosen as in figure 28, but now with a non-realistic Vp/Vs ratio of 2 (instead of the Vp/Vs ratio of 1.78 of figure 28) the importance of the Vp/Vs ratio is illustrated further. The iterative linearized least-squares inversion does not converge when a Vp/Vs ratio of 2 is used for the starting model.

Concluding, it can be stated that the choice of the starting model does play a role, but the most important part is formed by the Vp/Vs ratio of the starting model. Using a constant shear wave velocity as a reference model has as the advantage that it makes the modelling procedure easier. Furthermore, the focus then lies especially on the effects of a changing Vp/Vs ratio on the data fit. This is desirable, because of the above illustrated relatively high importance of the Vp/Vs ratio on the obtained final result. However, when having reliable a priori information about an indication of the values of the shear wave velocities at the location of interest, using a reference model with these values could result in a better final solution.

Damping

In addition to investigating the different starting models, the application of damping was studied. Damping has as a result that the iterative linearized least-squares inversion tries to find a final result that lies relatively close to the starting model. When a starting model is used with a constant shear wave velocity (which does not resemble the true Earth well), damping towards the reference model is totally unwanted. However, when a quite reliable starting model is chosen, damping can be desirable in a way that it can improve the obtained final end-solution. Nevertheless, for the starting models investigated in this study, no pronounced positive effects of damping on the obtained final result were noticed.

General approach developed

To obtain a good final model, a good fit of the phase velocity data and receiver function data is required. However, the joint inverse problem is highly non-linear which makes obtaining a good final model quite difficult. Therefore, it is tried to make the non-linear inverse problem as linear as possible. As mentioned before, the phase velocity data is less non-linear than the receiver function data. The Rayleigh wave phase velocity dispersion data determines the absolute shear wave velocity values quite well, but has no sensitivity to the shear wave velocity contrasts (i.e. discontinuities). Due to the fact that the phase velocity data is less non-linear than the receiver function data, more weight should be put on the phase velocity data in order to make the inverse problem more linear.

Recapitulating, the total normalized misfit function is given by:

$S_{total} = w_{recfn} S_{recfn} + w_{phasevel} S_{phasevel} + w_{groupvel} S_{groupvel}$, where *w* accounts for the relative weights of respectively the receiver function misfit, the phase velocity misfit and the group velocity misfit. *S* represents the normalized misfit function for the receiver function data, the phase velocity data and the group velocity data (see section 'Methods'), respectively.

As mentioned before, lower-frequency receiver functions are more smooth than higher-frequency receiver functions and therefore less non-linear. As discussed earlier in the section 'Methods' the low-pass Gaussian filter G(ω) removes high-frequency noise in the receiver functions. The Gaussian filter-width parameter *a* controls the frequency content. So, in order to make the inverse problem as linear as possible, smaller values for the Gaussian filter-width parameter *a* can be chosen for calculating the receiver function. When for example changing *a* from 1.0 to 0.6, this has as a consequence that G(ω) has decayed to a value of 0.1 for a frequency of about 0.3 Hz (instead of 0.5 Hz for an *a* of 1.0).

This strategy was followed and implemented in the way described below, which led to the development of a certain 'general approach' to tackle the non-linearity and non-uniqueness problems of the iterative linearized least-squares inversion as best as possible.

In order to be able to focus on the importance of the Vp/Vs ratio (i.e. for example to be able to try different Vp/Vs ratios easily and to study their effects clearly), constant shear wave velocity starting models were used to develop the general approach.

The best approach seems to be, to first fit the less non-linear phase velocity data as best as possible, but simultaneously try to fit the receiver function data reasonably well.

To enhance the chance of succeeding, the first step of the iterative linearized least-squares inversion was set-up in such a way, that it used lower frequency receiver function data (the Gaussian scale 'a' was changed from 1.0 to 0.6). This because, as discussed above, the lower frequency receiver function data is also less non-linear, which enhances the chance of getting a good data fit.

By putting relatively more weight on the phase velocity residual than on the receiver function residual (respectively 1:1/5), the goal of fitting especially the phase velocity data and also the receiver function reasonably, is generally achieved.

However, different weights can be investigated, thereby focusing on the effects on the data fit. In other words, by looking at the end-result fits of the phase velocity curves and the receiver functions, logical decisions could be made with respect to putting more weight on either the phase velocity residual or the receiver function residual.

The next step is to use the in this way obtained best final result as the reference model for the next iterative linearized least-squares inversion. This time, the Gaussian scale 'a' was set to 1.0, which results in higher frequency receiver functions.

In general, more weight is now desired on the receiver functions. So again, different relative weights of the residuals are studied, looking closely at the effects on the data fit. In addition, care must be taken that the shear wave velocity structure obtained until now does not change extremely. Because when it changes too extremely, this can be a clear indication that a possible improvement in the data fit does not have beneficial effects on the shear wave structure. This brings us again to the point that a better data fit not always results in a better shear wave velocity-depth plot. All these effects give a clear indication of the next weight distribution that should be investigated.

However, when no clear improvements of the data fit are visible, and the inversion stops in general rapidly, this can be an indication that the final result is reached (whether it is a solution that has become trapped in a local minima or not). To be really sure that the final solution is reached, extreme weights can be put on either the phase velocity residual or the receiver function residual (respectively 1:0 or 0:1). When the data fits do not change in these cases, and the inversion stops

rapidly, the final solution is almost certainly obtained. When the data fits corresponding to this final solution are not as good as desired, another starting model can be investigated (with a different Vp/Vs ratio or different shear wave velocity values). A schematic overview of the 'general approach' is visible in the flowchart below (figure 32).

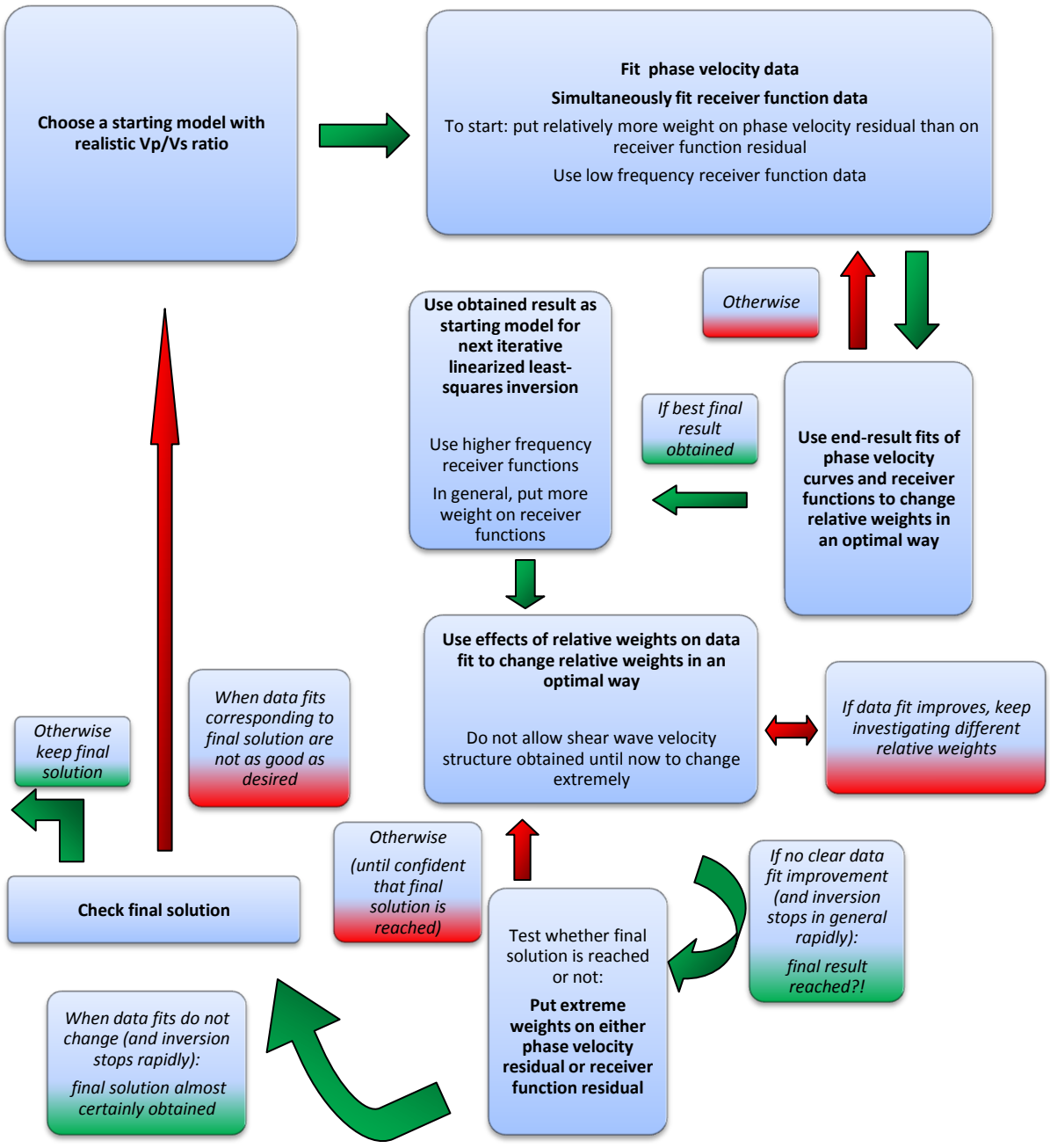

Figure 32: Flowchart showing a schematic overview of the developed 'general approach'.

With this approach, several solutions that seem at first hand trapped in a local minimum can come out of this local minimum. In other words, the difficulty of the non-linearity of the inverse problem is solved quite well by this approach. Unfortunately, the local minima are not always solved. In addition to this, as discussed earlier, changing the relative weights of the phase velocity and receiver function residuals improve certain parts of the shear wave velocity structure. However, there is a certain trade-off between either improving the upper crustal and upper mantle shear wave velocity values, or improving the lower crustal shear wave velocity value (and the discontinuities).
Furthermore, the end-result is still very dependent on the initial starting model (its absolute shear wave velocity values and its Vp/Vs ratio). That is why the shear wave velocity structure is not always resolved well. Another big problem is caused by the fact that a better data fit not always results in a better retrieved shear wave velocity structure. Unfortunately, the problem of non-uniqueness, as shown before, still remains.

Iterative linearized least-squares inversion with many layers

The approach of the iterative linearized least-squares inversion used in this study is completely different from the approach done e.g. in studies by *Julia et al. (2000) and Julia et al. (2008).*
Julia (2000) uses multi-layer synthetic modelling in the iterative linearized least-squares inversion. In contrast, in this study only a couple of layers (three layers over a half-space) are used for the synthetic modelling. Despite the fact that *Julia et al. (2000)*, obtains quite reasonable results after smoothing, several critical remarks can be made on their approach. To test their approach, an iterative linearized least-squares inversion was performed with a starting model that is shown in black in figure 33a. For the synthetic modelling, 18 layers were used (as visible in red in figure 33a). As can be seen in figure 33a, large discontinuities are visible in the final solution, where they are not present in the 'true' shear wave velocity model. Furthermore, the Moho discontinuity is retrieved completely wrong, despite the almost perfect data fit for both data sets (figures 33b and 33c). So, when the 'true' model is not known (which is off course the case dealing with the real Earth), a good interpretation of this end result is hardly possible. No smoothing or damping was applied to the shown results, but applying this does not influence the critical remarks stated above.
As has been demonstrated by the results of this study, the approach of modelling with only a few layers yields end-structures in which the main discontinuities are clearly recognizable. Furthermore, the values of the shear wave velocities are retrieved quite nicely. With a good reference model, the final result was in some cases even almost identical to the real structure (see figure 29). In addition, more stable results were found when modelling with only a few layers. The worse result of modelling with more layers was also already illustrated by the results of the Monte Carlo-search, when

modelling was done with only one layer more than the total number of layers of the 'true' structure. Concluding, it can be stated that modelling with only a few layers is preferable above modelling with many layers in combination with smoothing.

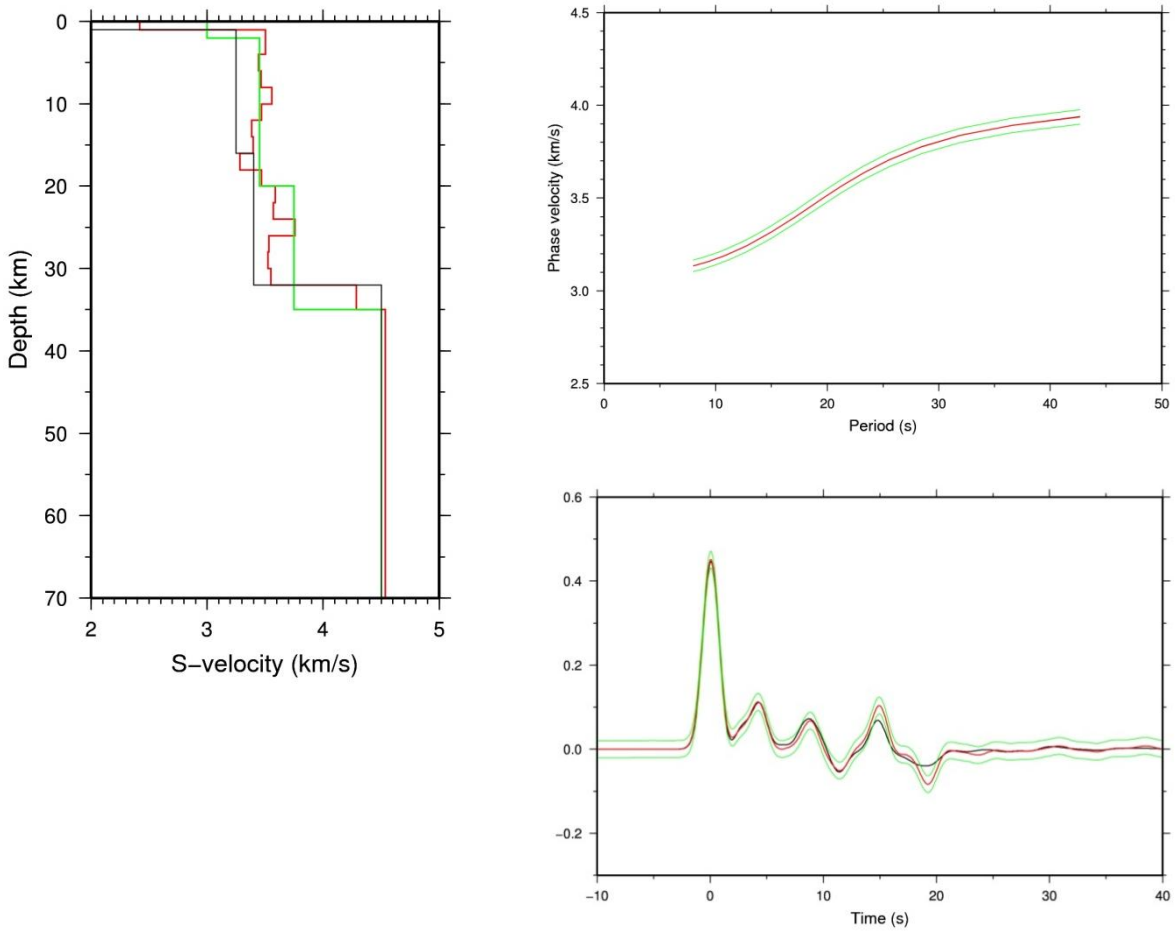

Figure 33:

- *a) Top left: shear wave velocity-depth plot, obtained with an iterative linearized least-squares inversion. The green line represents the true model, the red line the final end-model. The black line illustrates the starting model.*
- *b) Top right: phase velocity curve corresponding to the obtained model shown in Figure 33a. The red line indicates the true model, the black line represents the final end-model. The green lines illustrate the allowed uncertainty range (±1%).*
- *c) Lower right: Receiver functions corresponding to the accepted models shown of Figure 33a. The red line indicates the true model, the black line represents the final end-model. The green lines illustrate the allowed uncertainty range (±0.02).*

The above figure 33 shows also a clear example of the non-uniqueness problems encountered during the joint-inversion of phase velocity dispersion data and receiver function data: a perfect fit of the phase velocity data and receiver function data is obtained with the iterative linearized least-squares inversion, but the retrieved shear wave velocity structure differs significantly from the 'true' shear wave velocity structure, drawn in green. Or in other words, roughly the same data fit produces completely different end-results.

Iterative linearized least-squares inversion with phase velocity dispersion data, receiver functions and group velocity dispersion data

When adding group velocity dispersion data to the joint inversion, the general approach described in the last section had to be slightly modified.

Again, the first part of the iterative linearized least-squares inversion uses a Gaussian scale ´a´ of 0.6 (i.e. low-frequency receiver functions). Two approaches of adding the group velocity constraints are feasible. The first approach adds the group velocity constraint to the inversion, when the Gaussian scale ´a´ is changed to 1.0 (higher-frequency receiver functions). The alternative is to take the group velocity data already in consideration at the start of the iterative linearized least-squares inversion with the low-frequency receiver functions. In general, the best approach is to start in both situations with weights for the group velocity residual that lie between the weights for the phase velocity residual and the receiver function residual. Recapitulating, the total normalized misfit function is given by: $S_{total} = w_{recfn} S_{recfn} + w_{phasevel} S_{phasevel} + w_{groupvel} S_{groupvel}$, where *w* accounts for the relative weights of respectively the receiver function misfit, the phase velocity misfit and the group velocity misfit. *S* represents the normalized misfit function for the receiver function data, the phase velocity data and the group velocity data (see section 'Methods'), respectively. An example of a good starting weight distribution is: $w_{phasevel} = 1$, $w_{groupvel} = ½$ and $w_{recfn}=1/5$.

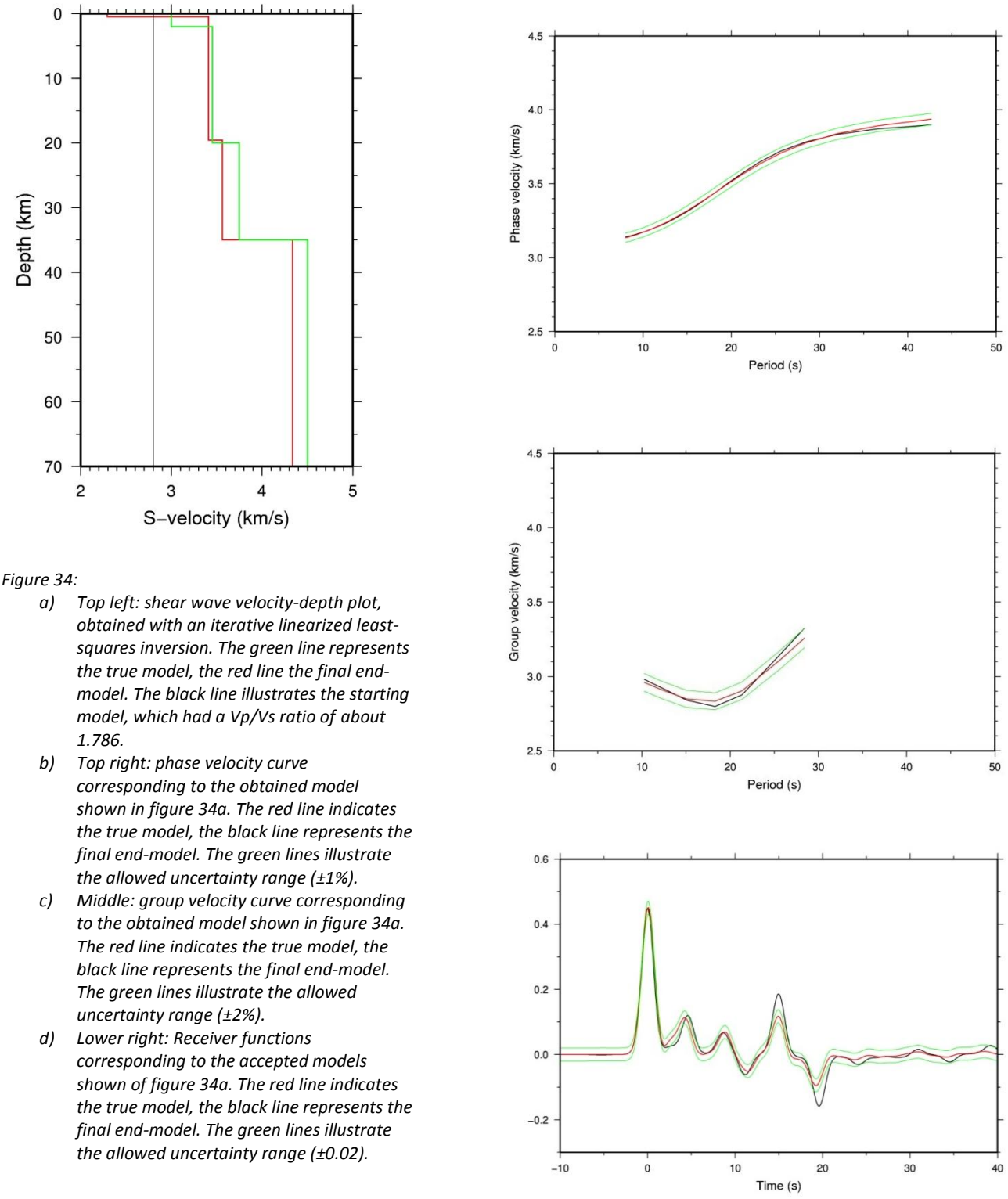

Figure 34:

- *a) Top left: shear wave velocity-depth plot, obtained with an iterative linearized least-squares inversion. The green line represents the true model, the red line the final end-model. The black line illustrates the starting model, which had a Vp/Vs ratio of about 1.786.*
- *b) Top right: phase velocity curve corresponding to the obtained model shown in figure 34a. The red line indicates the true model, the black line represents the final end-model. The green lines illustrate the allowed uncertainty range (±1%).*
- *c) Middle: group velocity curve corresponding to the obtained model shown in figure 34a. The red line indicates the true model, the black line represents the final end-model. The green lines illustrate the allowed uncertainty range (±2%).*
- *d) Lower right: Receiver functions corresponding to the accepted models shown of figure 34a. The red line indicates the true model, the black line represents the final end-model. The green lines illustrate the allowed uncertainty range (±0.02).*

Figure 34 above shows the final result of an iterative linearized least-squares inversion, where the group velocity constraint is added when the Gaussian scale ´a´ is changed to 1.0 (i.e. only a group velocity constraint when the higher-frequency receiver functions are used). A constant shear wave velocity model was used with a Vp of 5000 m/s and a Vs of 2800 m/s, which results in a Vp/Vs ratio of 1.786 (which corresponds to the Vp/Vs ratio of the 'true' model). This Vp/Vs ratio was used for both the approach of figure 34 and the approach of figure 35. As can be observed, the phase velocity data, group velocity data and receiver function data are not matched within the uncertainty bounds

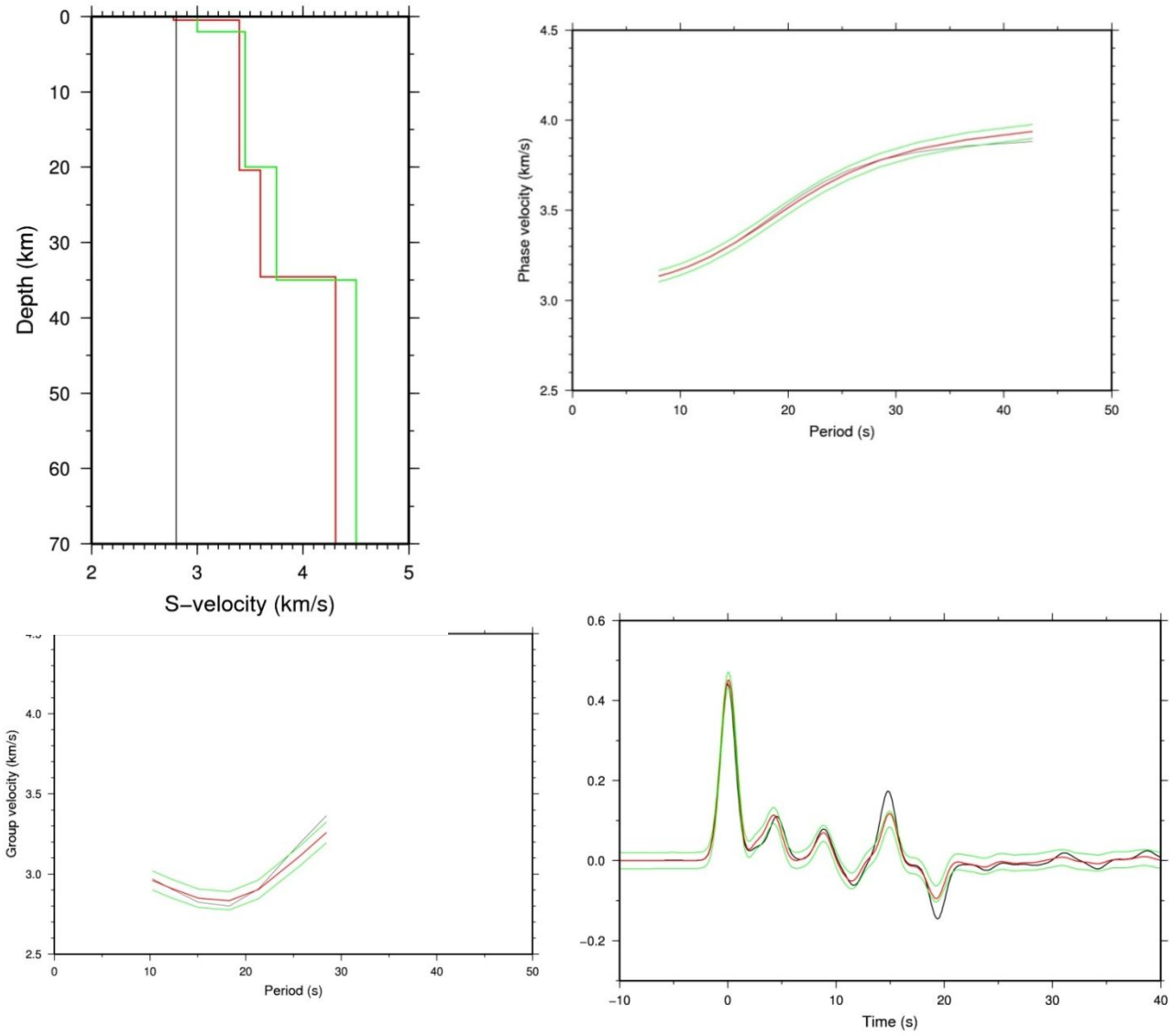

Figure 35:

- *a) Top left: shear wave velocity-depth plot, obtained with an iterative linearized least-squares inversion. The green line represents the true model, the red line the final end-model. The black line illustrates the starting model, which had a Vp/Vs ratio of about 1.786.*
- *b) Top right: phase velocity curve corresponding to the obtained model shown in figure 35a. The red line indicates the true model, the black line represents the final end-model. The green lines illustrate the allowed uncertainty range (±1%).*
- *c) Lower left: group velocity curve corresponding to the obtained model shown in figure 35a. The red line indicates the true model, the black line represents the final end-model. The green lines illustrate the allowed uncertainty range (±2%).*
- *d) Lower right: Receiver functions corresponding to the accepted models shown of figure 35a. The red line indicates the true model, the black line represents the final end-model. The green lines illustrate the allowed uncertainty range (±0.02).*

set. So, this implies that the obtained final model is not very reliable. This observation can also be made when looking at figure 35. So, the obtained final models are in both cases not very reliable (based upon the data fit). However, the obtained shear wave velocity structure resembles the true structure quite well in both cases. Furthermore, most parts of the three different data sets do fit the true data reasonably well. So, based upon that, the retrieved models can still provide some useful information on the shear wave velocity structure. However, care must still be taken when interpreting the obtained final models.
Comparing the approach that resulted in figure 34 with the alternative approach of taking the group velocity constraint into account from the beginning (results shown in figure 35), some small differences can be noticed, especially looking at the shear wave velocity-depth plots. The approach of figure 34 seems to have resolved the discontinuities a bit better. This can be explained by the fact that the synthetic receiver function of this approach, fits the data slightly better in this case. However, the results of model runs with other reference models, have shown that the approach of figure 35 yields the best results.
No clear conclusion about which approach is best can be drawn on the basis of the model runs performed in this study. The author's personal preference lies on the approach of figure 35, i.e. including the group velocity constraint already in the inversion with the low-frequency receiver functions. Which of these two approaches is chosen does not really matter, as long as the focus lies on the main steps of the general approach (i.e. investigate different weights, thereby focusing on the effects on the data fit).

Now, the results shown above are compared with the situation of the joint inversion with only phase velocity dispersion data and receiver function data (results are shown in figure 36 below). Again, a constant shear wave velocity model was used with a Vp of 5000 m/s and a Vs of 2800 m/s, which results in a Vp/Vs ratio of 1.786 (which corresponds to the Vp/Vs ratio of the 'true' model). The shear wave velocity-depth plot of figure 36 is the final result obtained with the general approach. The solution is trapped in a local minimum. Again, the phase velocity data and receiver function data are not matched within the uncertainty bounds set. This makes the final model unreliable. As can be seen when comparing this plot with the ones where the group velocity dispersion data is also used in de joint inversion, it can be seen that then the shear wave velocity structure is a little bit better resolved. The discontinuities are better retrieved (the receiver function data fit is improved by adding the group velocity constraint), and also an improved upper crustal shear wave velocity is visible (see figure 34). The results shown in figures 34, 35 and 36 are also a clear example of the non-uniqueness of this joint inverse problem. Looking at the phase velocity, group velocity and receiver function data,

roughly the same data fit is recognizable (except for very small differences). The obtained shear wave velocity structure however does differ significantly. Furthermore, the non-linearity problem of the joint inverse problem is also illustrated by these figures. The solution of the joint inversion of figure 36 is clearly trapped in a local minimum.

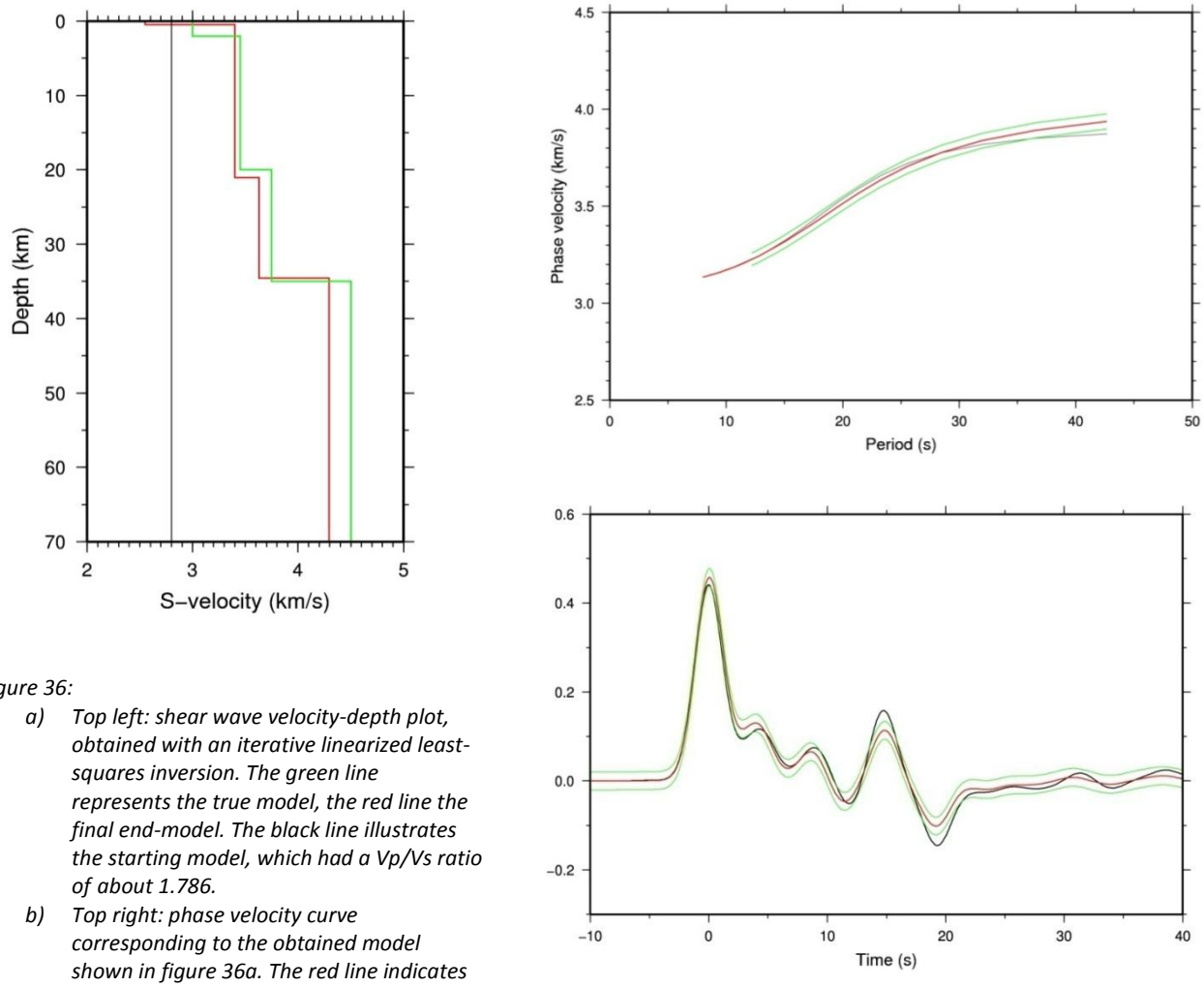

Figure 36:

- *a) Top left: shear wave velocity-depth plot, obtained with an iterative linearized least-squares inversion. The green line represents the true model, the red line the final end-model. The black line illustrates the starting model, which had a Vp/Vs ratio of about 1.786.*
- *b) Top right: phase velocity curve corresponding to the obtained model shown in figure 36a. The red line indicates the true model, the black line represents the final end-model. The green lines illustrate the allowed uncertainty range (±1%).*
- *c) Lower right: Receiver functions corresponding to the accepted models shown of figure 36a. The red line indicates the true model, the black line represents the final end-model. The green lines illustrate the allowed uncertainty range (±0.02).*

The fact that in all cases the upper-mantle shear wave velocity is not obtained perfectly, has to do with the bad data fit at the greater periods of the phase velocity curve and group velocity curve. As has been seen during this study, whenever this part of the dispersion curves improves, the upper-mantle shear wave velocity improves as well. During the application of the general approach on the iterative linearized least-squares inversion with group velocity dispersion data, the following was clearly recognized: as soon as the group velocity data fit improves, the upper and lower crustal shear wave velocity also improves significantly (and as mentioned above, when the data fit at the greater periods improves, the upper-mantle shear wave velocity gets better as well). This is clearly not the case when performing a joint iterative linearized least-squares inversion without group velocity constraints. As discussed before, in this case there is a trade-off between either improving the lower crustal velocity or improving the upper-mantle velocity and the upper crustal velocity. This trade-off problem seems to be solved by adding the group velocity dispersion data to the joint inversion.

Concluding it can be stated that adding the group velocity dispersion data to the joint inversion has significant beneficial effects on the obtained shear wave velocity structure, also for the iterative linearized least-squares inversion.
An important advantage of using group velocity dispersion data as an additional constraint in the iterative linearized least-squares inversion is, that the apparent trade-off between either improving the lower crustal shear wave velocity or the upper mantle and upper crustal shear wave velocity seems to be resolved. Furthermore, it is shown that the general approach developed for the case of jointly inverting only phase velocity and receiver function data also holds for the joint inversion with the additional group velocity dispersion constraint. However, none of the results presented above show a data fit for all data sets that lies in between the uncertainty bounds set. This means, that the obtained models are not so reliable yet. However, when not using the group velocity constraints the data fit of the final model is even worse when considering the same starting models. So, the addition of the group velocity data does help the convergence towards the right model.

Conclusions

From all the results shown and discussed above, it has definitely become clear that performing a joint inversion with surface wave dispersion data and receiver function data (whether this is a Monte Carlo-search or an iterative linearized least-squares inversion), significantly improves the retrieved shear wave velocity structure. The non-uniqueness problem of the receiver functions is tackled remarkably well by this joint inversion (unfortunately the problem of non-uniqueness cannot be completely solved). Adding the group velocity dispersion data to the joint inversion improves the retrieved shear wave velocity structure even more. Nevertheless, the joint inverse problem (especially the receiver function part) remains highly non-linear. Therefore, with the iterative linearized least-squares inversion, an final solution which resembles the true shear wave velocity structure perfectly is almost impossible to obtain, even with the application of the general approach developed in this study. A Monte Carlo-search is in general the best approach, while this results in a range of possible models, that give a clear indication of the real shear wave velocity structure. However, also the iterative linearized least-squares inversion results in quite good shear wave velocity-depth plots.

When the structure is modelled with a different number of layers than the number of layers of the true structure, the shear wave velocity structure is generally less well obtained than when modelling with the exact same number of layers. Modelling with one layer less than the 'true' structure yields better results than when modelling with one layer more than the 'true' structure. The results of the latter are significantly improved when in addition to the joint inversion of phase velocity dispersion data and receiver function data also group velocity dispersion data is taken into account. This holds also for modelling with one layer less than the true structure, but for this case reasonable results were already obtained with the use of only phase velocity dispersion data and receiver function data.

The approach of the iterative linearized least-squares inversion used in this study is completely different from the approach done e.g. in studies by *Julia et al. (2000) and Julia 2008.*

Julia et al. (2000) uses multi-layer synthetic modelling in the iterative linearized least-squares inversion. In contrast, in this study only a couple of layers (3 layers over a half-space) are used for the synthetic modelling. To test the approach of *Julia et al. (2000)*, an iterative linearized least-squares inversion was performed in this study, that used 18 layers for the synthetic modelling. This obtained final model showed large discontinuities at places where they were not present in the 'true' shear wave velocity model. Furthermore, the Moho discontinuity was retrieved completely wrong, despite

the almost perfect data fit for both data sets. So, when the 'true' model is not known (which is off course the case dealing with the real Earth), a good interpretation of this end result is hardly possible.

As has been demonstrated by the results of this study, the approach of modelling with only a few layers yields end-structures in which the main discontinuities are clearly recognizable. Furthermore, the values of the shear wave velocities are retrieved quite nicely. In addition, more stable results were found when modelling with only a few layers. Concluding, it can be stated that modelling with only a few layers (the approach of this study) is preferable above modelling with many layers in combination with smoothing (the approach of e.g. *Julia et al., 2000)*.

As has become clear during the development of a general approach for the iterative linearized least-squares inversion the choice of the starting model does influence the final result obtained, but the most important influencing part is formed by the Vp/Vs ratio of the reference model. So, for many purposes, using a constant shear wave velocity starting model with a realistic Vp/Vs ratio is sufficient to obtain good shear wave velocity structures.

However, when having reliable a priori information about an indication of the values of the shear wave velocities at the location of interest, using a reference model with these values could result in a better final solution.

The importance of the Vp/Vs ratio of the starting model was yet discovered, when performing the iterative linearized least-squares inversion. Due to lack of time, this parameter could not be (further) investigated in the Monte Carlo-search.

Recommendations for future research

Due to the great influence of the Vp/Vs ratio of the reference model on the obtained final solution of the iterative linearized least-squares inversion, it should be tried to improve the obtained shear wave velocity structure by changing the programs that are used for the iterative linearized least-squares inversion (and perhaps also for the Monte Carlo-search) in such a way, that Vp is changed separately from Vs (so that it is not coupled anymore via a constant Vp/Vs ratio).
However, this introduces 4 additional parameters, which results in 11 variables instead of 7. This will definitely require a longer computation time for the Monte Carlo-search.
Another negative consequence of introducing 4 more parameters, is that the chance that the solution of the iterative linearized least-squares inversion becomes trapped in a local minimum, is enhanced. With regard to the time-span of this study, this treating of Vp as a separate variable could not yet be investigated.
Furthermore, the effects of the choice of the constant Vp/Vs ratio could be investigated further (both in the iterative linearized least-squares inversion and also in the Monte Carlo-search).
In addition to the joint inversion, other a priori (geophysical) constraints, like e.g. refraction and reflection data, could be used to solve the problem of non-uniqueness further.
Because of the fact that a Monte Carlo-search is in general the best approach for this joint inverse problem, further research should be done on improving the Monte Carlo-search technique (such that for example its computation time is shortened).

Acknowledgements

I would like to thank my supervisor Dr. J. A. M. Paulssen, for her indispensable contributions to this study. Furthermore my acknowledgement goes out to Utrecht University (the Netherlands) for making all the tools available, necessary for performing this study.

References

Aki, K., and P. G. Richards, Quantitative Seismology (2nd edition), *University Science Books*, 2002.

Ammon, C. J., G. E. Randall, and G. Zandt, On the Nonuniqueness of Receiver Function Inversions, *Journal of Geophysical Research, 95*, 15.303-15.318, 1990.

Ammon, C. J., An overview of Receiver Function Analysis, 1997
(website: http://eqseis.geosc.psu.edu/cammon/HTML/RftnDocs/rftn01.html)

Harland, K. E., R. S. White, and H. Soosalu, Crustal structure beneath the Faroe Islands from teleseismic receiver functions, *Geophysical Journal International, 177*, 115-124, 2009.

Julia, J., C. J. Ammon, R. B. Herrmann, and A. M. Correig, Joint Inversion of receiver function and surface wave dispersion observations, *Geophysical Journal International, 143,* 99-112, 2000.

Julia, J., M. Assumpção, and M. P. Rocha, Deep crustal structure of the Paraná Basin from receiver functions and Rayleigh-wave dispersion: Evidence for a fragmented cratonic root, *Journal of Geophysical Research, 113*, 2008.

Kennett, B. L. N., Seismic Wave Propagation in Stratified Media, *Cambridge University Press,* 1983.

Kennett, B. L. N., Wavenumber and wavetype coupling in laterally heterogeneous media, *Geophysical Journal Royal Astronomical Society, 87*, 313-331, 1986.

Langston, C. A., Structure under Mount Rainier, Washington, inferred from teleseismic body waves, *Journal of Geophysical Research, 84*, 4749-4762, 1979.

Lin, F-C., M. P. Moschetti and M. H. Ritzwoller, Surface wave tomography of the western United States from ambient seismic noise: Rayleigh and Love wave phase velocity maps, *Geophysical Journal International,* 2008.

Moschetti, M. P., M. H. Ritzwoller and N. M. Shapiro, Surface wave tomography of the western United States from ambient seismic noise: Rayleigh and Love wave phase velocity maps, *Geochemistry, Geophysics, Geosystems, 8,* 2007.

Nolet, G., A Breviary of Seismic Tomography – Imaging the Interior of the Earth and Sun, *Cambridge University Press, Cambridge, UK,* 2008.

Oldenburg, D. W., A comprehensive solution to the linear deconvolution problem, *Geophysical Journal Royal Astronomical Society, 65*, 331-357, 1981.

Owens T. J., G. Zandt, and S. R. Taylor, Seismic Evidence for an Ancient Rift Beneath the Cumberland Plateau, Tennessee: A Detailed Analysis of Broadband Teleseismic P Waveforms, *Journal of Geophysical Research, 89*, 7783-7795, 1984

Owens, T. J., Crustal structure of the Adirondacks determined from broadband teleseismic waveform modeling, *Journal of Geophysical Research, 92,* 6391-6401, 1987.

Owens, T. J., D. E. McNamara, G. Zandt, K. F. Priestly, and G. E. Randall, Array analysis of teleseismic receiver functions using PASSCAL Basin and Range passive-source experiment data, *Seismological Research Letters, 60*, 11, 1989.

Özalaybey, S., M. K. Savage, A. F. Sheehan, J. N. Louie, and J. N. Brune, Shear-Wave Velocity Structure in the Northern Basin and Range Province from the Combined Analysis of Receiver Functions and Surface Waves, *Bulletin of the Seismological Society of America, Vol. 87, No. 1,* 183-199, 1997.

Pollitz, F. F., and J. A. Snoke, Rayleigh-wave phase-velocity maps and three-dimensional shear velocity structure of the western US from local non-plane surface wave tomography, *Geophysical Journal International, 180*, 1153-1169, 2010.

Shibutani, T., M. Sambridge, and B. Kennett, Genetic algorithm inversion for receiver functions with application to crust and uppermost mantle structure beneath eastern Australia, *Geophysical Research Letters, 23*, 1829-1832, 1996.

Snieder, R., and J. Trampert, Inverse Problems in Geophysics, *Reprinted from 'Wavefield Inversion'*, *ed. A. Wirgin, Springer Verlag, New York*, 119-190, 1999.

Stein, S., and M. Wysession, An introduction to Seismology, Earthquakes and Earth Structure, *Blackwell Publishing Ltd., Oxford, UK*, 2003 (6^{th} edition 2007).

Xia, J., R. D. Miller, and C. B. Park, Estimation of near-surface shear-wave velocity by inversion of Rayleigh waves, *Geophysics, 64*, 691-700, 1999.

Zandt, G., S. R. Taylor, and C. J. Ammon, Analysis of teleseismic waveforms for structure beneath Medicine Lake Volcano, northern California, *Seismological Research Letters, 58*, 34, 1988.

Zhu, L., and H. Kanamori, Moho depth variation in southern California from teleseismic receiver function, *Journal of Geophysical Research, 105*, 2969-2980, 2000.